Amazon Climate Reconstruction Using Growth Rates and Stable Isotopes of Tree Ring Cellulose from the Madre de Dios Basin, Peru

by

Hillary Sandford Jenkins

Department of Earth & Ocean Sciences
Duke University

Date:_____
Approved:

_____
Paul A. Baker, Supervisor

_____
Avner Vengosh

_____
Gary S. Dwyer

_____
Miles R. Silman

_____
Michael N. Evans

Dissertation submitted in partial fulfillment of
the requirements for the degree of Doctor
of Philosophy in the Department of
Earth & Ocean Sciences in the Graduate School
of Duke University

2009

ABSTRACT

Amazon Climate Reconstruction Using Growth Rates and Stable Isotopes of Tree Ring Cellulose from the Madre de Dios Basin, Peru

by

Hillary Sandford Jenkins

Department of Earth & Ocean Sciences
Duke University

Date:_____
Approved:

_____
Paul A. Baker, Supervisor

_____
Avner Vengosh

_____
Gary S. Dwyer

_____
Miles R. Silman

_____
Michael N. Evans

An abstract of a dissertation submitted in partial fulfillment of the requirements for the degree of Doctor of Philosophy in the Department of Earth & Ocean Sciences in the Graduate School of Duke University

2009

Abstract

The Amazon basin is a center of deep atmospheric convection and thus acts as a major engine for global atmospheric circulation. From this basin, one fifth of the world's freshwater flux is discharged into the Atlantic and nearly two-thirds of the global rain forest resides herein. Yet despite its significance, little is known about past Amazon climate variability and the response of the forest ecosystem to climate.

Here, I attempt to reconstruct the paleoclimate history of a portion of the Amazon basin using both tree ring growth and the carbon and oxygen isotopes of tree ring cellulose from the Madre de Dios department of Southeastern Peru. Bomb ^{14}C dating identifies annual rings in tropical species *Cedrela odorata* and *Dipteryx micrantha*. A ring width chronology spanning 189 years (1817-2006) is developed for *Cedrela odorata* and 5 trees of *Dipteryx micrantha* are utilized for isotope reconstruction. The oldest tree used in the isotope reconstructions has an error-adjusted age of about 473 years (1533-2006). Using the species *Cedrela odorata, Ceiba pentandra, Hymenaea courbaril, Myroxylon balsamum,* and *Tabebuia serratifolia*, I develop 5 tree ring chronologies using relative ring width measurements and chart the growth behaviors of over 40 trees. Ring width chronologies from tree species *Cedrela odorata* and *Ceiba pentandra* show a significant correlation with wet season precipitation ($r = 0.42$, and 0.37, respectively, $p<0.05$). The ring width chronology developed from the species *Hymenaea courbaril* is significantly correlated ($r = 0.68$, $p<0.05$) with January river

discharge. Correlations between wet season precipitation and ring growth in *Cedrela odorata* are used to identify extreme wet and dry events. Nine historic droughts of the 20th century are identified in the *C. odorata* record. An increase in the frequency of extreme events (mean recurrence interval = 5-6 years) is observed in the 20th century and both Atlantic and Pacific sea surface temperature (SST) forcing mechanisms are implicated. The chronology shows a moderate correlation with both ENSO and tropical North Atlantic SST anomalies, suggesting that both basins play a role in precipitation variability over tropical South America.

Carbon and oxygen isotopic measurements (proxies of moisture stress and precipitation amount, respectively), in tree ring cellulose from 5 *Dipteryx micrantha* trees are used to reconstruct an error adjusted 473 year long record of precipitation variability. Because an error correction factor is applied to the chronologies of the trees of this species, assessment of annual-scale variability is precluded. Instead lower frequency trends are examined. No long term trends are identified in the oxygen isotopic records from individual trees. The carbon isotopic records of all five individual trees track the depletion of atmospheric $\delta^{13}C$ during the 20th century due to the anthropogenic input of fossil fuel CO_2 (The Suess effect). Relatively large variability in the oxygen isotopic records between trees suggests that site-specific and tree-specific conditions dominate this signal. Carbon isotopic records reveal a better correlation between records from multiple trees ($r = 0.47$, $p<0.01$) suggesting that a common climate signal is more robustly recorded by the $\delta^{13}C$ of these trees. At interannual frequencies (5

year), both carbon and oxygen isotopic records correlate significantly with wet season precipitation ($r = -0.50$, and -0.55 respectively, $p<0.05$). Spectral analysis reveals dominant 8-10 year and 3-5 year periodicities in both the carbon and oxygen isotopic records of individual trees. The oldest tree examined reveals a shift from this 8-10 year periodicity during the early part of the record to a lower frequency (20-24 year) variability during the last century. The lower frequency variability identified in the records is associated with both the Pacific Decadal Oscillation and the decadal and multidecadal variability observed in the tropical North Atlantic.

Collectively, these data show that tropical tree ring growth and isotopic composition in the southwestern Amazon basin are precipitation dependent and these measures can be exploited to reconstruct a hydrologic history for this region.

Dedication

This dissertation is dedicated to my parents, Dr. Cheryl Sandford Jenkins & Dr. Jeffrey Alan Jenkins, whose unwavering love of learning and intellectual discovery has instilled within me a passion for this journey.

Contents

List of Tables

List of Figures

Acknowledgements

I would first and foremost like to acknowledge my committee members, Professors Paul A. Baker, Avner Vengosh, Gary S. Dwyer, Miles R. Silman, and Michael N. Evans for their critiques and helpful advice during this process. I would especially like to thank my advisor Paul Baker for his encouragement, critical comments, insight, support as well as his insatiable curiosity about all things paleoclimate. I acknowledge my field and laboratory assistants, Cesar Vela and Elizabeth Bramble. The work in Peru would not have been possible without the assistance of Cesar Vela, whose intimate knowledge of tropical tree species allowed identification of over 60 species *in-situ*. Liz Bramble provided invaluable assistance by processing a multitude of cellulose samples in our lab at Duke.

Lab work for oxygen isotope analyses was provided by Professor Michael N. Evan's Mass Spectrometry Lab at the University of Arizona. I would like to thank both Mike and his lab manager Adam Csank for their assistance in processing over 1500 oxygen isotope samples. Carbon isotope analyses were conducted at the Duke University Environmental Stable Isotope Laboratory. I thank Dr. Jonathan Karr for his tremendous help is processing >2000 isotopic measurements.

Professor John Terborgh provided valuable assistance in the selection of tree species for this analysis. I would also like to acknowledge Dr. Robinson Negron Juarez for his assistance in the selection of precipitation datasets over the

Amazon basin as well as for his love and support throughout this process. This work would not have been possible without support from the Mustard Seed Foundation and the National Science Foundation (NSF 04-597).

Introduction

In 2005, the southwestern Amazon Basin experienced one of its most severe droughts of the century. Thousands of hectares of forest burned and river and lake levels were so low that travel by boat (the main mode of transport in many places) was impossible in parts of western Brazil and eastern Peru. The drought caused such widespread problems that the collective countries of Peru, Brazil, Colombia and Bolivia declared a 'state of public calamity' in September of 2005 (Marengo et al., 2008). Though previous droughts in the Amazon basin have been linked to El Nino (Nepstad et al., 1999), the 2005 drought occurred during a period of slight cooling in the Pacific and an Atlantic ocean based forcing mechanism has been asserted instead (Marengo, 2006). A warming of ~0.5°C has been observed in the tropical Atlantic between 1920 and 2000 (Trenberth and Shea, 2006) and some studies have linked this heating and its effect on the Amazon basin to global climate change (Emanuel, 2005; Webster et al., 2005). Still others report that trends in Atlantic Ocean SST's are part of a natural climate cycle such as the Atlantic Multidecadel Oscillation (AMO) (Goldenberg et al., 2001). The exact mechanisms controlling atmospheric and hydrologic variability in tropical South America remain unclear and a poor historical record of climate information prior to 1950 prevents this debate from being resolved. It is unknown what role Atlantic and Pacific SST's have had on the precipitation variability of the basin and whether events similar to the drought of 2005 have occurred even in the very recent past. Even less well understood is how extreme

climate events have affected the growth of the forest. Some studies (Saleska et al., 2007) have suggested that the forest is resistant to drought and report increased growth during 2005 while still others (Phillips et al., 2009) report widespread tree mortality in the Brazilian Amazon in response to extreme drought. It is clear that both the behavior of climate and the response of the forest are poorly understood. The lack of sufficient data (both spatially and temporally sparse and discontinuous) prevents even very basic questions about this hydrodynamic hotspot from being answered and the future climatic and biologic fates of the Amazon basin remain poorly understood. Providing an annually resolved, temporally continuous, paleoclimatic record for the Amazon basin that will help to address these questions has been the driving movitation for this work.

Tree rings have been used by many researchers to assess climate change of the past millennium (Mann et al., 1999; Lara and Villalba, 1993) as ring width is often a function of growing season temperature in temperate regions. Less attention has been given to the application of dendrochronology and dendroclimatology in tropical regions, in large part due to a suspicion that annual rings do not form in tropical species. This pervasive view has led to a lack of information on both growth behavior and ring formation in many tropical tree species (Lang and Knight, 1983). However, a myriad of studies over the past decade have shown that annual growth bands do form in trees in the tropics (Dunisch et al., 2003; Enquist and Leffler, 2001; Worbes et al., 2003; Stahle et al., 1998). Thus, if tropical trees can be accurately ring counted, and their rings

related to climate variables, they hold powerful potential as paleoclimatic indicators. The objectives of this study are therefore as follows:

1. To identify and test the utility of tropical tree rings as paleoclimatic indicators.
2. To use those paleoclimatic indicators to extend our knowledge of climate for the Amazon basin beyond the instrumental record.
3. To use this new record to investigate the mechanisms and forcings (both natural and anthropogenic) that drive extreme climate events in the Amazon basin.

In chapter 1, I conduct a methodological study to validate the isotopic measurements used in chapter 4. There has previously been some concern over biases in $\delta^{13}C$ and $\delta^{18}O$ records due to a diversity of preparation and chemical extraction methods. Here I compare the isotopic results from 3 preparation methodologies and two well known extraction techniques for reducing bulk wood to α-cellulose (Brendel Method & Modified Brendel Method).

Chapter 2 examines the relationship between tree growth behavior and climate. By charting the growth rates of 5 tropical trees species from the Madre de Dios department of Southeastern Peru, I discuss differences in growth behaviors through time. I then construct chronologies for each species and compare them to instrumental records of precipitation and river discharge. Relationships with climate for tree species *Myroxylon balsamum, Tabebuia serratifolia, Ceiba pentandra* and *Hymenaea courbaril* have not previously been documented and this work represents the first assessment of these species as

climatic indicators. I then use the relationship identified between precipitation and tree growth to examine extreme climate events over the past 190 years and discuss the forcing mechanisms driving drought in the Southern Amazon basin.

In chapter 3, I discuss the annual nature of tree rings in the tropics and use the 'atomic weapon effect' to date growth zones in trees of the species *Cedrela odorata* and *Dipteryx micrantha*. I then validate the use of both of these species in paleoclimatic reconstructions, discussing the relationship between tree growth, leaf fall behavior and seasonality. I identify locations where tree growth is expected to be annual and discuss environmental mechanisms that induce cambial dormancy in tropical trees.

In chapter 4, I utilize the relationship between stable isotopes in tree rings and climate to reconstruct an approximately 473 year-long isotopic record for the Amazon basin. Because the $\delta^{18}O$ of meteoric water is well correlated with precipitation amount in the tropics (Vuille et al., 2003), the measurement of $\delta^{18}O$ in plant cellulose gives a first order approximation of precipitation (White et al., 1994; Roden & Ehrlinger, 1999). The $\delta^{13}C$ measurement in plant cellulose yields an estimation of drought stress (based on stomatal conductance) experienced by the tree (Farquhar et al., 1989). By measuring these isotopes in the annual rings of five Amazon trees and comparing them with historic climate records, I demonstrate a relationship between wet season precipitation and both isotopic variables. However, in measuring isotopes from five individual trees, I reassess the notion that these variables are reproducible on annual time scales. Many studies currently average sample material from multiple trees prior to isotopic

analysis and this study demonstrates that averaging may be inappropriate given the differences between tree ring records. Longer time scale changes are consistent between both oxygen and carbon isotopic records, however, and a dominant 8-10 year periodicity is identified in both the carbon and oxygen isotopic records from all 5 trees. This periodicity is consistent with both the Pacific Decadal Oscillation (PDO) and the decadal and multidecadal variability of the tropical North Atlantic.

Each of these chapters provides a critical component to the story of Amazon basin paleoclimate. By examining the growth behavior of trees and the relationship between growth and climate, I am able to address how these species respond during extreme conditions. The use of isotopic measurements in tree rings provides a first glimpse into the history of climate variability on decadal time scales for the Amazon basin, while ring width measurements from species *Cedrela odorata* and *Hymenaea courbaril* provide the first annually resolved paleoclimate record for the region. And finally, integrating both of these measurements enables me to discuss the mechanisms forcing climate variability in tropical South America.

Instrumental Datasets Used throughout this Work:

There is currently a dearth of instrumental precipitation data across the Amazon basin. According to the IAWA, fewer than 30 measurement stations exist for the southwestern Amazon basin and many of these do not have data prior to 1970 (Figure 1). Data are both spatially and temporally heterogeneous making difficult the development of a consistent and reliable record. The earliest measurements date to 1901, though most station data begin after 1950. Often decades of data are missing from a single station and problems can arise in accounting for this error within a large dataset. Great effort has been put forth to produce quality-controlled datasets for this region and a variety of options currently exist (e.g. GHCN, CRU, GPCC). These datasets each have distinct advantages and disadvantages; some cover short time periods, some have low spatial resolution.

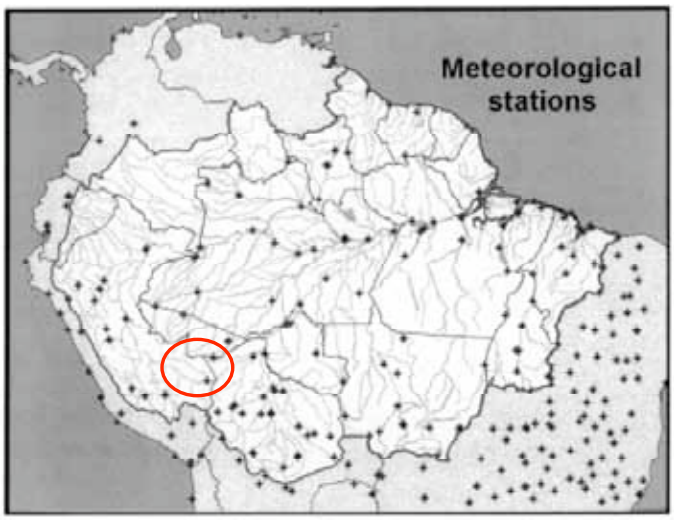

Figure 1. Map of South America showing Meteorological Stations across the basin. The field area for this study is outlined in red. Figure courtesy of Nepstad et. al., 1999.

Costa and Foley (1997) compared datasets over the Amazon basin and found that long-term spatial patterns of annual precipitation were in good agreement between rain gauge-only datasets. They found that reanalysis datasets contained biases that they associated with lack of good topographical resolution. Discrepencies were also found in the interannual signal between datasets. Negron Juarez et al. (2009) conducted a recent comparison between precipitation datasets over the Amazon basin using rain gauge, and combined rain gauge and satellite measurements and found that, although seasonal precipitation patterns are similar between datasets, large discrepancies are observed in both the spatial and temporal domains. They note particular differences in the sign of the interannual anomalies detected after 1998. The two datasets that showed the strongest correlation over the Amazon basin were from the Climate Prediction Center (GPC) and the Global Precipitation Climatology Centre (GPCC) rain gauge only measurements.

Three instrumental datasets are used in this study. The first is from a rain gauge dataset from one meterological station in the city of Puerto Maldonado, Peru. The second is a monthly gridded precipitation dataset from the GPCC. The third is a river discharge dataset (RIVDIS). The river discharge dataset provides an area-integrated measure of effective moisture (precipitation minus evaporation) taking into account processes occurring at the land surface. A detailed description of each of the three datasets is available below.

OBS Dataset

The Observational precipitation dataset (OBS) is a tabulation of monthly rain gauge data collected at the airport in Puerto Maldonado, Peru (12°30'S; 69°10'W) (SENAMHI, 2008). Rainfall has been collected daily at the station since 1973. However, the data have not been quality assessed and are therefore raw measurements. No systematic method has been applied to account for missing data or gauge measurement error. Despite issues associated with the quality of the dataset, the Puerto Maldonado station is one of the few stations in the entire region of the Madre de Dios to contain a precipitation record. All data computed using this dataset come from average monthly values in millimeters. The total length of the time series is 25 years from 1973-2008.

GPCC Dataset

The Global Precipitation Climatology Center (GPCC) dataset is a rain gauge only 0.25°x0.25° globally gridded precipitation dataset (Rudolf and Schneider, 2005). Rain gauge data are interpolated using the gridded method SPHEREMAP (Willmot et al., 1985). The full dataset is from 1901-2007, however the number of rain gauges used to interpolate the gridmap varies from 45,000 in the 1980's to less than 20,000 by 1950. An estimate of gauge measuring error is used to correct the dataset taking into account weather conditions during any given month of measurement. Because the number of rain gauge stations drops off rather dramatically in the early 1980's, I only use GPCC data going back to

1970. The Puerto Maldonado station is included in the GPCC gridded dataset. The GPCC gridbox used in this study is centered roughly over 10.8°S, 69.4°W.

RIVDIS Dataset

The third instrumental dataset, henceforth referred to as RIVDIS, is a compilation of river discharge data from Porto Vehlo, Rio Branco, and Brasileia, Brazil. Unfortunately no river discharge data are available from southeastern Peru; however the Brasileia site (11°1'17''S; 68°45'10''W) is located less than 50 kilometers away from the main tree localities. Discharge data from Rio Branco and Brasileia come from the Rio Purus and the Porto Vehlo discharge data is from the Rio Madeira. Discharge values are calculated by using a rating curve that relates local water level height measurement (stage) to discharge. The rating curves used to calculated discharge rates are periodically rechecked and recalibrated on-site. The data from Rio Branco come from the international dataset RIVDIS and the data from Porto Vehlo and Brasileia are unpublished (personal communication, da Silva, 2008). Both the Porto Vehlo and Rio Branco datasets span the time period 1967-2007. The Brasileia record spans 1984-2007. The RivDIS dataset has been compiled using UNESCO river archives by the University of New Hampshire. Data have been quality assessed against discharge records from the Global Runoff Center in Koblenz, Germany. Data are available as monthly average discharge values in cubic meters per second. Both monthly means and wet season means are calculated and used in this work.

Comparisons between datasets

All three datasets demonstrate the seasonality of precipitation and are highly correlated with each other ($r_{average}$ = 0.89). There is strongest agreement between the GPCC and OBS datasets (r = 0.99) showing a wet season peak during December-January (Figure 2). Although the two preciptiation datasets are well-correlated, there is a consistent offset in their absolute values of precipitation. The GPCC dataset yields consistently higher values of precipitation (up to 100 mm during the wet season) than the OBS dataset. All datasets show the dry season occurs between May and September. As expected, maximum discharge lags the precipitation maximum by about one month.

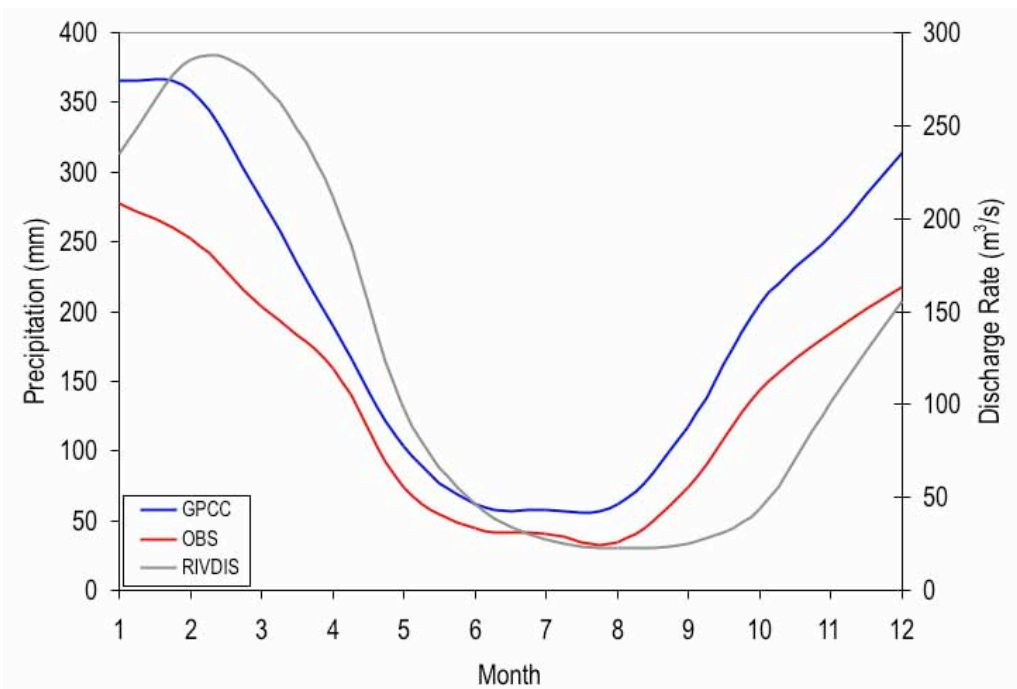

Figure 2. Mean monthly values of precipitation and river discharge derived from the 3 datasets. Rainy season (>100 mm/month) is from October through April.

The interannual variability derived for the three datasets is not as well correlated as might be expected. They are partially divergent between 1998 and 2004 (Figure 3). River discharge is poorly correlated with both precipitation datasets (OBS & RIVIDS: r = 0.25; GPCC & RIVDIS: r = 0.23). The two precipitation datasets show better agreement (r = 0.42), however much of this apparent agreement is driven by the largely coherent anomaly in 1982-83. As I will demonstrate, this lack of good agreement between instrumental records limits my ability to assign climatic significance to my paleoclimate data.

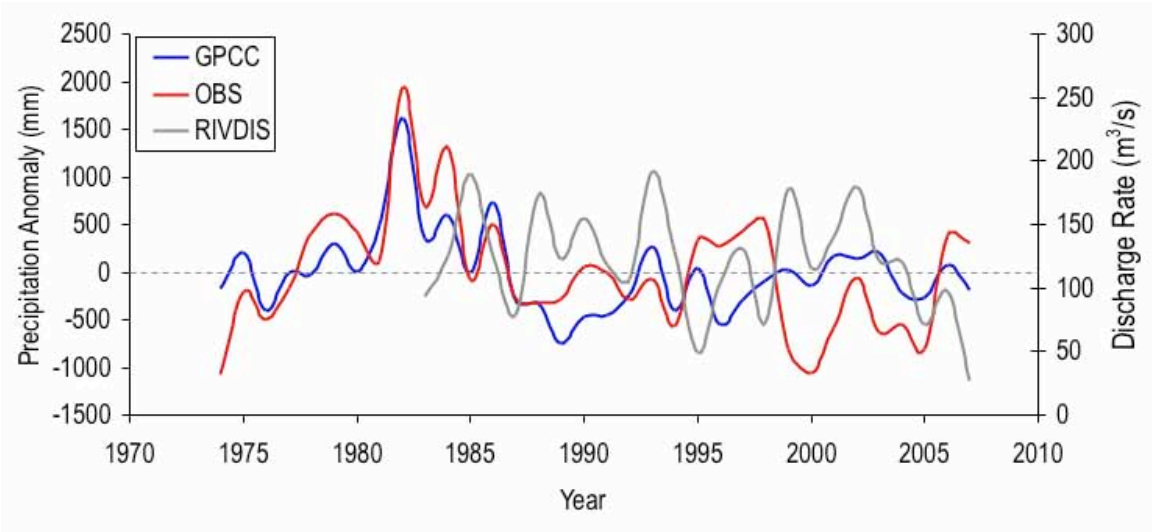

Figure 3. Precipitation anomalies and discharge rates for the hydrological year (Oct-Sep) for GPCC, OBS, and RIVDIS datasets during the overlapping period (1973-2007).

1. An Intralaboratory Comparison of Preparation Methods for α-Cellulose and the Consequences for Carbon and Oxygen Isotopic Measurements

1.1 Introduction

Cellulose comprises the majority of the woody xylem tissue that makes up plant cell walls and is the major component in tree rings (Taiz and Zeiger, 1998). The carbon and oxygen atoms that make up this long-chained polymer do not undergo exchange with atoms of carbon and oxygen in water, sucrose, or any other compound traveling through the tree after the cellulose is formed. Because its atomic signature remains fixed in time, this makes cellulose an excellent recorder of past environmental conditions (Anchukaitis et al., 2008; Evans, 2008; Evans, 2007; Roden et al., 2000; Farquhar et al., 1989; Benner et al., 1987; Burk and Stuiver, 1981).

However, only about one half to two thirds of bulk wood is composed of cellulose. The remaining one third to one half is made up of hemicellulose and lignin. These two compounds both bind to cellulose fibers serving to harden and strengthen the cell walls. However, hemicellulose is amorphous and easily hydrolyzed making it susceptible to isotopic fractionation. Lignin also lacks a distinct structure. Lignin is involved in facilitating water transport through the xylem. Because of this, lignin constantly undergoes isotopic fractionation, thus cannot preserve a permanent record of any environmental signal. Therefore, extracting pure α-cellulose from bulk wood is a crucial step in isolating any permanent environmental record preserved in the tree rings. Some work has

been done (Borella et al., 1998) to derive climate information from bulk wood itself by accounting for a constant offset between α-cellulose and lignin formed at the same time. However, problems can arise due to incomplete removal of extractives (e.g. resins) which can vary considerably between heartwood and sapwood.

While a variety of methods have been put forth in the last half-century regarding the chemical extraction process to isolate α-cellulose, little attention has been given to the preparation method for removing bulk wood from the tree sample itself. Prior to cellulose extraction, tree ring samples must be manually removed from tree core, stem wedge, or stem disc samples. A wide variety of techniques exist for this process, from thin-sliced micromilling to hand drilling to non-motorized scalpel removal. Each of these techniques results in a different treatment of the wood prior to cellulose extraction. In some cases, the cellulose compositions may be altered by burning of the wood. Clearly, if the initial preparation technique for wood removal is biased toward preserving/removing α-cellulose, lignin, or hemicellulose, then the final isotopic measurement may be inaccurately biased as well. However, no systematic comparison of sampling techniques and their effect on cellulose isotopes has been conducted. Here I examine the effect of 3 different bulk wood preparation techniques on the isotopic signature of α-cellulose. I compare carbon and oxygen isotopic data from tropical tree samples prepared using a hand drill (Dremel) operated at high speed, a (Dremel) drill operated at low speed, and a rotary microtome that sliced thin (20 μm) sections of wood. This comparison was done to answer one basic

question; do the different preparation techniques result in different carbon and oxygen isotopic outcomes for a given tree sample? Such differences would presumably result from the partial burning of cellulose during high-speed drilling.

A myriad of chemical procedures exist for the extraction of α-cellulose, and previous laboratory comparisons have been undertaken to examine the difference (if any) between these methods in yielding final carbon and oxygen isotopic results. Recently, Gaudinski et al. (2005) compared 5 different extraction methods and found that the original Brendel method produced significantly different values of $\delta^{18}O$ ($p<0.05$) than other methods. In 2008, Anchukaitis et al. compared the Brendel, Modified Brendel and classical methods using both stable isotope and infrared measurements. While they found no significant difference between the $\delta^{18}O$ of the standard Brendel technique and other methods, their absorbance spectra do show a peak in the region associated with cellulose acetate which they attribute to a slight (~3%) acetylation of cellulose during Brendel method processing. Thus, I conduct an additional comparison of the Brendel and Modified Brendel extraction methods here.

1.2 Methods

Two tropical tree species (*Dipteryx micrantha* and *Cedrela odorata*) were examined for isotopic variation in this analysis. Both species are relatively abundant (2-6 trees per hectare) in both the northern and southern Amazon basin, though *C. odorata* has a larger geographical extent ranging from southern

Mexico to Northern Argentina (Cintra, 1997). Though they are widely known for their export value as commercial timber (*C. odorata* – Spanish mahogany in particular), the clear growth rings present in both species suggest that they may record past environmental conditions at annual resolution.

Here I examine wood samples of *C. odorata* and *D. micrantha* wood samples from logging concessions in the Madre de Dios department of southeastern Peru. These samples were collected in the summers of 2004 and 2007 in and around the city of Puerto Maldonado, Peru. Twenty samples (10 samples each of *C. odorata* and *D. micrantha*) were analyzed using the three preparation methods of low speed dremel drilling, high speed dremel drilling, and rotary microtoming and their oxygen and carbon isotopic values were measured (Table 1). A cross-species comparison was also conducted to determine the effect of density on preparation method (*D. micrantha* is much denser than *C. odorata*). Finally, the Brendel and Modified Brendel extraction methods were conducted on both species to determine the importance of the final NaOH step in the extraction process.

Table 1. Sample Information detailing extraction and preparation methods used for each sample set and elemental analyses conducted.

Sample Set	Tree Species	Sample Location	Sample Size	Extraction Method Used	Preparation Method Used	Analyses
1	*Cedrela odorata*	Puerto Maldonado, Peru	10	Brendel Method, Modified Brendel Method	Low Speed Drilling, High Speed Drilling, Microtome Slicing	$\delta^{13}C$ %C
2	*Dipteryx micrantha*	Inapari, Peru	10	Brendel Method, Modified Brendel Method	Low Speed Drilling, High Speed Drilling, Microtome Slicing	$\delta^{13}C$ $\delta^{18}O$ %C

1.2.1 Preparation Methods

Three different preparation methods were utilized on the tree samples and their isotopic responses were compared. The three preparation methods used were high speed dremel drilling, low speed dremel drilling, and wood slicing using a rotary microtome. Prior to sample removal, tree slab surfaces were sawed, sanded and polished up to 400 sand grit. Both high and low speed dremel drilling was conducted using a 300 Series Variable Speed Dremel Rotary tool with a diamond bit tip. For high speed drilling, pressure was applied to the tree sample surface and the drill rotary was set to 35,000 rpm. This is the highest level available on the drill and a burned wood smell was associated with its use, however, no charring was present on the wood surface. After drilling, samples were ground using a mortar and pestle until powdered. The diamond bit tip was cleaned in ethanol between each sample. For low speed drilling, the drill rotary was set to 5,000 rpm and little pressure was applied to the tree surface. On occasion a slightly charred smell was detected in the laboratory though no charring was visible on the sample surface. The final preparation technique was employed using a non-electric flat-cutting rotary microtome. Samples were cut into sections and then sliced in 20 micron increments prior to powdering. The microtome blade was cleaned in ethanol between each sample. 10 Samples from both *C. odorata* and *D. micrantha* were subjected to each of the three preparation methods, extracted and measured for oxygen and carbon isotopic ratios.

1.2.2 Extraction Methods

The extraction method used on all samples in this study is the Modified Brendel Method, however I employ an additional comparison between the Brendel and Modified Brendel methods to confirm the results of Gaudinski et al. (2005) which found the Brendel method to yield significantly different $\delta^{18}O$ values than other methods. For all samples used in this comparison, a rotary microtome was used to slice and prepare samples. The Brendel method was developed as a rapid way to process crude cellulose into pure α-cellulose (Brendel et al., 2000). The original procedure for cellulose extraction, the Jayme-Wise method, involved solvent extraction with benzene and ethanol in a Soxhlet system followed by an acid sodium hypochlorite bleaching to remove lignin from the sample (Green, 1963). Leavitt and Danzer (1993) modified this method using toluene instead of benzene to reduce laboratory exposure to carcinogens and included an NaOH rinse to further purify the sample. α-cellulose is defined as the cellulose that does not dissolve in a 17.5% solution of NaOH. The Brendel method uses an acetic and nitric acid mixture instead of toluene and ethanol to remove both lignin and noncellulose polysaccharides (hemicellulose). The acetic/nitric acid mixture does not require a Soxhlet apparatus, therefore cuts processing time from 30 hours (Jayme-Wise method, Soxhlet) to 30 minutes, making the Brendel method the preferred method for processing large numbers of samples. The original Brendel method does not include a final NaOH rinse and was therefore thought to produce holocellulose, a combination of pure α-cellulose and hemicellulose. Because hemicellulose can contain residual bonded

lignin, the additional NaOH step is added to ensure the removal of all non α-cellulose material. For a complete description of the Brendel and Modified Brendel methods, see Appendix I.

1.2.3 Elemental and Isotope Analysis

Both carbon and oxygen isotopic values are recorded for samples in all of the sample sets. All isotope data are expressed using standard notation where

$$\delta^{18}O = \frac{\left(\frac{^{18}O}{^{16}O}\right)_{sample} - \left(\frac{^{18}O}{^{16}O}\right)_{standard}}{\left(\frac{^{18}O}{^{16}O}\right)_{standard}} \; x\ 1000$$

and

$$\delta^{13}C = \frac{\left(\frac{^{13}C}{^{12}C}\right)_{sample} - \left(\frac{^{13}C}{^{12}C}\right)_{standard}}{\left(\frac{^{13}C}{^{12}C}\right)_{standard}} \; x\ 1000$$

The values for both $\delta^{18}O$ and $\delta^{13}C$ are measured in parts per thousand (‰) or per mil. The standard for $\delta^{13}C$ measurements is the Vienna Peedee Belemnite (VPDB) and the standard for $\delta^{18}O$ is the Vienna Standard Mean Ocean Water (VSMOW).

All isotopic measurements are made on a Finnigan MAT Delta Plus XL continuous flow mass spectrometer system interfaced with a thermochemical elemental analyzer (TC/EA). Pyrolized $\delta^{18}O$ and combusted $\delta^{13}C$ samples are respectively packed into silver and tin capsules, and thermally combusted to produce CO (for oxygen) and CO_2 (for carbon). Internal standards of Duke sucrose, Duke cellulose and COSTECH Actenalide are used to correct for the

normal daily changes in instrument environment and parameters as well as any standard gas drift. For $\delta^{13}C$ values, internal standards are calibrated against NIST/IAEA Reference Material NBS-22, Sucrose ANU, and PERFl foil. For $\delta^{18}O$, standards are calibrated against IAEA 601, IAEA 602, and Sucrose ANU. Precision for both $\delta^{13}C$ and $\delta^{18}O$ values is +/- 0.2 ‰. Percent C measurements are made incidentally when the $\delta^{13}C$ data are processed and are therefore less precise (+/- 0.5% to 5%). The %C of the COSTECH Actenalide is used as a proxy standard.

1.2.4 Statistical Analyses

I employ an Analysis of Variance (ANOVA) test to examine the differences (if any) between the three preparation methods (high speed drilling, low speed drilling, and microtome slicing) for each sample set. In all cases, the number of replicates is 3. For $\delta^{13}C$ and %C data, the number of samples is 10. For $\delta^{18}O$ samples, the number of samples is 5. For comparisons between sample sets, a paired t-test is used to determine whether the sample sets are significantly different. In cases where the ANOVA test revealed significant differences among preparation methods, I conducted a post hoc Tukey's HSD test to determine which of the 3 preparation methods differed significantly. For comparisons between extraction methods (Brendel and Modified Brendel methods), a one-way ANOVA test was used. For the extraction method data, the number of replicates is 3 but the number of samples is variable (e.g. only 3 non-extracted bulk wood samples were measured for oxygen and carbon isotopes). In this case,

the mean of these 3 samples was used as an estimate for the remainder of the sample set.

1.3. Results

1.3.1 Preparation Methods

All three preparation methods resulted in significantly different $\delta^{13}C$ values in both tree species (Figures 4a and 4b, Appendix II). A progressive depletion of 1-1.5 per mil was observed between each preparation method with non-motorized microtome slicing resulting in the most isotopically enriched value (-24.66‰) and high speed drilling with the most isotopically depleted (-27.35‰). This suggests a preferential loss of ^{13}C during the drilling preparation methods, with the highest loss occurring during high speed drilling. An ANOVA test showed this difference to be statistically significant at the 99% significance level (Table 2). A Tukey's HSD Post Hoc Test revealed that all three methods result in significantly different $\delta^{13}C$ values (Table 3).

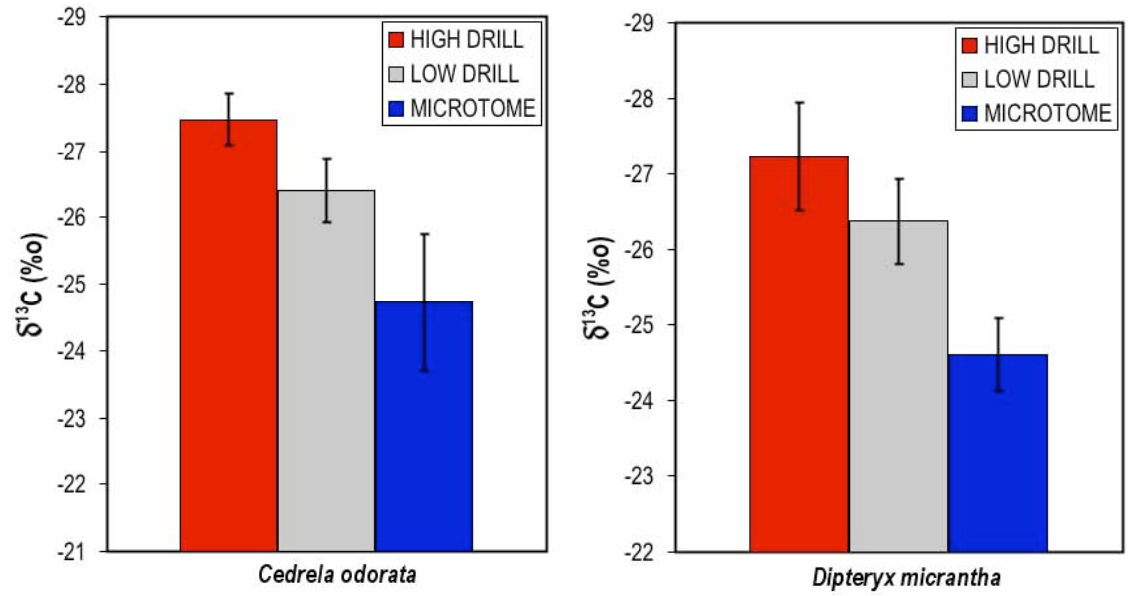

Figures 4a and 4b. Average $\delta^{13}C$ values for 10 *Cedrela odorata* and *Dipteryx micrantha* cellulose samples treated with the 3 different preparation methods of microtome slicing, high speed drilling, and low speed drilling. Error bars for each average are +/- 1 standard deviation.

The $\delta^{18}O$ data show a somewhat similar trend, where both high and low speed drilling samples are on average 1.21‰ lower values than microtome samples (Figure 5). However, this relationship is weaker than that observed in the $\delta^{13}C$ data and is statistically significant only at the 90% level. Low and high speed drilling methods both result in isotopically depleted values, and the Tukey's HSD shows no significant difference between the two methods (Table 3). Percent carbon is 5-10% higher in low speed drilled samples than in microtomed or high speed drilled samples. A Tukey's HSD Post Hoc Test shows that low speed drilling results in significantly different %C output than either of the other two preparation methods.

Figure 5. Average $\delta^{18}O$ values for 10 cellulose samples treated with the 3 different preparation methods of microtome slicing, high speed drilling, and low speed drilling. Error bars for each average are +/- 1 standard deviation.

Table 2. ANOVA results comparing extraction methods for $\delta^{13}C$, $\delta^{18}O$ and %C in *Cedrela odorata* and *Dipteryx micrantha*.

Variable Measured	F Value	Degrees of Freedom (between samples)	Degrees of Freedom (within samples)	MSE (mean square error)	F-critical value (p<.05)
δ13C *Cedrela*	39.97	2	27	0.48	3.35
δ13C *Dipteryx*	50.16	2	27	0.36	3.35
δ18O	2.58	2	12	1.00	2.81*
%C *Cedrela*	2.86	2	27	118.11	2.51*
%C *Dipteryx*	1.21	2	27	103.55	2.51*

*Indicates the F-critical value for p<.10

Table 3. Tukey's HSD Analysis results for comparisons between the three preparation methods of High speed drilling, low speed drilling, and microtome slicing and their effect on $\delta^{13}C$, $\delta^{18}O$, and %C content in the tree rings.

Preparation Method	$\delta^{13}C$ *Cedrela*	$\delta^{13}C$ *Dipteryx*	$\delta^{18}O$	%C *Cedrela*	%C *Dipteryx*
High Drilling	a*	a*	a	a	c
Low Drilling	b*	b*	b	b"	c
Microtome	c*	c*	b	a	c

Results are reported in the same format as Gaudinski et. al., 2005, such that significant differences between preparation methods are expressed by different letters in the same column
Letters within the same column should be compared.
*Indicates differences significant at the 99% level.
"Indicates differences significant at the 90% level.

1.3.2 Extraction Methods

Not surprisingly, bulk wood samples that received no chemical cellulose extraction resulted in significantly different results in all three measurements ($\delta^{13}C$, $\delta^{18}O$, and %C) (Table 4). Bulk wood $\delta^{13}C$ measurements were, on average, 1.5-2.5‰ lighter than samples processed using the Brendel and Modified Brendel methods (Figure 7a and 7b). $\delta^{18}O$ measurements were ~2.0‰ lighter and %C was 5-8% higher in non-processed samples (Figure 6).

Table 4. ANOVA results from a comparison between extraction methods (Brendel Method, Modified Brendel Method, and No Treatment) for both sample sets.

Variable Measured	F Value	Degrees of Freedom (between samples)	Degrees of Freedom (within samples)	MSE (mean square error)	F-critical value (p<.01)
δ13C *Cedrela*	32.84	2	27	0.18	5.488
δ13C *Dipteryx*	123.22	2	27	0.16	5.488
δ18O	6.16	2	12	0.33	3.885*
%C *Cedrela*	10.08	2	27	19.78	5.488
%C *Dipteryx*	6.8	2	27	29.29	5.488

*Indicates the F-critical value for p<.10

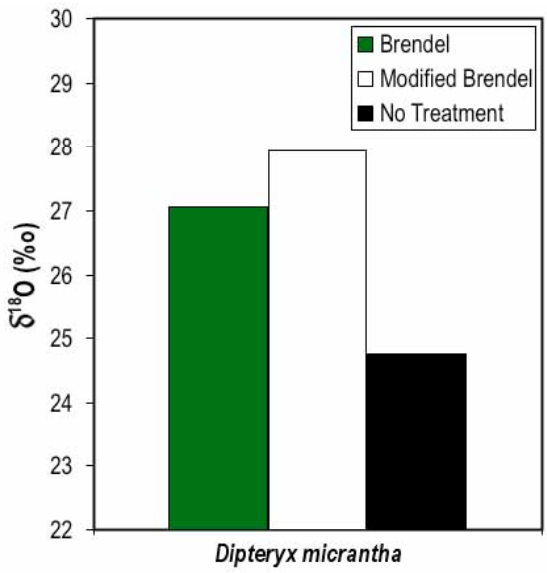

Figure 6. Average $\delta^{18}O$ values for cellulose samples treated with the Brendel Method and Modified Brendel Method as well as an untreated bulk wood. $\delta^{18}O$ values are for samples from the tree species *Dipteryx micrantha* only.

The Brendel and Modified Brendel methods did not result in significantly different $\delta^{18}O$ values. Both methods resulted in higher $\delta^{18}O$ values relative to bulk wood. The $\delta^{13}C$ values were significantly different ($p<0.01$) between the two methods for *D, micrantha* samples, but for *C. odorata* no significant difference was detected (Table 5). In the case of the *D. micrantha* samples, the Modified Brendel method resulted in values 0.85‰ lower than those extracted using the Brendel method.

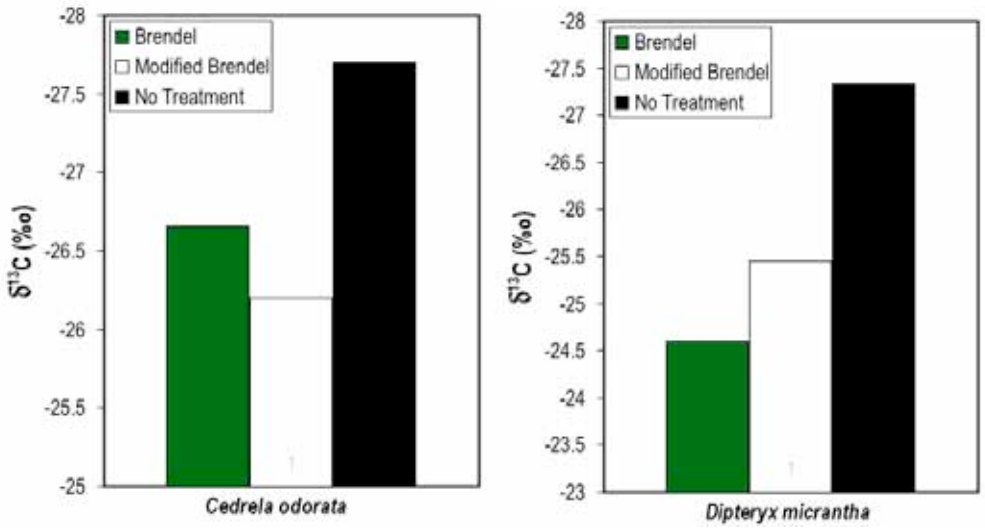

Figures 7a and 7b. Average $\delta^{13}C$ values for cellulose samples treated with the Brendel and Modified Brendel Methods of extraction as well as an untreated bulk wood.

Table 5. Tukey's HSD Analysis results for comparisons between the Brendel and Modified Brendel methods and a bulk wood for each of the following variables; $\delta^{13}C$, $\delta^{18}O$, and %C.

Extraction Method	δ13C *Cedrela*	δ13C *Dipteryx*	δ18O	%C *Cedrela*	%C *Dipteryx*
Brendel	a	a	a	a	a
Modified Brendel	a	b*	a	a	a
No Treatment	b*	c*	b"	b*	b*

Results are reported in the same format as Gaudinski et. al., 2005, such that differences between preparation methods are expressed by different letters. Letters within the same collumn should be compared.
*Indicates differences significant at the 99% level.
"Indicates differences significant at the 95% level.

1.4 Discussion

The preferential loss of ^{13}C within the high speed drilling samples is consistent with the samples having been heated or burned slightly. During the carbonization of wood, thermally labile carbon compounds are more likely to be

lost to the system. Lignin is non-labile carbon and is more likely to be preserved during carbonization (Baldock and Smernik, 2002; Czimczik et al., 2002; Harden et al., 2004). The formation of lignin occurs secondarily to initial carbon fixation at the plant leaf surface and is therefore relatively more ^{13}C depleted than holocellulose (Benner et al., 1987; Loader et al., 2003). Therefore, when holocellulose is preferentially volatilized during burning, the overall isotopic signature of the bulk wood decreases and approaches that of lignin. Turney et al. (2005) found similar results to those of this study by conducting a systematic carbonization of bulk wood from *Eucalyptus*, *Quercus*, and *Pinus*. They found a similar depletion of up to 1.3‰ during this process which, they suggest, may lead to up to a 7% error in paleoclimatic reconstruction.

The results for oxygen isotopic values are similar to those of $\delta^{13}C$. Both high and low speed drilling results in a decrease of $\delta^{18}O$. This is likely also due to the preferential volatilization of holocellulose relative to lignin. Initial carbon fixation results in the formation of holocellulose, but secondary metabolism fractionates the oxygen isotopes further, yielding a much more negative signature for lignin formation. Both methods of drilling result in a depletion of $\delta^{18}O$, suggesting that even low speed drilling volatilizes cellulose at the wood surface. This may also be due to the hardness of the tropical wood being sampled, such that drilling at any speed generates enough friction to volatilize organic compounds. Both the $\delta^{13}C$ and $\delta^{18}O$ data reveal that drill-prepared samples result in an isotopically depleted bias in sample measurements. Thus I

conclude that the application of drilling as a method to prepare wood samples for extraction is inappropriate and a rotary microtome is highly preferable.

Gaudinski et al. (2005) found the carbon content of unprocessed wood to be ~45-53% while woods that had been treated with extraction methods resulted in lower values (37-49%). By weight, pure cellulose is 44.5% carbon and the results of this study find that wood samples processed using both the Brendel and Modified Brendel methods approach this value (Brendel average = 41.25, Modified Brendel average = 42.19). Though Gaudinski et al. (2005) find that Brendel method resulted in an isotopically enriched $\delta^{18}O$ relative to the Modified Brendel method, the difference is not statistically significant here. The Brendel method does yield an enriched value relative to the Modified Brendel method, but the difference is minimal. However, for $\delta^{13}C$ of *D. micrantha*, the Brendel method values yield significantly higher values of $\delta^{13}C$ than does the Modified Brendel method. Anchukaitis et al. (2008) used NMR spectroscopy to identify this difference in cellulose from a Peruvian *Prosopis* tree from Piura, Peru. They attribute this offset to a partial acetylation of cellulose that occurs during the nitric/acetic acid delignification process.

1.5 Conclusion

This analysis has shown that the $\delta^{13}C$ value of alpha cellulose is affected by sample preparation technique. $\delta^{13}C$ values become progressively more negative (up to 2.5 ‰) when an electric drill is used to remove the sample from the wood surface and are significantly different ($p<0.01$) from those derived using a microtome. The increased friction caused by drilling apparently

preferentially volatilizes the more mobile carbon (cellulose) leaving behind the isotopically depleted lignin. This results in a systematic bias in $\delta^{13}C$ estimates for alpha cellulose prepared with this technique. The $\delta^{18}O$ results show the same bias with a decrease of ~1.5‰ between drilled and non-drilled samples. This result is reproduced in two tree species of varying hardness suggesting that drilling results in a systematic bias in the isotopic ratios of tree ring 'cellulose.' Microtome slicing (or removal with a scalpel) is therefore the recommended preparation technique for removal of sample from the wood surface.

A comparison between the Brendel and Modified Brendel methods did not yield statistically significant results in $\delta^{18}O$, but did result in significantly different values from bulk wood. The $\delta^{13}C$ values were similar, though a statistically significant difference was found in the $\delta^{13}C$ values of *Dipteryx micrantha*. Gaudinski et. al., 2005, found evidence to suggest that the Brendel method may not effectively remove lipids from samples, which may result in slightly lower values (lipids contain more ^{12}C), though I did not find this to be the case. Although no systematic difference was found between these two methods, the additional NaOH rinse in the Modified Brendel Method ensures the removal of any molecules bearing readily exchangeable oxygen and is thus the preferred procedure.

2. Relating Tree Growth and Precipitation in 5 Tropical Tree Species: An Analysis of Extreme Climate Events

2.1. Introduction

A pervasive view that annual rings do not form in tropical trees has led to a lack of information on both growth behavior and ring formation in many tropical tree species (Lang and Knight, 1983). However, Worbes (1999) points out that for many species, a period of at least 2 consecutive months with <60 mm of rainfall is enough to induce cambial dormancy, causing a distinct growth zone to form. If the precipitation signal is strongly seasonal, tree rings are likely to form in association with the annual cycle and this has been demonstrated by numerous studies in tropical regions (Detienne 1989; Dunisch et al., 2003; Fichtler et al., 2004). The method of cross-dating has been widely used in temperate regions by matching trees of unknown date with trees of known date using a pattern of shared variability but has only recently been attempted in the tropics (Worbes et al., 2003; Brienen and Zuidema, 2005). Site-specific and species-specific conditions can influence the behavior tree growth and it is unknown how strong the shared climate signal is for trees from tropical South America.

In this study, I present dendrochronologic records from 5 tropical species from the department Madre de Dios in southeastern Peru and compare these records with the region's climate. Three of the five species (*Cedrela odorata, Ceiba pentandra*, and *Hymenaea courbaril*) have previously been shown, via methods of cambial wounding, ^{14}C dating, and cross-dating (Mauriax, 1967; Worbes, 1995;

Brienen and Zuidema, 2005) to produce annual rings. I validate these findings via cross-dating methods and correlations with annual precipitation and river discharge. The species that show greatest correlation with climate variables are then examined for extreme low (dry) and high (wet) tree growth over the past 190 years. Trends in precipitation from historical records for the Amazon basin are related to tree growth and possible forcing mechanisms are discussed. A comparison between growth rates for each of the 5 species is also conducted.

2.2 Study Area

2.2.1 Site Localities

The samples used in this study were collected from the Madre de Dios department of Southeastern Peru. Samples were retrieved both from logging concessions and private property (farmland). Based on the diversity of sampling sites, I divide the region into 4 localities (Figure 8). All of the sites are located in Peru, adjacent to the interoceanic highway which enabled access to some of the more remote locations. The first locality (Inapari) encompasses the town of Inapari near the border between Peru, Bolivia and Brazil (12°3′0S, 69°24′0W). This site is the northernmost locality in this study. The second and third localities (Iberia and Alerta, respectively) are located in the Tahuamanu province and are slightly farther south (11°40′0S, 69°13′60W, and 11°20′60S, 69°34′60W). The southernmost site includes the town of Puerto Maldonado and these samples were collected from concessions and farmland in the surrounding areas. Samples from each of the 5 species used in the chronologies are dispersed throughout these 4 localities with the exception of *Cedrela odorata* (CO) and *Ceiba pentandra*

(CP). The CO tree samples were collected from the Puerto Maldonado locality only while the CP samples were taken from the Alerta locality. Both CO and CP tree samples come from logging concessions only. Trees from the remaining 5 species are a mixture of concession and *in-situ* samples. Only trees that had been cut during the year of field collection were sampled.

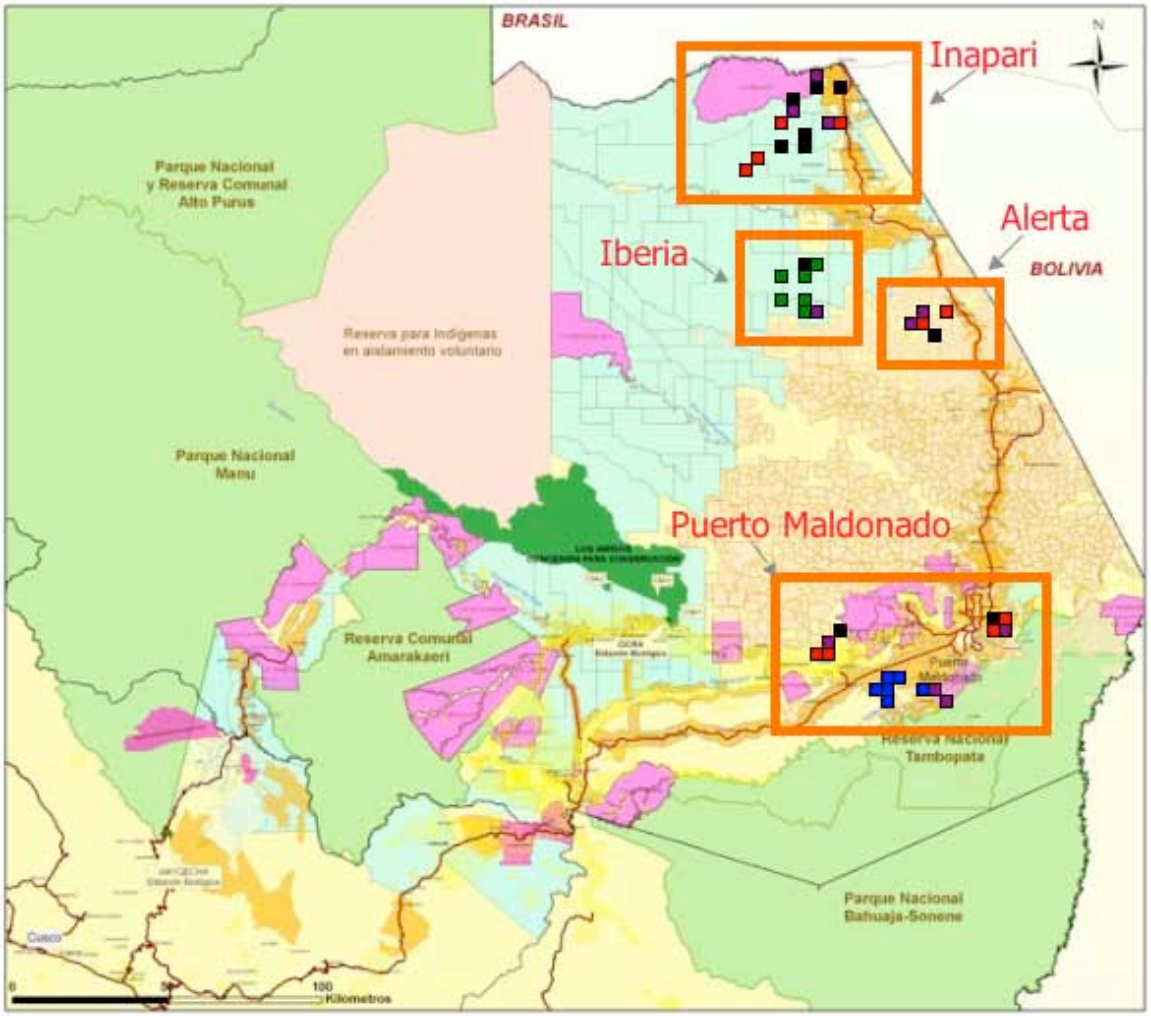

Figure 8. Map of the 4 site localities in this study. Localities outlined in orange boxes and labeled on the map. Smaller boxes denote approximate locations of individual trees. Color coding is as follows: Red = *Hymenaea courbaril,* Purple = *Myroxylon balsamum*, Blue = *Cedrela odorata*, Green = *Ceiba pentandra*.

2.2.2. Climatology

The climate is not significantly different between these 4 sites. The Inapari locality sits at 238 meters above sea level while the Puerto Maldonado site is only 183 meters altitude. The two intermediate sites (Alerta and Iberia) are both 235 meters above sea level. The average annual temperature for all 4 sites is 26° C with little seasonal variation (+/- 1° C) (Figure 9). The seasonality of rainfall, however, is strong, with monthly rainfall averages of >200 mm during the wet season and <75 mm during the dry season (Figure 10). At all four localities, the rainy season runs from October through April where it is defined as monthly rainfall >100mm. The dry season runs from May through September. Average annual rainfall for the Inapari site is 1761.33 mm while average rainfall at the Puerto Maldonado site is 1711.81 mm.

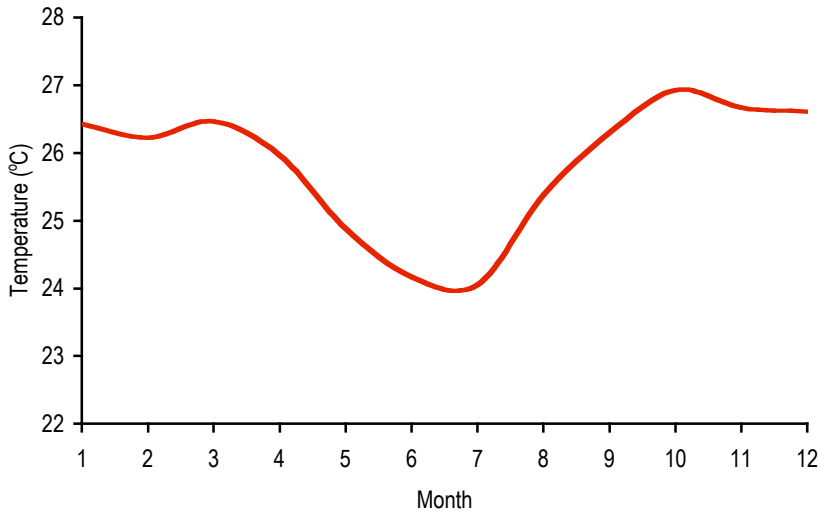

Figure 9. Mean monthly temperature recorded at the meteorological station in Puerto Maldonado, Peru. Averages are based on monthly values recorded between 1972 and 2007.

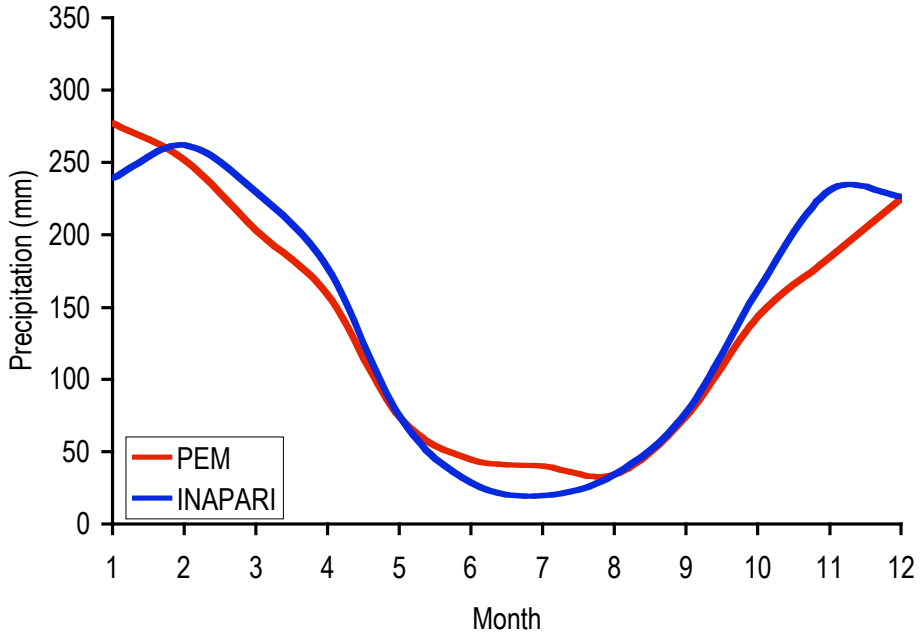

Figure 10. Mean monthly precipitation for the Puerto Maldonado and Inapari localities. The Puerto Maldonado data are based on rain gauge measurements recorded daily at the meteorological station in Puerto Maldonado, Peru. The Inapari data are globally interpolated rain gauge data from the Global Precipitation Climatology Center (GPCC) interpolated using the gridded method SPHEREMAP (Wilmott et al., 1985) and come from a 0.25°x0.25° gridbox centered over the Inapari, Alerta, and Iberia study sites (12°3'0S, 69°24'0W). Both datasets span 1973-2008.

2.2.3 Climate Datasets

Because the instrumental climate data for this region is extremely sparse, I compare both precipitation and river discharge data with the tree ring chronologies. The precipitation data come from a rain gauge station located at the airport in Puerto Maldonado. This is the only rain gauge station with available data for the Madre de Dios department. The closest meteorological station is located in Rio Branco, Brazil. River discharge data come from two

stations located in Brasileia and Rio Branco, Brazil. Discharge is measured in cubic meters per second and data are given as monthly averages from 1984 and 1967 to present.

2.3 Materials and Methodology

2.3.1 Study Species

I selected 5 species for this study. Each of these species was selected primarily because of the appearance of visibly distinct growth bands and because of the relatively high number of individual tree samples obtained (>5 trees). These species differ in growth rate, hardness, and leaf-fall behavior. Further information for each species discussed in this study is presented below.

1. *Hymenaea courbaril*

Also known as the Brazilian Cherry Tree, this leguminous Fabaceae is a canopy tree and can grow up to 45 meters in height (Vozzo, 2002). The tree bears small red flowers at the onset of the rainy season and through the austral summer. *H. courbaril* grows on sandy drained ridges, from sea level up to 900 meters elevation (Vozzo, 2002). As a hardwood with a specific gravity of 0.71-0.82 g/cm^3, *H. courbaril* is also a timber product used in furniture, boatbuilding and cabinets.

2. *Myroxylon balsamum*

Another legume, this Fabaceae is an emergent tree, typical of the mature forest. It is found in evergreen forests and grows well on moderate slopes between 100 and 600 meters elevation (Marin and Flores, 2003). *M. balsamum* is found between 20°N and 15°S ranging from Southern Mexico through central

American and into the Peruvian and Brazilian Amazon. It grows to 45 meters in height with a 1 meter diameter breast height (dbh) and can be planted to shade coffee tree plantations owing to its growth of 10 meters in the first 10 to 12 years and 20 meters within 25 years of life. It is extremely dense and hard with a specific gravity of 0.74-0.81 g/cm^3 (Marin and Flores, 2003). Fruit production occurs just before this during the onset of the rainy season (October to November). *M. balsamum* is used as timber for flooring, furniture, interior trim, and railroad crossties (Chudnoff, 1984). It is also known for its balsam which is used in perfumes, produced mainly in El Salvador, though plantations of *M. balsamum* have also been established in India, West Africa, and Sri Lanka for this purpose.

3. *Ceiba pentandra*

Ceiba pentandra is a fast growing, light demanding, pioneer species that flourishes between sea level and 500 meters elevation. This deciduous Malvaceae (formerly Bombaceae) is an emergent species that can grow as high as 50 meters (Alvarado et al., 2003). The large umbrella shaped crown emerges above the canopy and the trunk is often heavily buttressed. *C. pentandra* is found throughout the American tropics ranging from Mexico to Bolivia and Brazil. It is also found in West Africa. It is a drought-deciduous species meaning that it loses its leaves during the dry season. Flowering occurs during the rainy season with fruits produced between January and April (Joker and Salazar, 2000). *C. pentandra* is neither hard nor dense with a specific gravity of 0.26-0.4 g/cm^3 and has been used commercially for plywood (Richter and Dallwitz, 2000). The fluff

of kapok that surrounds the seeds is water resistant and lighter than cotton, making it useful as the stuffing of life preservers, seat cushions, and mattresses. The wood is also used by local communities to make giant canoes.

4 *Cedrela odorata*

Also known as Spanish cedar, this meliaceae is one of the most commercially important trees of the tropical Americas. Ranging from the pacific coast of Mexico (26°N) through Central America, the South American lowlands and into Argentina (28°S), *C. odorata* is widely distributed though not common (averaging an individual tree per 2-6 hectares). It is a deciduous tree that flowers at the beginning of the rainy season. *C. odorata* is a secondary forest colonizer and can exceed 50 meters in height (Rendle, 1969; Ricker and Daly, 1997). It is a moderately lightweight wood (specific gravity 0.4) and is used commercially for plywood, furniture and cabinets.

5. *Tabebuia serratifolia*

From the family, bignoniaceae, this dicot is most widely distributed in the Caribbean, but it ranges from the Southern United States through Central America and as far south as Bolivia. It grows up to 37 meters high with a wide (3 meter) trunk diameter. The yellow flowers of *T. serratifolia* bloom during the dry season and the tree is known for its hardness (3684 lb on the Janka scale). It is commercially used for making beds, house posts, and building bridges.

2.3.2 Field Collection & Ring Width Measurements

In June, July and August of 2007, I collected over 250 tree samples (>800 kilograms total) from the Madre de Dios department in southeastern Peru. Because the majority of old growth tropical tree species are extremely hard, traditional coring methods proved impossible and stem disks or tree slabs were obtained instead. This sampling method enabled the entire circumference of the stem disk to be utilized during cross-dating, which minimized error associated with locally absent rings and indistinct tree ring boundaries. Stem disks were cut with a chainsaw between 1 and 3 meters up from the base of each tree, depending on the degree of buttressing and the amount of trunk material available. In the case of buttressing, we sampled above the buttress, where the trunk was more circular. Because entire stem disks were required, I adjusted my sampling strategy to utilize only trees that had already been cut down by logging mills or farmers living on the edge of the forest. This limitation favored a multi-species sampling approach as this enabled me to maximize the amount of same-species overlap between site locations.

In our laboratory at Duke, the tree samples were sawed, sanded, and polished up to 400 sand grit. In cases of extreme bowing or gradational offset, a mechanical planer was used on the sample prior to sanding. For each full stem disc, up to 4 radii were measured depending on the level of coherence between radii. In the case of slab samples (smaller sections of the stem disk), one to two radii were used. Multiple radii tracks enabled elimination of within-tree error due to locally absent rings. Each radii was measured along a straight line

approximately perpendicular to the ring boundaries. Tree ring boundaries were identified manually using a microscope and measured using a Velmex tree ring measuring system (Velmex Inc. Bloomfield, NY, USA) that is accurate to the .001 mm.

2.3.3 Data Analysis

Once the ring widths for each radii were entered into a spreadsheet, I used the quality control program COFECHA to detect regions of misalignment or low correlation between individual series (Holmes, 1983; Grissino-Mayer, 2001). This allowed me to reexamine radii for incorrect measurements, ring counting, or missing rings. COFECHA considers each series in 50 year segments and calculates the correlation of these segments with various points along the master chronology (the average of the remaining series). By sliding these segments along the master chronology, errors in measurements which may have caused a shift in the chronology (missing rings) can be detected. If a higher correlation value is calculated for a position other than the dated position of the series, the radii are reexamined and a correction is made.

In order to calculate a master chronology, non-climatic trends were removed from the individual tree series. These non-climatic trends may be due to tree geometry (a larger tree circumference will result in a thinner ring width to distribute an equal amount of material around a trunk), physiology (in some species juvenile trees grow faster than adults), and ecology (changes in site conditions, e.g. stand competition and disturbance). The method of removing

these non-climatic trends or so-called 'noise' is referred to as standardization. While traditional standardization methods have used simple linear regressions or negative exponential curves (Fritz, et al., 1969) for semiarid sites (e.g. Southwestern United States), closed-canopy forest dynamics can be much more complex requiring additional detrending methods (Cook and Peters, 1980). The conventional method used in closed-canopy stands is the cubic smoothing spline, and I applied this detrending method here. The smoothing spline is a curve made of cubic polynomial segments that have preset conditions around their inflection points. These conditions assume that the data contain experimental error and have continuous first and second derivatives. Following Reinsch (1967), the equation for the smoothing spline is as follows:

$$W = \beta X^2 + \int_{x_o}^{x} [f''(x)]^2 \, dx$$

where W is minimized and integrating the square of the second derivative quantifies spline curvature. χ^2 is a chi square test that measures how closely the spline function fits the given data:

$$X^2 = \sum_{i=0}^{n} \left[\frac{f(x_i) - y_i}{\sigma_i} \right]^2$$

where y_i is the measured tree ring series, n is the number of data points (rings) and σ is a predetermined weight (set to 1.0 (Cook and Peters, 1980)). The coefficient β is measured in the frequency domain (1/period, values 0-1) and

determines the relative stiffness of the spline. If $\beta = 0$, this eliminates the χ^2 value and the spline will become a straight line. If β is close to 1, this places a high emphasis on minimizing χ^2 and forces the spline to interpolate between every data point. The smoothing spline is applied to remove the complex ecological effects that can perturb tree ring growth in closed-canopy conditions and is utilized here only to remove the non-climatic anomalies that would otherwise be interpreted as extraordinary climatic events. Indeed, Cook and Peters (1980) assert that this spline should in fact be as stiff as possible yet still remove the variance that is not in common to all tree-ring series.

For each tree species, I applied the cubic smoothing spline over a range of flexibilities (5 to 80 year; β=.2-.0125) including no spline ($\beta = 0$) and calculated the effect of the removal of this variation on overall interseries correlation. The results of this analysis are given below (Figure 11). The spline rigidity that resulted in the highest interseries correlation was chosen as the standardization method for that species.

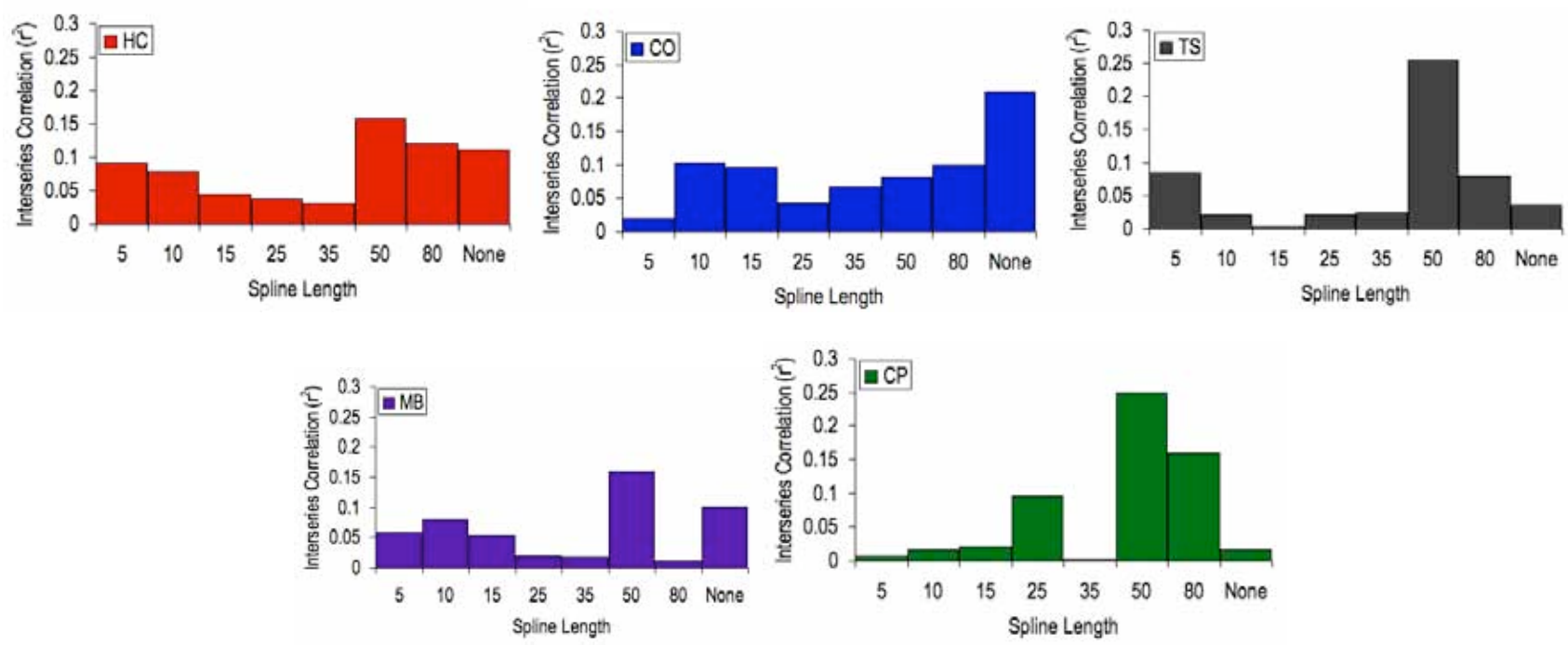

Figure 11. Interseries correlation results of the Spline Rigidity Analysis for each tree ring chronology. The spline length that resulted in the highest interseries correlation was chosen for each chronology. The resulting splines used are as follows: CO series received no spline detrending, HC, TS, MB, and CP series were detrended using a 50 year spline.

Once the standardization technique was chosen and the individual series corrected for any dating errors using COFECHA, a master chronology was developed for each of the 5 species examined. Using the program ARSTAN, the tree ring series were averaged together to create a master chronology for each species. Prior to this, however, the spline-detrended residual series were calculated by dividing each data point by the fitted spline value. This method prevented individual tree ring series with abnormally large ring widths or standard deviations from dominating the composite signal. The master chronologies developed for each of the 5 species, *M. balsamum* (MB), *C. pentandra* (CP), *H. courbaril* (HC), *C. odorata* (CO), and *T. serratifolia* (TS), were then normalized to a mean of zero and standard deviation of 1 to enable cross-species comparisons. The summary statistics for the composite chronologies are listed below (Table 6).

Table 6. Summary Statistics for the 5 chronologies from the program ARSTAN.

Species	Number of Trees	Time Span	Common Period	Mean Sample Segment Length	Standard Deviation	Skewness	Kurtosis	Mean Corr. of Radii with Chronology	Explained Var. PC1 (%)
TS - Tabuia serratifolia	7	1824-2006	1880-2006	151	0.23	1.24	2.44	0.36	29.52
HC - Hymenaea courbaril	6	1820-2006	1876-2006	154.67	0.36	0.34	0.76	0.50	35.68
CO - Cedrela odorata	5	1817-2006	1942-2006	108.5	0.64	2.69	10.32	0.47	36.83
CP - Ceiba pentandra	5	1819-2006	1927-2006	123.33	0.55	1.09	1.43	0.46	41.63
MB- Myroxylon balsamum	10	1836-2006	1914-2006	117.63	0.27	1.23	2.08	0.35	17.32

2.3.4 Data Uncertainty

To assess the relative uncertainty of the tree ring chronologies, I employed the expressed population signal (EPS) as a metric. Derived by Wigley et al. (1984), the EPS has been the standard method in dendrochronology used to assess how well a chronology of n ring width series represents the theoretical population signal. It is calculated as follows:

$$EPS = \frac{n(r_{between\ trees})}{[1 + (n-1)(r_{between\ trees})]}$$

where n is the number of ring width series used in chronology construction and r is the mean interseries correlation. Using the EPS, the Standard Error (SE) and Signal-to-Noise Ratio (SNR) are also calculated:

$$SE^2 = \frac{(1 - r_{between\ trees})}{n}$$

$$SNR \cong \frac{EPS}{1 - EPS}$$

The SNR can be used to compare the strength of the common variance signal in tree ring chronologies from various regions (Wigley et al., 1984). In the Southwestern USA for example, the SNR = 15 with an n = 10 series. As tree ring chronologies have not been developed for this region prior to this study, I report these values below, for comparison with other areas (Table 7).

As prescribed by Wigley et al. (1984), an EPS cutoff value of 0.85 is the convention for a statistically robust chronology. However, this threshold value is arbitrary and has been derived empirically from oak tree ring width data from 3 sites in England (K.R. Briffa and P.D. Jones). As stated by Wigley et al. (1984), the

threshold value should be chosen according to the accuracy needs of a given site. The so-called 'chronology uncertainty' should therefore simply be a much smaller value than the uncertainty that arises from the climate-chronology reconstruction. Based on this, the EPS threshold value should be much larger than the variance explained by climate, resulting in the smallest loss possible of explained climate variance due to chronologic uncertainty. As the largest variance explained by climate in my study is 36%, I find that an EPS value of 0.80 hypothetically reduces the explained climate variance from 36% to 28% (0.8 x 0.36). An EPS value of 0.85 reduces the explained variance from 36% to 30% (0.85 x 0.36). The loss of explained climate variance is not significantly different (30% versus 28%) for these two threshold values, therefore I choose an EPS value of 0.80 for these sites.

Table 7. Expressed Population Signal values for each of the 5 chronologies used in this study.

Species	Number of Trees (radii)	Expressed Population Signal (EPS)	Standard Error (SE)	Signal to Noise Ratio (SNR)
CO	5 (15)	0.84	0.04	5.32
TS	7 (16)	0.84	0.05	5.33
HC	6 (12)	0.60	0.08	1.48
CP	4 (16)	0.84	0.05	5.33
MB	8 (14)	0.71	0.07	2.47

2.4 Results

2.4.1 Ring Structure & Growth Behavior

Worbes (1995) defines four different types of tree ring structures: (1) density variations, (2) marginal parenchyma bands, (3) a repeating pattern of

alternating fibers and parenchyma bands, and (4) variations in vessel distribution and size. Density variations can be detected via X-ray densitometry to measure differences in density between the earlywood and latewood of trees. However, the complex nature of hardwood species is such that often the alternations of fibers, parenchyma bands, and vessels serves to muddle the density signal and wild variations in density can be detected intraannually (Worbes, 1995). I therefore did not employ this method for the detection of ring boundaries, relying instead on visual identification under the microscope.

There was some variation between the growth rings of individual species. *C. odorata* and *C. pentandra* both had easily identifiable and distinct ring boundaries, marked by clear marginal parenchyma (Figure 12). They are both type 2 species with clear marginal parenchyma banding. In *C. odorata* there was no consistent variation in vessel size or vessel density relative to the parenchyma band. In a number of the rings, *C. pentandra* showed a higher density of vessels near the latewood, though this was not a consistent finding throughout the rings. *T. serratifolia* showed a difference in vessel distribution (type 4) such that vessels were clustered in the middle of the ring. The beginning of each ring is marked by a region where vessels are completely absent. This created a color variation between rings that made identifying the ring boundaries easier. *M. balsamum* specimens also show this difference in vessel distribution. In *M. balsamum*, the beginning of the ring vessel is marked by an increase in vessel density and size followed by a decrease which is easily marked by a color change in the ring.

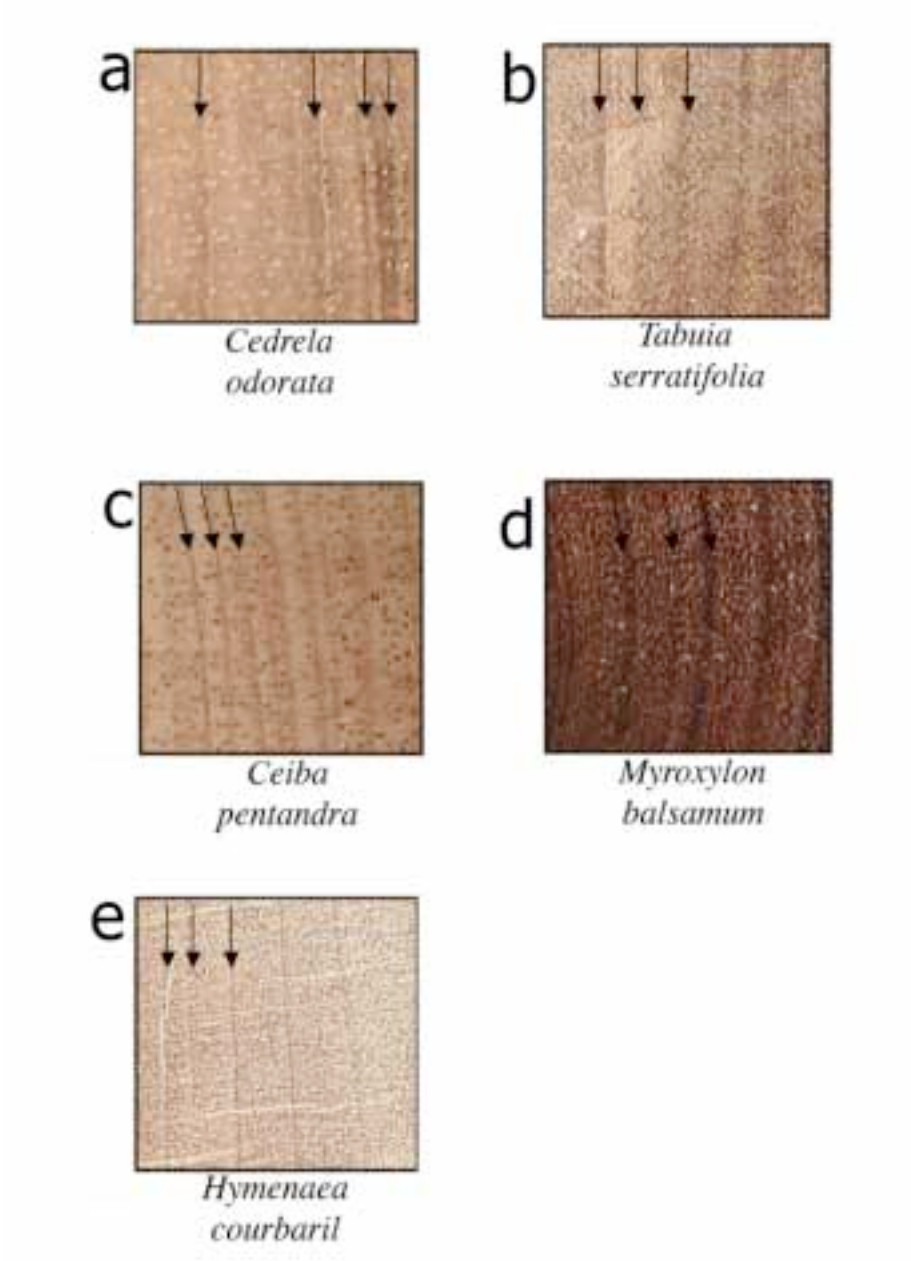

Figure 12. Ring structures for each of the five species examined in this study. Arrows mark ring boundaries, though only the first 3 rings are marked to show boundary. Growth direction is from left to right (i.e. pith to the left, bark to the right).

T. serratifolia and *M. balsamum* are both classified as type 4. *H. courbaril* is identified by a type 3 ring structure of alternating fibers and parenchyma bands. The parenchyma bands were sometimes difficult to identify as they became

progressively smaller towards the outer part of the tree. All 5 species showed false banding in places, and this was most difficult to identify in *M. balsamum*. Identification of false bands was done by examination of the entire circumference of the tree, or where appropriate, identification of the parenchyma.

The growth behaviors of each of the five species vary significantly. Based on raw averages of growth per year in each tree, I have compiled a growth anomaly index for each species. By taking the nth year of growth in each tree for a given species and averaging the ring width for that year, a growth rate may be calculated. I have subtracted the mean from the growth index and standardized the 5 species for interspecies comparison. Average growth rates and standard deviations are available in Table 8. *C. pentandra* on average has the largest growth rings (3.71 mm) and the largest variability of growth ring width between years (1.92). This is not surprising, given that this is a fast growing pioneer species. The two species with the lowest growth rates are *H. courbaril* and *T. serratifolia.* Both species also show the lowest standard deviation between years. *M. balsamum* and *C. odorata* show similar ring width averages and standard deviations, suggesting that their growth rates are similar on average. It is important to note that none of the trees used in this study are older than 150 years, though this is likely that due to logging pressures on these two species, such that the only trees still available are smaller, younger trees.

Table 8. Growth parameters for each of the 5 species based on ring counting and ring width measurements.

Species	Number of Trees	Average Age (Years)	Average Ring Width (mm)	Standard Deviation
Tabuia serratifolia	7	143.20	1.50	0.45
Hymenaea courbaril	6	126.25	1.48	0.67
Cedrela odorata	5	107.50	1.94	1.69
Ceiba pentandra	5	105.75	3.71	1.92
Myroxylon balsamum	10	111.30	1.99	0.70

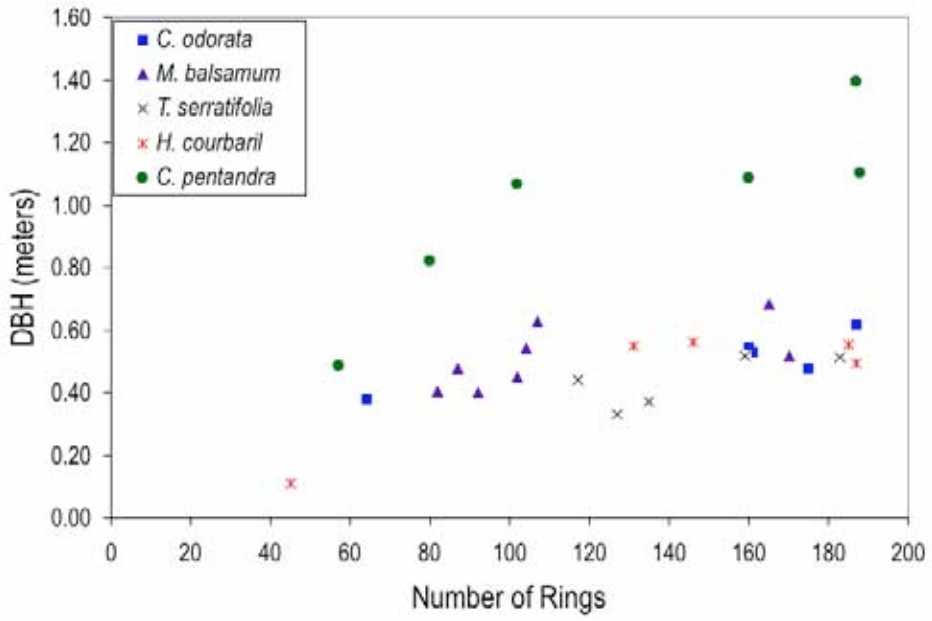

Figure 13. Diameter at Breast Height (DBH) versus the number of rings for each of the 5 species examined in this study.

The average growth trend in each of the 5 species varies from linear to exponential to polynomial (Figure 14). All of the species show a decline in growth rate with age, though this is also due to the geometry of the trees. *C. pentandra* shows a strong spurt in growth at the beginning of life and then exponentially declines with age. Both *C. pentandra* and *T. serratifolia* show a

higher variability in ring width in the early part of tree growth. In the case of *C. pentandra*, both ring width and standard deviation are much greater in this species than others, likely related to its behavior as a fast-growing pioneer in the forest. The species *T. serratifolia* and *C. odorata* both show roughly linear declines in growth rate such that as the trees age, their growth rates decline. *M. balsamum* shows a positive linear trend in growth up through ~50% of the lifetime of the tree before decreasing again in later life. *H. courbaril* does not show much change in growth behavior over time, showing a roughly linear pattern.

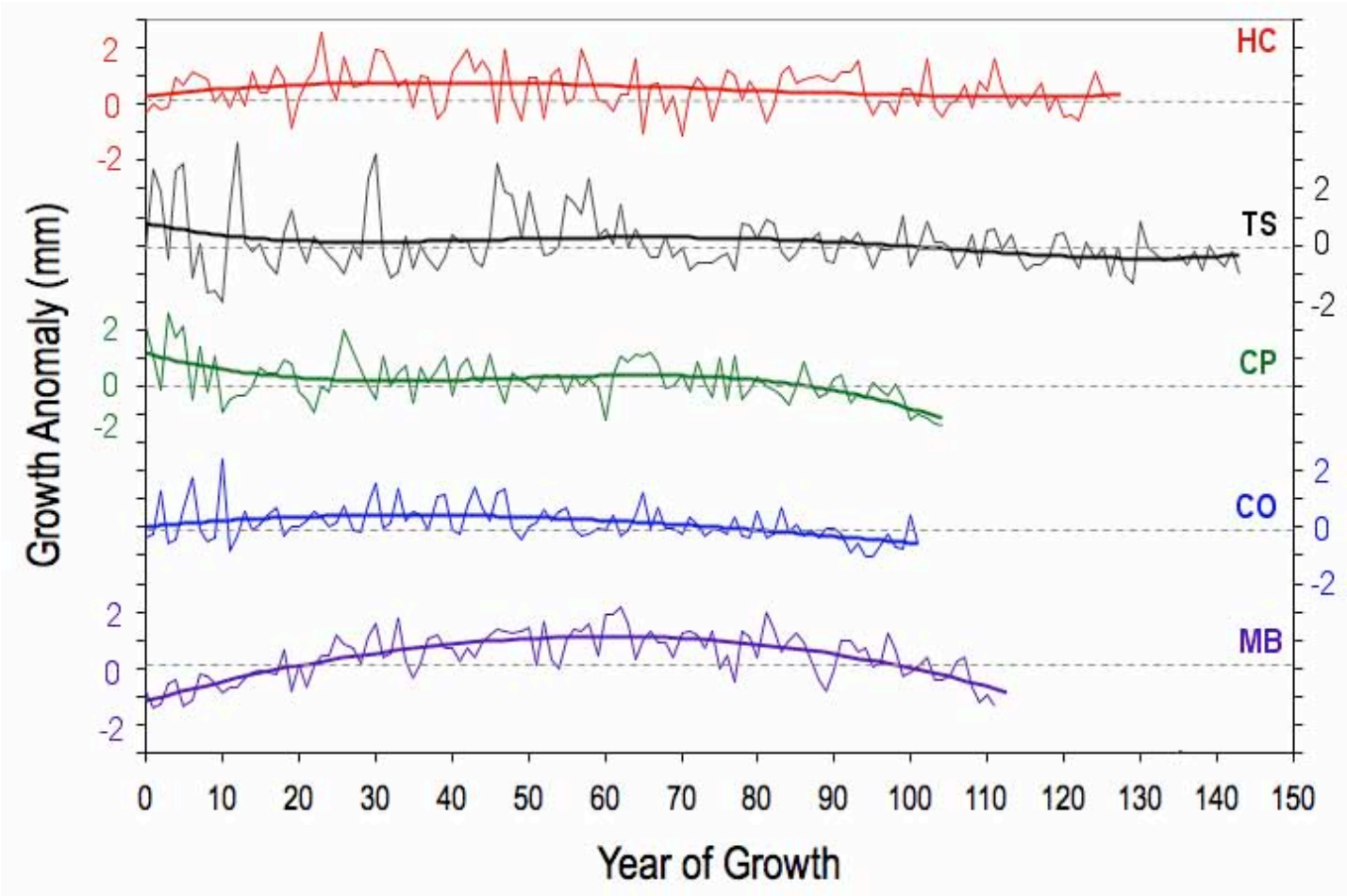

Figure 14. Growth rate anomalies for each of the 5 species examined in this study. Growth anomalies were computed by calculating the average rate of growth for each year of life for a given species. These rates were then subtracted from the mean to calculate the anomaly. A negative value in this case represents below average growth over the course of the life of the tree while a positive value represents above average growth.

2.4.2 Tree Ring Chronologies

There is a large degree of variability in the tree chronologies among trees of different species. Statistics for the 5 chronologies are listed in Table 6. HC shows the strongest correlation between ring width series and the first principle component of the series explains a significant portion of the variability (35.68%). Both *C. pentandra* and *C. odorata* also show a significant portion of the variance explained (41.63% and 36.83%, respectively). Though the tree ring chronologies are diverse, some long term trends are apparent and all of the chronologies show lower frequency trends (5 and 8 year frequencies). Some of these similarities are highlighted below (Figure 15). All 5 chronologies show a progressive decline in growth between ~2001-2006. *H. courbaril* and *C. odorata* show a spike of growth in 1996-1997. *C. pentandra, C. odorata, M. balsamum* and *H. courbaril* show a period increased growth around 1960. Between 1964 and 1968 is a low growth period for *C. pentandra, M. balsamum*, and *T. serratifolia*. All three of these chronologies also show a low period of growth in the early 1920's.

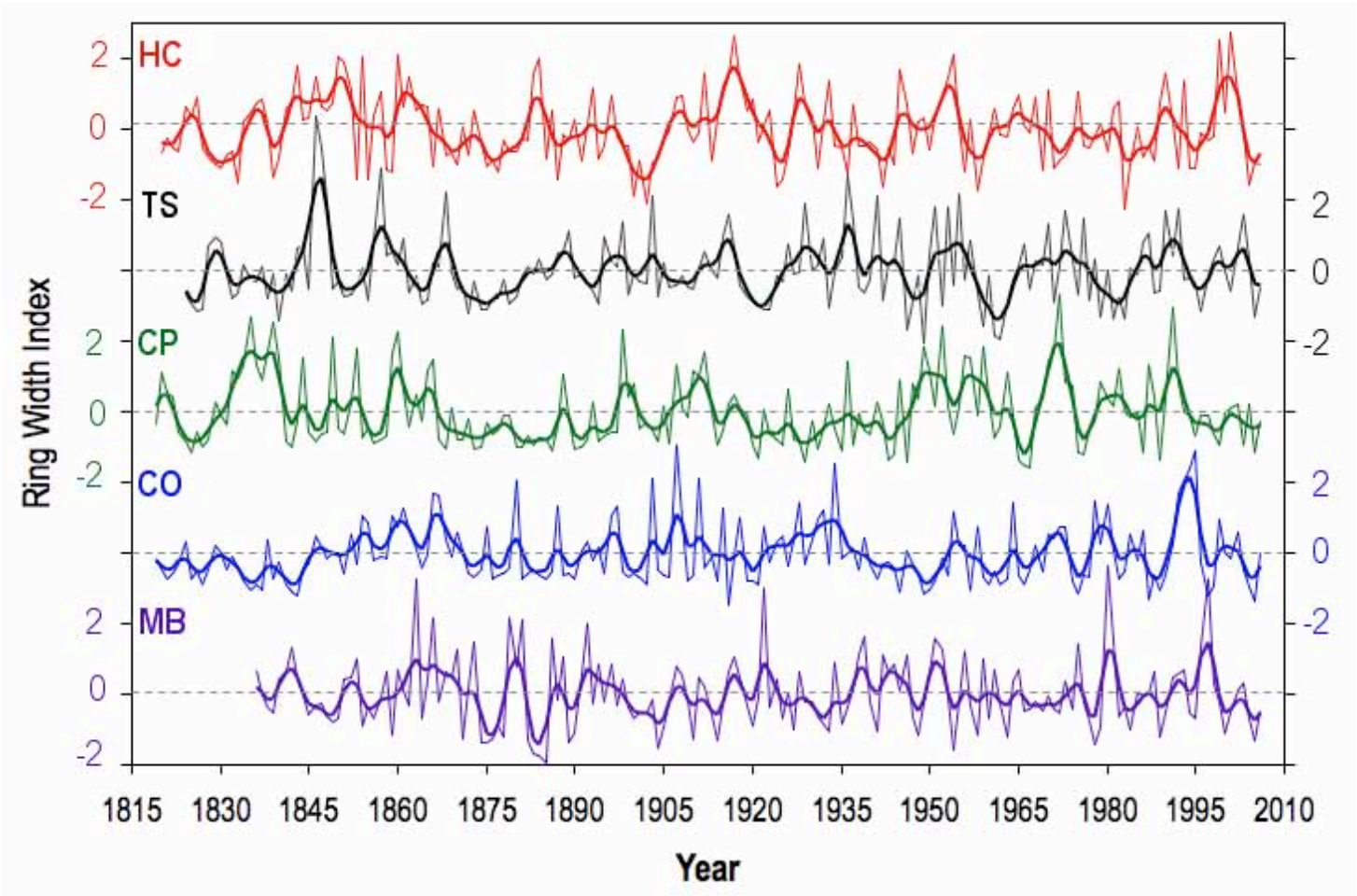

Figure 15. Standardized ring width indices for each of the 5 chronologies. Chronologies were compiled using the program ARSTAN where only the standard chronologies were used. Chronologies have been normalized to a mean of 0 and a standard deviation of 1 for interspecies comparisons. Bolded lines represent 5 year running means.

2.4.3 Response Functions

I compared each of the 5 chronologies to climate variables, precipitation and river discharge. Because temperature is near constant (26° +/- 1° C) between wet and dry seasons for this region, I did not consider this variable. To compare the tree ring chronologies with the remaining climate variables, however, I generated a series of correlation coefficients between each tree ring chronology and the given climate variable (e.g. monthly precipitation). This series of correlation coefficients collectively comprises a response function which identifies how the climate variable relates to tree growth. A sequence of monthly precipitation (discharge) values that begin many months prior to the current growing season of the tree are compared with the chronology and a series of correlation coefficients for each of these months is generated. This is done because the width of each tree ring may be influenced by processes extending beyond simply the current growing season (Fritz, 1976). In this study, I compare my chronologies with monthly precipitation and river discharge data over a period of 19 months beginning with the onset of the previous wet season (September) and extending through the current growing season (May). For precipitation data, total monthly values were computed (mm/month) and compared with the chronologies. River discharge values were calculated as monthly averages (m^3/sec).

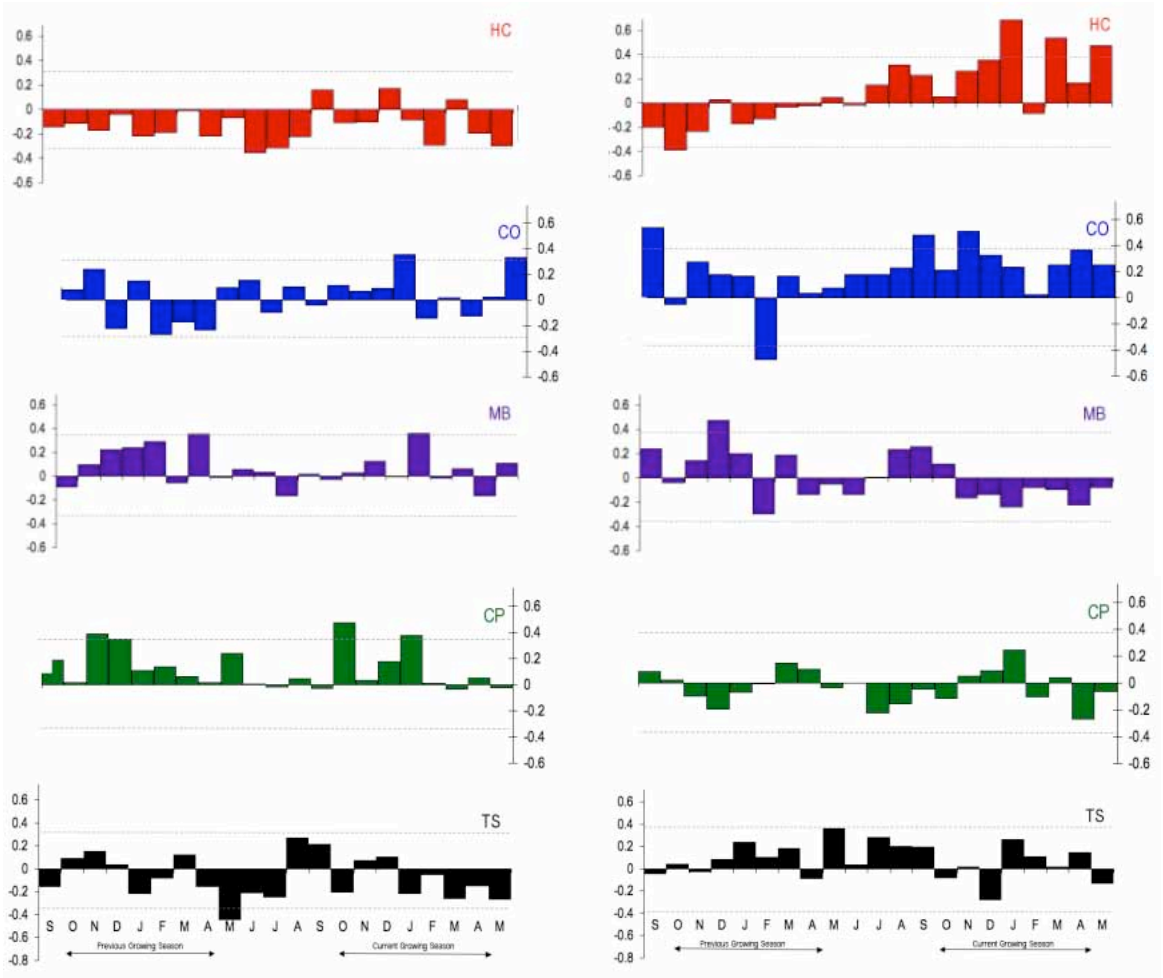

Figure 16. Response functions for each of the 5 chronologies. Correlation coefficients for precipitation are plotted on the left and correlation coefficients for river discharge are plotted on the right. Precipitation data come from the Puerto Maldonado meteorological station (1973-2006) and river discharge data come from the Rio Branco and Brasileia stations in Brazil (1973-2006, and 1984-2006, respectively). 95% significance levels plotted as dashed lines.

2.4.3.1 Ring-width and Rainfall

Two of the 5 chronologies (*C. odorata* and *C. pentandra*) show similar growth behaviors, with the majority of growth occurring during the early to middle part of the wet season (Figure 16). *C. odorata* and *C. pentandra* all show correlation with December precipitation. *C. pentandra* shows a positive

correlation with precipitation over both the previous and current wet seasons ($r = .39$, $p<.05$) from October through January. *C. odorata*, however, only shows significant correlation during December of the current growing season ($r = .40$, $p<.05$). *M. balsamum* shows correlation with March ($r = .38$, $p<.05$) of the previous growing season and January of the current season ($r = .39$, $p<.05$). The remaining two chronologies (*H. courbaril* and *T. serratifolia*) do not show any correlation with the growing season and instead show negative correlation with dry season precipitation, suggesting that in years when dry season precipitation is high, tree growth is low. *H. courbaril* shows a significant correlation with June and July precipitation ($r = -.35$ and $-.31$, respectively, $p<.05$) and TS shows negative correlation with May, June and July, though only correlation with May is statistically significant ($r = -.44$, $p<.05$). No species showed significant correlation with total annual precipitation.

Two of the 5 chronologies show correlation with total precipitation during portions of the wet season. In fact, correlations improve when the chronologies are compared with total rainfall from multiple months during the wet season, suggesting that tree growth is dependent on rainfall throughout the season. *C. pentandra* correlates with rainfall from October through January. The *C. odorata* chronology is correlated with rainfall sums from October through December (Figure 17). The *C. pentandra* chronology also shows a correlation with rainfall during the previous wet season as well, indicating a dependence on rainfall during multiple years. The *T. serratifolia* and *H. courbaril* chronologies do not show correlation with wet season rainfall during multiple months, however, they

both correlate with portions of the previous dry season (Table 9). This suggests the influence of dry season precipitation rather than wet season for these species. *M. balsamum* does not show significant correlation with any cluster of months throughout the year.

Table 9. Correlation coefficients of wet and dry season precipitation with each of the chronologies. All values reported are statistically significant at the 95% level (p<.05).

Chronology	Current Wet Season	Current Dry Season	Previous Wet Season	Previous Dry Season
CP	0.37 - Oct-Jan	--	0.36 - Nov-Dec	--
CO	0.42 - Oct-Dec	--	--	--
MB	--	--	--	--
HC	--	--	--	0.37 - May-Aug
TS	--	--	--	0.40 - May-July

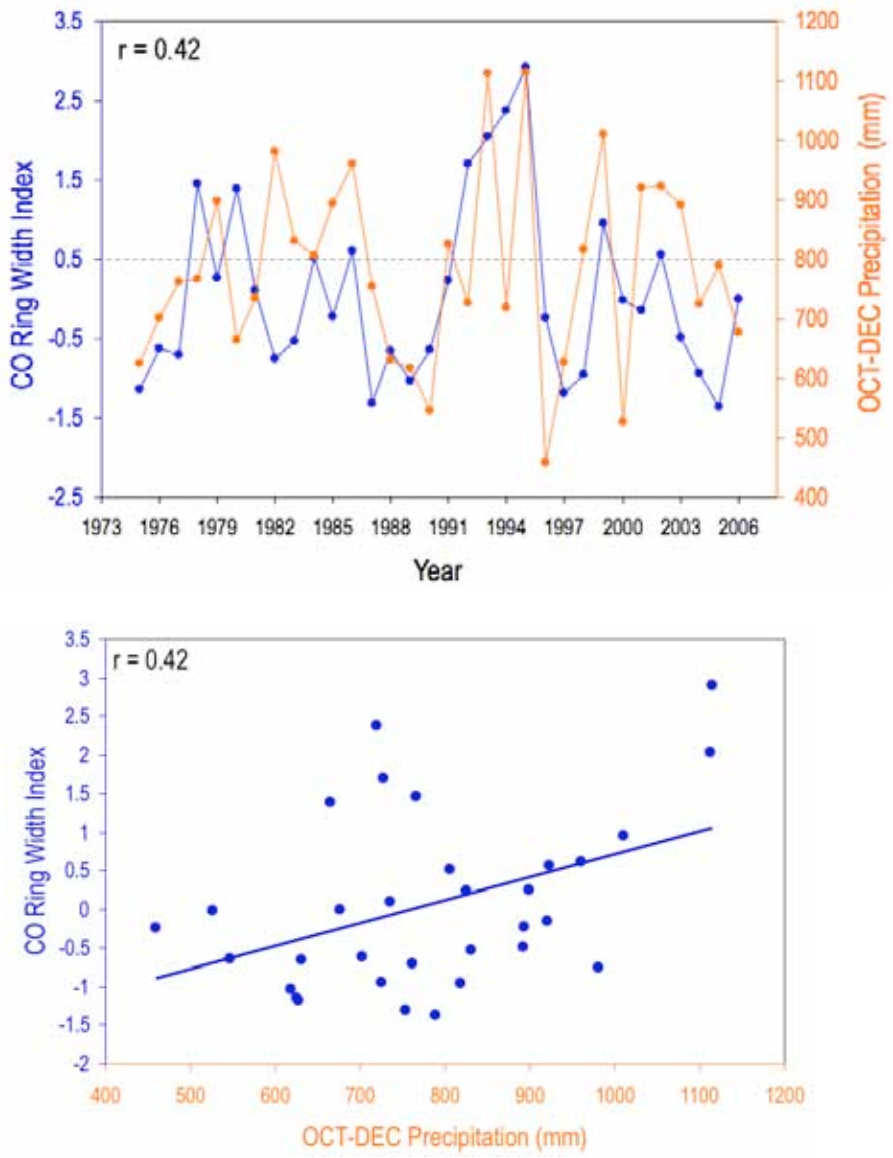

Figure 17. Top panel: the *C. odorata* chronology plotted against wet season precipitation during the months of October through December. Bottom panel: scatterplot of wet season precipitation against the *C. odorata* chronology.

2.4.3.2 Ring-width and River discharge

The *C. odorata* chronology shows significant correlation with discharge at the onset of the rainy season in September and November. *M. balsamum* is correlated with discharge during the month of December of the previous

growing season ($r = .47$, $p<.05$). *C. pentandra* does not reveal any significant correlation with river discharge, though the month of highest correlation ($r = .24$) is January. Both *H. courbaril* and *T. serratifolia* show correlation with discharge during the dry season (May) though *H. courbaril* also shows correlation with January and February of the rainy season ($r = .68$ and $.53$, respectively, $p<.05$) (Figure 18). *T. serratifolia* only shows correlation with the dry season, though this correlation is not statistically significant. None of the chronologies show a correlation with mean annual river discharge.

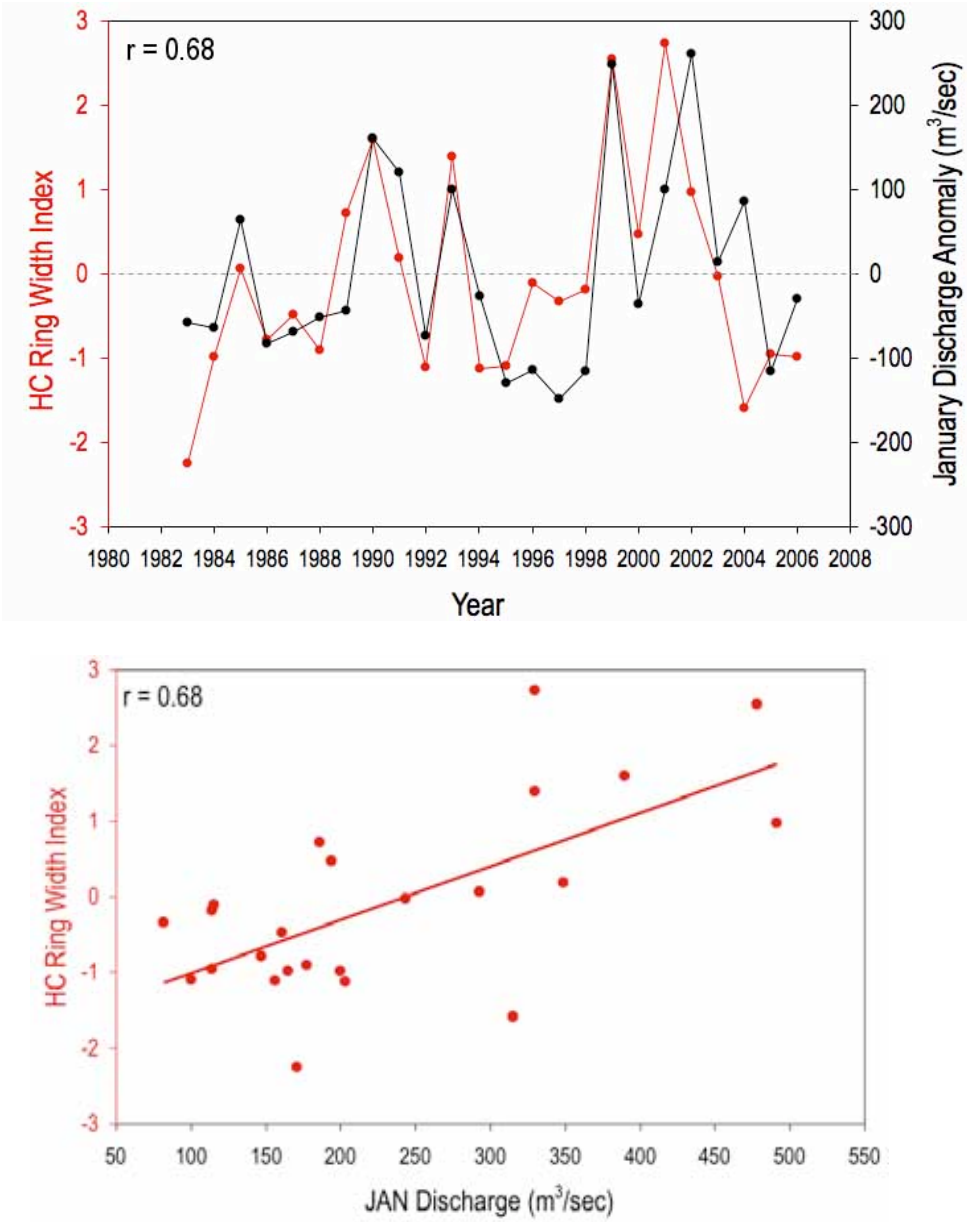

Figure 18. Top panel: plot of ring width for the *H. courbaril* chronology and January river discharge. Bottom panel: scatterplot of January river discharge against the *H. courbaril* chronology.

2.4.4 Analysis of Extreme Events

Because the *C. odorata* chronology shows a strong correlation (r=0.42, p<.05) with wet season precipitation, I examine extreme events within this record

over the last 124 years. I use a quantile method for this analysis where values that fall above the 80th percentile are considered extreme wet events and values that fall below the 20th percentile are droughts. The threshold values are calculated from the *C. odorata* chronology itself. These extreme events are referred to as 'wet' and 'dry' events, but it is important to note that this is not a quantitative reconstruction of the wet season precipitation index, rather an examination of these events based on the observed relationship between precipitation and ring width for this species. I then compare the extreme events with historic dry events that have been documented for the southern Amazon basin. These records are sparse and from diverse geographical locations across the basin, but give some measure of drought history over the last century (Table 10). The chronology identifies 9 periods of extreme low growth that correlate with known droughts that have occurred in the basin over the last century.

Twenty-four extreme dry events occur throughout the record with a mean recurrence interval of 8 years. Sixteen of these events are of duration 1 year, 3 of duration 2 year, 4 of duration 3 year and 1 of duration 4 year occurring between 1834-1837 (Figure 19). The 20th century shows more droughts than the 19th century with a mean recurrence interval of 6 years and a total of 16 dry events. The 19th century shows a mean recurrence interval of 10.5 years with a total of 8 dry events during this period. The longest period between drought events is 30 years and occurs between 1843 and 1873. The two most severe dry events occur in 2005 and 1916.

There are 29 extreme wet events that occur throughout the record with a mean recurrence interval of 6 years. Twenty-one of these events are of duration 1 year, 6 of duration 2 year, and 2 events of duration 4 years (1992-1995, and 1859-1862). There is a difference in the number of wet events in the 19th and 20th centuries, with the 20th century having 19 events and the 19th century only having 10 events. The mean recurrence interval for the 19th century is 8 years while the recurrence interval during the 20th century is 1 extreme wet event occurring every 5 years. The longest period between wet events lasts 20 years and occurs between 1834 and 1854, though there is also a 36 year period at the onset of the record where no extreme wet events are recorded.

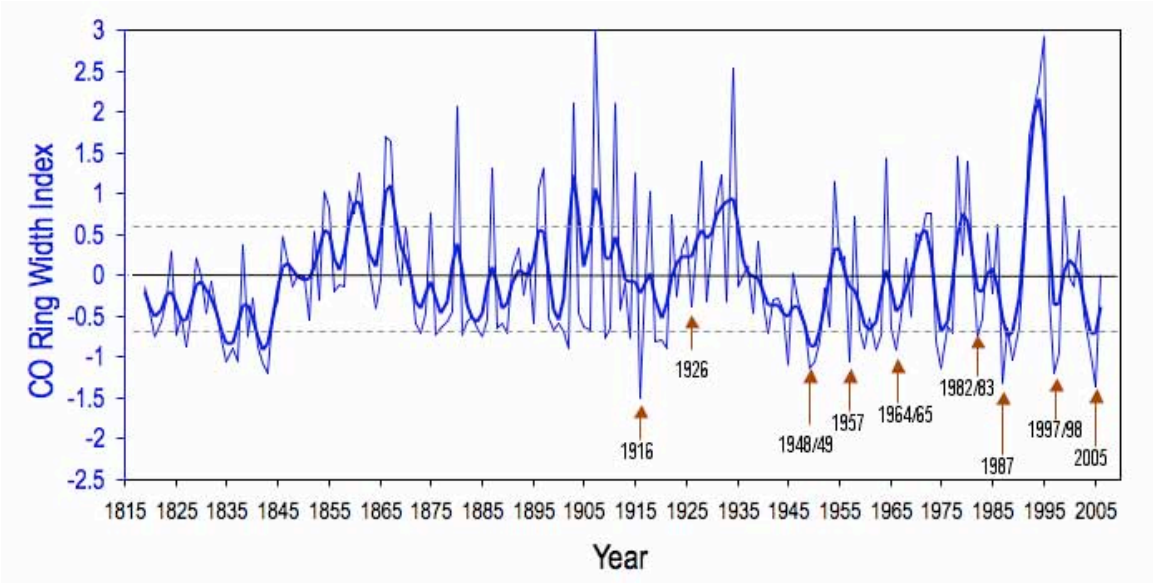

Figure 19. CO Tree Ring Chronology plotted with known Amazon basin drought events highlighted by brown arrows. Bold line is a 5-year running average. Gray dashed lines represent 20% and 80% percentile thresholds for extreme events.

Table 10. Table of historic droughts identified for the Amazon basin between 1900 and 2009.

YEAR	Drought Identified in the chronology	El Nino Year	Location	Measurement Used	REFERENCE
1906	No	Yes	Rio Negro, Manaus	ANA, PORTOBRAS River Discharge Data	Marengo et al., 2005
1912	No	Yes	Rio Negro, Manaus	ANA, PORTOBRAS River Discharge Data	Marengo et al., 2005
1916	Yes	No	Rio Negro, Manaus	ANA, PORTOBRAS River Discharge Data	Marengo et al., 2005
1925	Yes*	Yes	Rio Negro, Manaus	River Stage Height	William et al., 2005
1936	No	No	Manaus, Manicore	Rain Gauge Station Data (Interpolated)	Sternberg, 1968
1948	Yes	NO	Manaus	ANEEL Dataset	Sombroek, 2001
1957/58	Yes	No	Entire Basin	VIC Model with NCEP/NCAR Reanalysis	Sheffield et al., 2007
1964-1973	Yes	No	Southern Basin	Rainfall anomalies (-1 stdev)	Chen et al., 2002
1979-1981	No	No	Rio Branco, Brazil	River Discharge	Marengo et al., 2005
1982/83	Yes	Yes	Southern Basin	NCEP Reanalysis	Aceituno et al., 1988
1987	Yes	Yes	Rio Branco, Brazil	River Discharge	Marengo et al., 2005
1997/98	Yes	Yes	Southern Basin	NCEP Reanalysis CMAP	Nepstad et al., 1999 Xie and Arkin, 1997
2005	Yes	No	Southwestern Basin	CMAP NCEP Reanalysis River Discharge	Marengo et al., 2005

*Indicates drought is identified as a negative excursion in the reconstruction but does not fall below the 20th percentil cutoff.

2.5 Discussion

2.5.1 Droughts: The 20th Century

1926

1926 has been described by some as the greatest drought of the 20th century (Williams et al., 2005). Intense subsidence over the central Amazon basin as well as an anomalously northward displacement of the ITCZ over oceans suppressed rainfall in the western portion of the basin. This drought occurred during an El Nino year where anomalously warm SST's were observed in the eastern equatorial Pacific in 1925 and continued to increase until April of 1926 (Williams et al., 2005). An extreme effect on river stage height is evidenced by the measurements from the Rio Negro at Manaus, Brazil, implying a large reduction in rainfall. This reduced rainfall occurred as a direct result of the enhanced subsidence over the central Amazon, however it has been posited that rainfall was further suppressed by wide-spread forest fires. Numerous fires broke out in 1926. Knoch (1926) and Williams et al. (2005) speculate that the increase in smokiness due to the presence of aerosols may have suppressed the formation of cloud condensing nuclei. Discharge levels are estimated at 30-40% of the mean. The *C. odorata* chronology shows this year to have been an anomalously low growth year, although not extreme by the quantile definition.

1935/36 & 1948

These two droughts periods are both documented in river discharge data from the Rio Negro in Manaus, Brazil. The drought of 1936 falls lower than 1.5

standard deviations from the wet season mean. The drought of 1948 was less severe than the 1936 drought, showing a deviation of ~1 standard deviation below the mean value. Little is known about the climatic conditions of the two drought periods. They did not occur during El Nino years. The drought of 1948 is recorded in the tree ring record as a period of low growth which continued until 1949. The 1935/36 drought is not recorded in the record.

1964-1973

Chen et al. (2002) demonstrate a period of weak, but sustained below-average rainfall between 1964 and 1973 for the Amazon basin. This period was initiated by a drought in 1964 when anomalously warm tropical Atlantic SST's contributed to anomalous subsidence over the adjacent Amazond. Marengo et al. (2008) found subsidence anomalies over western Amazonia and upward motion over the central part of the basin. This is in contrast to the typical El Nino pattern where subsidence occurs over the central and eastern parts of the basin. In 1964, the strongest subsidence was observed over ~15°S between January and April. This is similar to that observed in the 2005 drought (Marengo et al., 2005). The *C. odorata* tree ring chronology records this period as a negative departure from the mean, though the most extreme events occur in 1964/65. River discharge from instrumental measurements (Rio Branco, Brazil) show below average values persist between 1965 and 1972. The *C. odorata* chronology shows abnormally low growth during this entire period. Growth returns to normal or above-average values by 1973.

El Nino Years: 1982/83, 1987/88, 1997/98

Previous studies have related drought in the Amazon basin with ENSO (Richey et al., 1989; Meggers, 1994; Fu et al., 1999; Liebmann and Marengo, 2001). Indeed, some of these studies have shown a relationship between circulation anomalies over the northern part of Amazonia related to strong El Nino (La Nina) events and a resulting lower (higher) than average rainfall. Examples of strong El Nino years are 1925/26, 1982/83 and 1987/88, and 1997/98. The latter 3 El Nino's have been characterized by weakened northeast trades over the tropical Atlantic and (for the northern Amazon basin) anomalous westerly flow along the equatorial Pacific (Marengo, 2004). Though the *C. odorata* chronology shows decreased growth during 3 of these strong El Nino droughts, there is not a consistent El Nino like periodicity to the record nor does ENSO correlate significantly with this record (r=0.10, Nino 3.4 and *C. odorata*). Marengo et al. (2004) note that more intense and frequent El Nino events occurred during the period between 1976 and 1998 than in earlier years (1940-1975), however they observe negative rainfall excursions in only the northern part of the basin, likely due to changes in surface circulation along the tropical Pacific and Atlantic. An increase in drought frequency or drought intensity is not observed during the 1976-1998 period in the *C. odorata* chronology. Rather, multiple wet events are observed in the early part of this period (1976-1980) and are consistent with warm surface water in the tropical Atlantic but not for the tropical Pacific (Marengo et al., 2004).

2005

The drought of 2005 was one of the most severe droughts of the previous century for the Amazon basin. Unlike in El Nino years when drought effects are concentrated in the northeast portion of the basin, this drought was most severe in the western and southern portions of the basin. Amazon river flow was below normal, the Amazon plume was reduced in aerial extent, and rainfall in the southern part of the basin was 39% of the normal average (Marengo et al., 2008). Air temperature was 3-5°C above normal and numerous forest fires broke out over the basin in the dry season of 2005. The drought developed in the hydrological wet season of 2004-2005 and extended through September of the dry season of 2005. During this period, equatorial Pacific surface waters had near normal SST's while the tropical North Atlantic experienced anomalously high SST's. This suggests the drought was linked not to a Pacific (El Nino) forcing, but rather to an Atlantic SST forcing. During both the onset and peak of the rainy season of 2005 (ONDJF) moisture transport from the tropical North Atlantic was suppressed. The North Atlantic subtropical high weakened and moved northward, the northeast trades weakened and the South American low level jet (SALLJ) showed abnormally low southerly flow anomalies (Marengo et al., 2008). The fact that the SALLJ was reduced demonstrates that the source of moisture loss was from the Atlantic as strong northeast trades are associated with low level flow into the Amazon basin. Marengo et al. (2008) note that no SALLJ events occurred at all during this season while the average number of events per

year is ~12. A SALLJ event is a local wind maximum identified at roughly 3 kilometers height over Santa Cruz, Bolivia, and is defined by several conditions; meridional winds more predominant than zonal winds, there is no northerly wind flow, near surface winds (925 hecta-pascals, hPa) are greater than 12 meters per second, and the wind flow difference between 950 hPa and 700 hPa must be at least 6 meters per second (Marengo et al., 2004). During El Nino drought related years, the number of SALLJ events is typically unaffected. The *C. odorata* chronology shows abnormally low growth for this year. Indeed, the trees show a decline in growth beginning in 2003 which continues to its lowest level in 2005. This is consistent with a drying over this region due to the warming of the subtropical North Atlantic during the same period.

2.5.2 Droughts: The 19th Century

There are a smaller number of extreme events during the 19th than during the 20th centuries in the *C. odorata* chronology. The mean recurrence of both wet and dry events was lower in the 19th century by ~25%. Also, low frequency variability (20-24 year) appears in this portion of the record that is not present during the 20th century. Indeed there is a period of above average growth that begins in 1845 and is sustained for almost 30 years. This is preceded by a period of below average growth from 1819-1840. However caution should be applied to interpretation of this portion of the early record as it is based on ring width measurements from only 3 trees.

2.5.3 Drought and Sea Surface Temperature

Roughly half of the 11 major droughts that have occurred in the Amazon basin over the last century have been associated with El Nino. However, an equal number of events occurred during non-El Nino years when equatorial Pacific temperatures were normal or even anomalously low. During 2005, the difference between the tropical North and South Atlantic sea surface temperatures was ~1.2°C. Several studies have invoked anomalous warming of the subtropical North Atlantic to explain this extreme drought (Zheng et al., 2008; Marengo et al., 2008). Near surface circulation and moisture transport from the tropical Atlantic were greatly reduced over southwestern Amazonia and weaker convection occurred over the region, resulting in greatly reduced rainfall. Furthermore, interdecadel variability in the SST's of the tropical Atlantic has been identified (Nobre and Shukla, 1996) and the steady increase in the SST's between 1995 and 2005 may be linked to the extreme nature of the 2005 drought (Marengo et al., 2008). However, the link between Atlantic tropical sea surface temperatures and Amazon drought frequency remains enigmatic due in part to the interaction between the Atlantic and Pacific as well as a poor understanding of drought behavior over the Amazon basin.

To examine the relationship between SST and drought over the Amazon basin, the SST anomalies from both the Atlantic and Pacific between were compared with the *C. odorata* ring width chronology. SST anomalies from a gridbox over the subtropical North Atlantic (5-20°North, 60-30°West) were

calculated between 1950 and 2009 using the observed Reynolds SST field (Reynolds and Smith, 1994). SST anomalies for the Pacific were calculated using Nino 3.4 (5° North-5° South, 170-120° West).

The *C. odorata* Chronology is equally well correlated with both the Atlantic and Pacific SST anomalies (r = -0.20) (Figure 20). Extreme warm anomalies in the Atlantic in 2005, 2003, 1987 are all associated with a corresponding decrease in growth. All three records align during 1950-1955, 1987, and 1996-1998. However, there are a few periods when the ring width chronology diverges from both SST records. The most notable difference occurs between 1974 and 1978 where the tree ring chronology shows a period of increased growth while anomalously warm waters are detected in both SST fields.

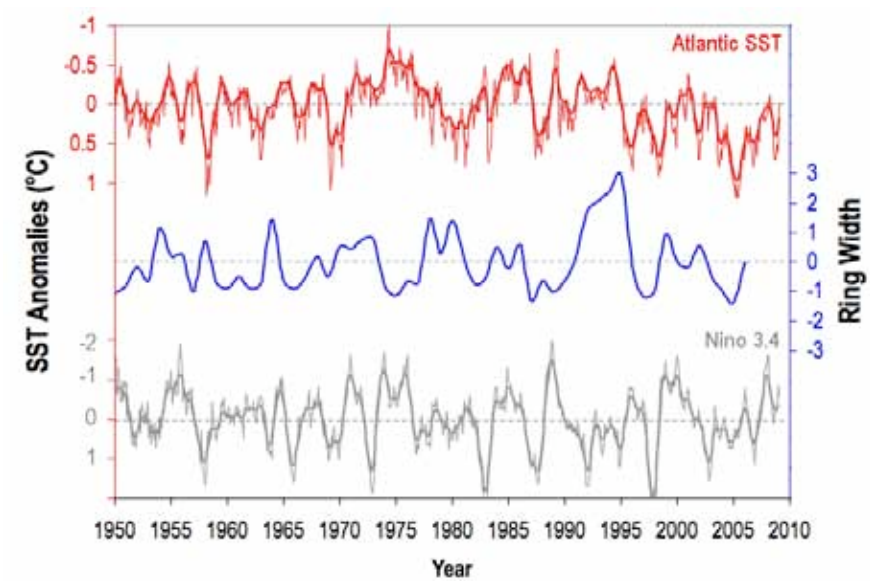

Figure 20. Pacific (gray) and Tropical North Atlantic (red) SST anomalies between 1950 and 2010 plotted against the *C. odorata* chronology. Pacific ocean anomalies are based on monthly averages from the Nino 3.4 index, Atlantic ocean SST anomalies are from a gridbox (5-20°North , 60-30°West) and are also plotted as monthly averages. 1 year smoothing means are applied to both of these datasets. SST anomalies are plotted on a reverse axis such that warm events are oriented down and cold events oriented up.

2.6 Conclusions

Growth behaviors and ring structures are investigated in 5 tree species from the Peruvian Amazon basin. These species show a variety of growth behaviors from negative linear to sinusoidal trends, though all species except *H. courbaril* do show a decline in growth rate with time. However, this pattern is also enhanced by the geometry of the trees. Ring structures are identified and clear enough to establish ring counting in each of these 5 species. From this ring counting, chronologies were developed and compared with climate variables of precipitation and river discharge.

Two of the five species (*T. serratifolia* and *M. balsamum*) did not show significant correlations with rainfall or river discharge. This may be explained by the timing of their growth. Flowering occurs during the dry season in *T. serratifolia* and just before the start of the rainy season for *M. balsamum*, suggesting that growth continues well through the length of the dry season. In general, tree ring growth in the other 3 species is well correlated with rainfall at the beginning to middle of the wet season but less well correlated with the late rainy season. It has been suggested that this decreased growth in the latter part of the rainy season may be due to a decrease in the photosynthetic capabilities of older leaves (Mooney et al., 1981; Brienen and Zuidema, 2005) or that this effect may be the result of a shift from active growth to storage during the latter part of the season (Iwasa and Cohen, 1989). It is also possible that heavy rainfall during the onset of the rainy season may saturate the soil horizon such that trees can

maintain positive growth rates regardless of the amount of rainfall through the remainder of the season (Brienen and Zuidema, 2005).

Growth behavior was significantly correlated with wet season precipitation and river discharge in 3 of the 5 species examined, with *H. courbaril* showing the most significant correlation with January discharge (r = 0.6). *C. odorata,* and *C. pentandra* both correlate well with total wet season precipitation, though peaks of growth correlated with individual months are detected in the response functions. The *C. odorata* tree ring chronology is most strongly correlated with wet season precipitation (r = 0.47) and a comparison of extreme events in this record with historic dry events of the Amazon basin reveals an accurate record of 9 of the 13 documented droughts of the 20th century. The 4 droughts that are not recorded in the chronology occur in 1906, 1912, 1936, and 1979-81. Three of these droughts (1906, 1912, 1936) are historically identified based on river discharge data from the Rio Negro (Manaus) and thus it is possible that the southwestern basin did not experience a strong drought during these years. The drought of 1979-81 is identified based on anomalously low discharge rates recorded on the Acre River in Rio Branco, Brazil, though this is not detected in the growth of the trees. The *C. odorata* chronology shows that there has been an increase in the number of both extreme wet and dry events since the turn of the century, with events showing a mean recurrence interval of 5-6 years during the 20th century. A comparison between Atlantic and Pacific SST's and the *C. odorata* chronology reveals that both basins have contributed to drought over the Amazon over the last century. This is corroborated by the fact that ~50% of the largest droughts recorded in the record coincided with El Nino

years while an equal number occured during non-El Nino years. While this chronology is only a preliminary indicator of the relationship between historic drought and tree growth, it is clear that variations in ring width correlate with changes in wet season precipitation. Both *Hymenaea courbaril* and *Cedrela odorata* show great promise as climate recorders for this region.

3. Assessing the Annual Nature of Tropical Tree Rings: A ^{14}C Study

3.1 Introduction

A pervasive view that annual rings do not form in tropical trees, in part due to the lack of appreciation that many tropical forests grow in regions with pronounced seasonality of precipitation, has contributed to a lack of information on both growth behavior and ring formation in many tropical tree species (Lang and Knight, 1983). Those researchers who have addressed this issue have applied a variety of methodologies (Worbes and Junk, 1989; Worbes et al., 2002; Westbrook et al., 2008; Verheyden et al., 2005). Worbes et al. (1995) used phenological characteristics such as leaf fall behavior combined with dendrometer measurements to determine the annual nature of tree rings in several species in the Caparo forest in Venezuela. Cambial wounding was developed by Mauriaux in 1967 to measure the rate of tree growth in real time. The wound causes a callous to form at the ring boundary, thus providing a marker from which to measure growth in future years. The method of cross-dating, widely used in temperate regions by matching trees of unknown date with trees of known date using a pattern of shared variability, has only recently been attempted in the tropics (Worbes et al., 2003; Argollo et al., 2004; Brienen and Zuidema, 2005).

An additional marker that can be used to measure growth in trees is the so called 'atomic weapon effect' (Worbes, 1995) that takes advantage of the increase

in atmospheric ^{14}C that occurred in the mid-20th century as a result of atmospheric testing of atomic bombs. During the 1960's, 404 aboveground nuclear explosions due to nuclear bomb testing nearly doubled the amount of ^{14}C in the troposphere (Nydal and Lovseth, 1970). In 1963, the Limited Test Ban Treaty was signed and many countries limited nuclear bomb testing to the underground arena only, though China continued atmospheric testing until 1980. Atmospheric ^{14}C has steadily declined due largely to uptake by the ocean and assimilation into plant biomass. The peak of this spike occurred in 1963 in the Northern Hemisphere and 1966 in the Southern Hemisphere (Hua and Barbetti, 2004). This effect is both delayed and diluted in the Southern Hemisphere because all bomb testing took place in the Northern Hemisphere. Trees growing during this time period record the bomb ^{14}C signal. By matching ^{14}C measurements in tree rings determined by ring counting with the ^{14}C measurements of the atmosphere, the annual nature of the tree rings can be confirmed or disproven.

In this study, I examine 2 tropical tree species using this ^{14}C method to determine whether or not their growth rings are annual. Samples from the two species, *Dipteryx micrantha* and *Cedrela odorata*, come from the Southwestern Amazon basin, in the Madre de Dios department of southeastern Peru. This is a region of strong precipitation seasonality. Here, the dry season (May – September) experiences an average of 75 millimeters of rain per month and the wet season (October – April) greater than 200 millimeters per month. Worbes (1995) has shown that regions with a dry season of at least two months duration

and less than 60 millimeters of rain per month are sufficiently seasonal to induce cambial dormancy, thus annual ring formation, in tropical trees. Both of these species possess distinct growth zones or banding which imply a period of growth alternating with a period of cambial dormancy. Previous studies strongly imply that *C. odorata* forms annual bands, although none of these studies employed ^{14}C dating to further test this inference (Brienen and Zuidema, 2005; Worbes, 2005). Annual ring structure has also been suggested in various members of the *Dipteryx* genus based on dendrographic measurements, but no detailed study has thus far been conducted on this member of the genus (Worbes, 1999). If the rings from these species can be confirmed to be annual, their utility as paleoclimatic indicators would be greatly enhanced.

3.2 Methods

Stem discs from 2 individual trees from *D. micrantha* and *C. odorata* were used in this study. Samples were collected from the Madre de Dios department of Southeastern Peru in the summer of 2007. Both samples were obtained from sawmills. The *C. odorata* sample was cut down 3 kilometers south of Puerto Maldonado and the *D. micrantha* tree was cut down ~5 kilometers southeast of Inapari, Peru. After cutting, polishing, and sanding each stem disc up to 400 sand grit, rings were identified visually using a microscope. After the rings were counted, approximately 8 samples were chosen from each tree at varying points believed to be between 1950 and 1975, on the basis of ring counting. Five to six milligrams of each sample were removed from the stem discs using a flat-cutting

non-electric rotary microtome and ground using a mortar and pestle. Samples were treated using the Modified DeVries Method (MDM, Hoper et al., 1998) for cellulose extraction and purification. For further details on the MDM, see Appendix I. Purified cellulose was diced and weighed into quartz test tubes, combined with a small amount of CuO and Ag, and sealed for combustion. Samples were baked at 900°C and combusted to form CO_2 gas. The samples were then combined with H_2 reducing the carbon to graphite using an Fe catalyst (Vogel et al., 1987). These graphite targets were used to measure $\Delta^{14}C$ values in accordance with Stuiver and Polach (1977). All samples were measured on the accelerated mass spectrometer at the Lawrence Livermore National Laboratories, CA. The error associated with each measurement is ~+/-5‰. Measurements are age-corrected using the methods of Stuiver and Polach (1977) and a background measurement of ^{14}C free coal is subtracted from the sample data. Correction for isotopic mass fractionation is made using the measured $\delta^{13}C$ value (in the case of *D. micrantha*) or an assumed value of $\delta^{13}C$ = -25‰ (in the case of *C. odorata*).

3.3 Results

Both trees clearly record the presence of elevated ^{14}C in their rings. The annual nature of the rings in *C. odorata* is clearly confirmed by the nearly perfect agreement with the known ^{14}C record (Figure 21). On the other hand, the *D. micrantha* tree shows significantly lower ^{14}C values than predicted (Figure 22). The only measured value in a ring that was elevated over the pre-bomb background occurs at the end of the sample period predicted to date 1972. This

value, 98.9‰, best fits the date of 1959, suggesting an undercount of rings by 13 years out of a total of 47 years (1959-2006).

An alternative possibility to an undercount is that the tree itself did not form an annual ring during 13 of the past 47 years. Missing rings are generally the result of two phenomena; stress and ring-wedging. Trees that live very near the environmental limit of their range may only form a partial ring during stressful years. Trees from the subalpine forests of New Zealand have been shown to form partial rings during relatively cool summers (Norton et al., 1987). If only a core sample is taken, these partial rings may be missed during ring counting. However, by obtaining cross-sectional discs of *D. micrantha* specimens, rings are unlikely to be missed due to an incomplete view of the trunk.

Another process that results in missing rings is ring-wedging, where rings form on only one side of the trunk for a period of time. This often occurs following the death of major branches and resulting variations in food and growth supplies. By again examining the complete cross-section of the tree, I am able to detect these regions and avoid missing rings due to wedging. I therefore believe that it is more likely that the rings has been miscounted due to their narrow width at the edge of the stem disk, and I present a method for correcting the tree-ring chronology based on this assumption.

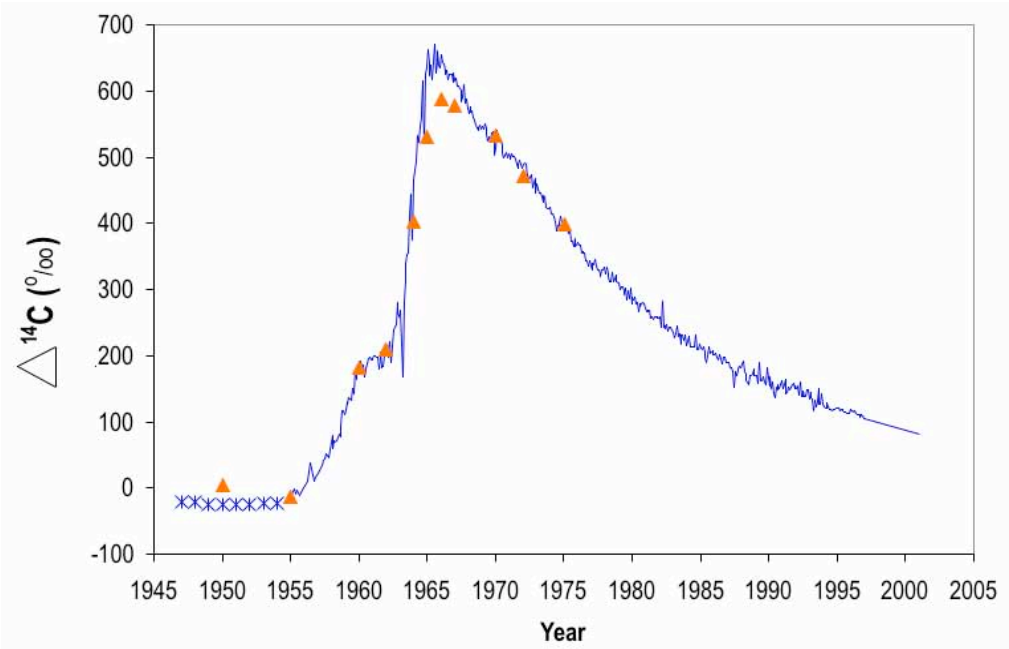

Figure 21. The blue line is a compilation of ^{14}C measurements from both tree rings and atmospheric measurements for the southern hemisphere (Hua and Barbetti, 2004). Stars are from a reconstruction of atmospheric ^{14}C based on two Douglas fir trees trees (Stuiver and Quay, 1999). The average value of ^{14}C between 1800 and 1935 is –4.99‰. Measurements for samples of the specimen of *C. odorata* in the present study are plotted in orange triangles.

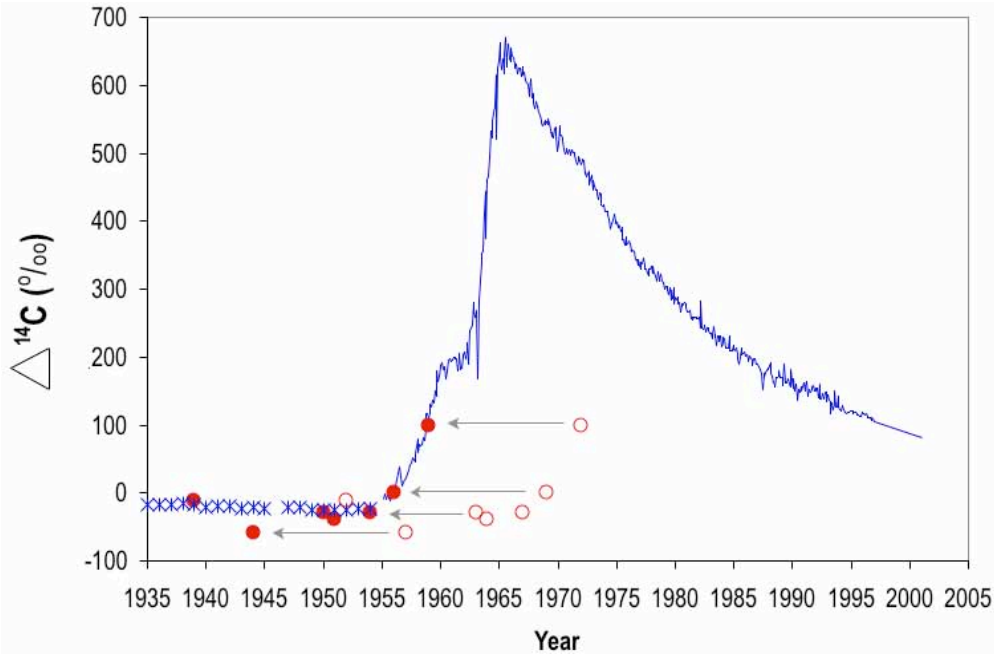

Figure 22. The blue line is a compilation of ^{14}C measurements from both tree rings and atmospheric measurements for the southern hemisphere (Hua and Barbetti, 2004). Stars are from a reconstruction of atmospheric ^{14}C based on two Douglas fir trees trees (Stuiver and Quay, 1999). Open circles represent *D. micrantha* samples using predicted years based on ring counting. Closed circles represent *D. micrantha* data adjusted to the bombed ^{14}C curve.

3.3.1 Corrected Tree Ring Chronology

Because bomb ^{14}C is detected in the trees rings of *D. micrantha*, the predicted chronology based on ring counting can be corrected by matching the *D. micrantha* data to the ^{14}C bomb curve. By fitting the tree ring radiocarbon measurements to the bomb ^{14}C curve, an offset of 13 years is determined. This suggests that 13 rings are either missing from this tree or have been miscounted on the stem disc. When the chronology is adjusted to account for these 13 missing rings, the radiocarbon present in the tree matches that of the bomb ^{14}C spike.

3.4 Discussion

Based on the results of this analysis, tree species *C. odorata* shows the clear formation of annual rings that can be counted accurately and dated. This is in large part due to the clear structure of the rings in *C. odorata* making them easily identifiable, despite relatively low rates of growth. It is clear that this species can be successfully dated for use in dendroclimatic and dendrochronologic reconstructions and such an application was previously employed in Chapter 2.

On the other hand, ring counting did not result in an accurate prediction of age in the *D. micrantha* specimen. Only 34 rings were counted over the period 1959-2006, suggesting that 13 rings were either missing or did not form in this tree between 1959 and 2006. There are several possible explanations for this result. One possibility is that, because the ring boundaries are continuous and gradational rather than discrete, smaller rings are not detected visually and therefore were missed in the ring counting process. Verheyden et al. (2006) found that annual ring boundaries defined by changes in vessel density in Kenyan mangroves became difficult to detect visually in trees with growth rates of <0.5 mm per year. In fact, trees with slow growth rates on average showed fewer rings than years (Verheyden et al., 2006). Because the transition between growth zones in *D. micrantha* is dependent on a gradational shift between high and low vessel density, a slow growth rate blurs the visual distinction between the two, and rings can be missed altogether.

Furthermore, the growth rate of a *D. micrantha* tree declines with age, such that older trees produce narrower growth zones (<1mm) on average than

younger trees (Figure 23). This pattern is partly enhanced due to the geometry of the tree, such that a larger tree circumference requires a thinner ring width to distribute an equal amount of material around a trunk than does a smaller tree circumference. Comparing the growth rates in five *D. micrantha* trees by counting their growth zones from pith to bark reveals a decrease of extension rate with age (Figure 24). The variability between growth curves for individual trees may be explained by tree-specific effects such as nutrient supply, light availability, and stand competition. However, an emergent pattern present in all 5 trees is a general decline in growth rate with age. The average growth in a tree after its 300th ring is ~0.86 mm, while the average growth rate in the first 100 rings is ~2.77 mm. Rings that form in later/outer years of an older tree are thinner and much more difficult to detect than rings that form near the pith where the tree is younger (Figure 25).

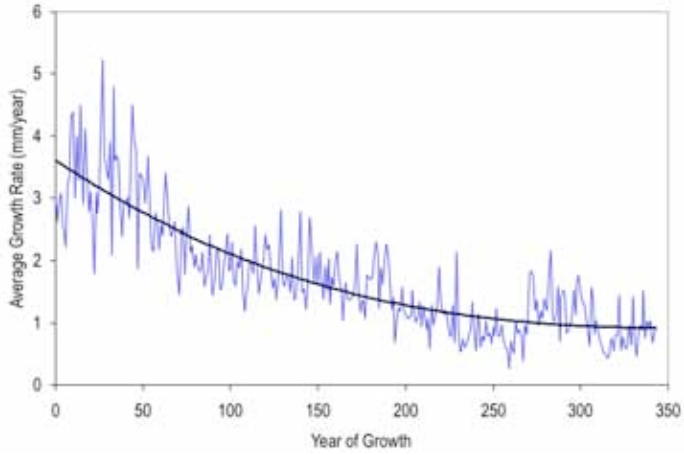

Figure 23. Average growth rate for the 5 *D. micrantha* trees examined in this study. Year of growth is calculated based on the number of rings, assuming that 1 ring = 1 year.

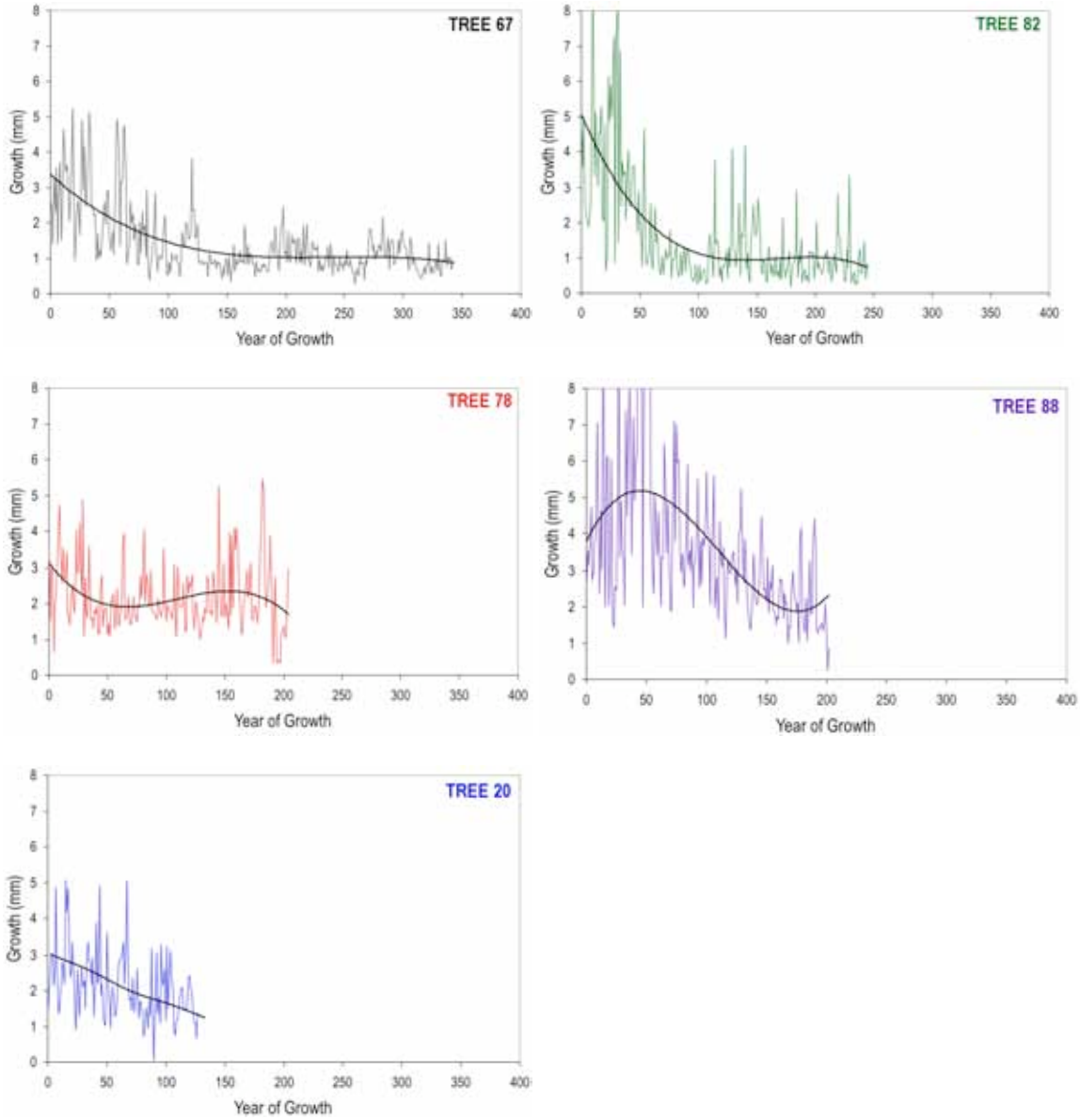

Figure 24. Growth Curves for each of the 5 trees examined in this study. They are plotted from oldest (i.e. greatest number of rings) to youngest (fewest rings).

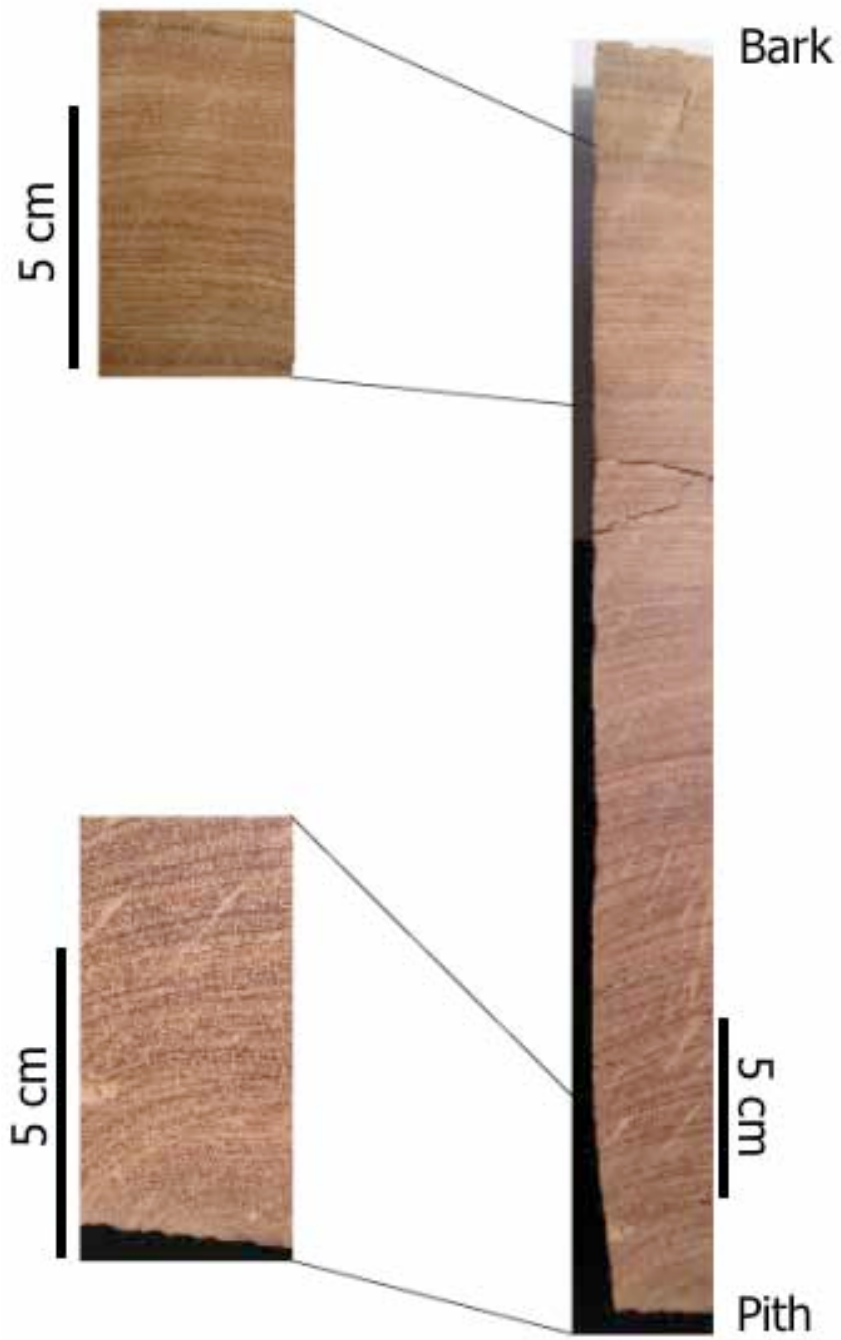

Figure 25. Photograph of ring structures in *D. micrantha* from pith to bark.

The tree samples used in the bomb ^{14}C measurements came from a specimen of *D. micrantha* (Specimen 67) with 343 counted growth rings. This tree is the oldest sample used in this study, thus, shows the narrowest growth rings during the 'atomic weapon effect' period. It is therefore likely that the gradational nature of the ring boundaries in this species prevented a visual detection of small (<0.5mm) rings that formed in the last 50 years of tree life. This is the most parsimonious explanation for the offset detected in the ^{14}C measurements, implying that rings were missed due to their miniscule size.

Another interpretation of the ^{14}C offset observed in this species could be that these rings are not annual at all and that cambial dormancy is linked to something other than the seasonality of precipitation in this region. This interpretation would demand that no tree rings were missed in the identification of ring boundaries and that fewer than 1 ring forms per year (such that 34 rings formed in 47 years as identified by the ^{14}C measurements). Periods of cambial growth and dormancy are the physiological behaviors that result in tree ring formation. During xylogenesis, cells erupt from the cambial layer, mature, produce secondary cells walls, and eventually lyse becoming passive water transporters. In deciduous species, the timing of xylogenesis mirrors that of shoot and leaf activity, such that cell eruption begins just before budding and continues until just after full leaf expansion. *D. micrantha* is a deciduous tree species and budding occurs at the onset of the wet season (Cintra, 1997). If the growth zones that form in the tree were not related to the annual cycle, a

disconnect is required between budding and leaf fall behavior and that of wood growth.

In some species, multiple leaf flushings occur each year leading to multiple rings within a single year (Worbes, 1989; Ng 1988). However, the formation of these rings is still tied to the leaf-fall behavior of the tree, and *D. micrantha* shows no evidence of multiple leaf flushings within 1 year (Cintra, 1997). False rings can form within a given year thus muddling the relationship between the growth zone and the annual cycle. Villalba and Veblen (1996) found false rings in *Austrocedrus chilensis* due to drought-like conditions that result in false latewood bands during the rainy season in Argentina. Cherubini et al. (2003) note the Mediteranean 'double stress' effect that can produce multiple rings per year due to decreased winter temperatures in addition to strong summer drought conditions. However, the accidental assignment of false rings as true annual rings would result in a prediction of more rings than actual years, while the opposite is true for *D. micrantha*.

What environmental factors are strong enough to both overwhelm the seasonal cycle of precipitation and disjoint the relationship between leaf fall behavior and wood growth? This factor must cyclically create favorable and unfavorable conditions for growth and it must operate on a time scale that is greater than 1 year. Worbes (1995) identifies three factors that can influence cambial dormancy in the tropics; precipitation, temperature, and flooding.

In Malaysian Borneo, dipterocarp trees were found to form 1 ring approximately every two years, though this pattern is consistent with the leaf

flushing behavior of the trees, which can take up to 2 years in mature trees (Ng, 1988). Additionally, this region does not show any climatic seasonality, and Jacoby (1989) point out that absence of seasonality is the main reason for poorly defined or non-existent annual growth rings in tropical trees.

Temperature remains roughly constant in this region (26°C +/- 1°C), making this environmental variable an unlikely candidate. However, exceptionally cold nighttime temperatures can occur during the dry season, when a dramatic change in wind currents brings cold Patagonian air northward into the Peruvian Amazon. This friaje or 'cold surge' occurs when a cold core high-pressure center moves from the Pacific ocean onto the southern tip of South America (Marengo, 1984). Over Amazonia, there is an increase in surface pressure and strong southerly winds can reduce nighttime temperatures to 5°C (Garreaud, 1999). A friaje is a short-lived event usually resulting in low nighttime temperatures for 5-6 days (Marengo et al., 1997). Though these events can be frequent (up to 10 per season, Doan, 2004), they are too short-lived to induce complete cambial dormancy (Worbes, 1995). A sudden drop in temperature could result in the formation of a false-band, which occurs when growth is abruptly slowed or temporarily halted. However, because friajes occur during the dry season, the trees have already entered a dormant state, and growth is likely to be unaffected by a cold surge. Garreaud (1999) noted the cold core anticyclone responsible for the cold surge can also form during the austral summer (wet season). However, the deep thermal trough located over the central

part of the continent prevents the northward propagation of the anticyclone thus suppressing a cold surge during the wet season (Garreaud, 1999).

Flooding by large rivers in the tropics (Amazon and Rio Negro) has been observed to induce dormancy in some tree species (Worbes, 1985, 1989). When water floods the tree, the roots begin to suffer anoxia, growth is slowed, and cambial dormancy ensues. Inundation forests in the central Amazon can be flooded up to 3 meters for approximately 8-9 months of the year. Water level fluctuations of 15 meters occur on all tributaries of the Amazon and Negro rivers, but these fluctuations are closely linked to the annual cycle. Furthermore, the trees of *D. micrantha* collected for this study are located above the flood plain and do not experience significant periods of inundation. Thus, the cyclicity of flooding likely cannot explain the growth zones observed in the trees.

Given the strong seasonality of precipitation in this region, even in the most anomalous of years on record, precipitation seems the preferred explanation for inducing cambial dormancy and growth zone formation in *D. micrantha* trees. It thus seems most likely that the growth zones detected in the *D. micrantha* trees are annual and that some annual rings have simply not been identified in the region near the edge of the stem disc due to their narrow width and gradational ring boundaries. This type of error in ring counting has been identified previously using bomb ^{14}C measurements in numerous other tree species (Lisi et al., 2001; Worbes and Junk, 1989). For example, Worbes (1989) found that older specimens of the species *Quercus costaricensis* from Germany contained such narrow radial increments near the bark that the trees were

significantly older than the estimates made by ring counting. Likewise, Amazon floodplain species *Annona sp.*, *Pseudobombax munguba*, and *Sorocea duckei* were all age-corrected after ^{14}C dating revealed miscounting in all 3 species (Worbes and Junk, 1989). I therefore conclude that the growth zones apparent in *D. micrantha* trees are 1) annual in nature, 2) formed in response to the seasonality of precipitation, and 3) are undercounted, potentially, in exterior regions of older trees.

4. Identification of Decadal and Multidecadal Trends in Stable Isotopes from Tropical Tree Rings of the Madre de Dios, Peru

4.1 Introduction

Oxygen isotopic ratios in meteoric water have been utilized to reconstruct past climate with a particular emphasis on past temperatures derived from high latitude ice cores, corals, and high latitude tree rings (Becker et al., 1991; Epstein, 1995). Numerous studies have documented a relationship between the $\delta^{18}O$ of precipitation and the $\delta^{18}O$ of tree ring cellulose (Anderson et al., 1998; Roden et al., 2000; Saurer et al., 2000; McCarroll and Loader, 2002; Evans and Schrag, 2004; Poussart et al., 2004; Anchukaitis et al., 2008; Evans, 2008). Recent attention has been given to the value of oxygen isotopes as a precipitation proxy in the tropics, as the temperature-$\delta^{18}O$ correlation is not statistically significant at low latitudes (Dansgaard, 1964; Rozanski et al., 1993). Instead, the oxygen isotopic composition of tropical precipitation is inversely correlated with precipitation amount. This so called "amount effect" (Gat, 1996) is the process by which precipitation preferentially removes the heavier (^{18}O) isotope from a moisture-laden air mass, such that the remaining water vapor and subsequent rainout is depleted in ^{18}O. The $\delta^{18}O$ of tree cellulose has been modeled by Roden et al. (1999) as a function of source water $\delta^{18}O$ and leaf water $\delta^{18}O$. Evans and Schrag (2004) demonstrate that during the wet season in the tropics, the amount effect will dominate the isotopic signal of α-cellulose and thus produce isotopically light cellulose values. During the dry season, on the other hand,

evapotranspiration is increased due a reduction in humidity. Increased evaporation at the leaf site causes an enrichment of the heavy isotope (^{18}O) and an overall increase in leaf water $\delta^{18}O$, which is mirrored in the $\delta^{18}O$ value of tree cellulose. This relationship also holds true for variations on annual times scales, so that drier years will be recorded by higher $\delta^{18}O$ values and wetter years by lower $\delta^{18}O$ values in tree rings. Poussart et al. (2004) used this relationship to identify a shared pattern of interannual variability in the $\delta^{18}O$ of two Javanese teak trees and linked this pattern to climate in Indonesia. Despite poorly defined or nonexistent rings structures in several species, the seasonal cycle of $\delta^{18}O$ was detected allowing the construction of a chronology and comparison of isotope records between multiple trees. In northern Japan, Tsuji et al. (2006) showed that the $\delta^{18}O$ of spruce (*Picea jezoensis*) trees is well correlated with summertime precipitation. Miller et al. (2006) used the relationship between $\delta^{18}O$ precipitation and the $\delta^{18}O$ of the latewood cellulose from longleaf pine in Georgia to identify major Altantic hurricane events of the last century. Liu et al (2008) identified patterns in the East Asian summer monsoon (EASM) using $\delta^{18}O$ measurements in several Helan mountain tree species and showed an increase in precipitation, recorded in the $\delta^{18}O$ of tree rings, since 1970.

Carbon isotopes in tree rings have also been used in many studies both to reconstruct past climate and the history of atmospheric $\delta^{13}C$ (e.g. Leavitt and Long, 1991; Lipp and Trimborn, 1991; Leavitt, 1993; Robertson et al., 1997; Saurer et al., 1997; Helle et al., 2002). The $\delta^{13}C$ of cellulose is a measure of the $\delta^{13}C$ of the atmosphere and the ratio of intracellular to atmospheric partial pressure of CO_2

(Farquhar, 1989). The latter is mediated by rates of photosynthesis and stomatal conductance. Under dry conditions, stomatal conductance will decrease in an attempt to minimize water loss resulting in greater ^{13}C incorporation during CO_2 uptake and a resulting increase in the $\delta^{13}C$ value of tree cellulose. Under wet conditions, stomatal conductance will increase and a greater discrimination of ^{13}C in favor of ^{12}C will result in a decreased $\delta^{13}C$ value. Recently, Gebrekirstos et al (2009) found a synchronous pattern of interannual pattern of $\delta^{13}C$ of several deciduous tree species from Ethiopia and linked this pattern to precipitation. Roden and Ehleringer (2007) showed the $\delta^{13}C$ of latewood in Ponderosa pine from Arizona declined with increasing precipitation during the hydrological year. Skomarkova (2006) related the $\delta^{13}C$ of wood with mid-season climate conditions in stands of beech in Germany and Italy but noted a high variability between individual trees. Because the α-cellulose of tree rings records the environmental conditions during the period of ring formation, measurement of stable isotope ratios from tree rings are potentially valuable sources of paleoclimatic information.

Here I present oxygen and carbon isotopic records from five *Dipteryx micrantha* trees from southeastern Peru. These records span nearly the last 5 centuries, with the oldest tree reaching a maximum error adjusted age of 473 years. The variability between isotopic records of individual trees is compared and the influence of site-specific conditions is discussed. Both records are compared with precipitation and river discharge datasets for this region to assess the relationship between the isotopic proxy and climate. Multiple trees are

analyzed to determine the relative strength of this common signal across the region. A spectral analysis is used to identify periodicity within the isotope records from each of the five trees and significant peaks are compared with variability of known South American climate forcings.

4.2 Isotope Theory

4.2.1 Oxygen Isotopes

Meteoric water is incorporated into tree ring cellulose through a series of processes beginning with root uptake and transport through the xylem to the leaf surface. At the leaf surface, this water is used during photosynthesis to make carbohydrate. This carbohydrate is then transported as sucrose through the phloem to the vascular cambium (site of cellulose synthesis) where the sucrose is broken down and incorporated into a developing cell. The $\delta^{18}O$ value of cellulose is thus a mixture of the $\delta^{18}O$ of meteoric water incorporated through the roots and the $\delta^{18}O$ of leaf water used during photosynthesis. The $\delta^{18}O$ of cellulose can thus be represented by the following equation:

$$\delta^{18}O_{cellulose} = f_o(\delta^{18}O_{sw} + \varepsilon_o) + [(1 - f_o)(\delta^{18}O_{lw} + \varepsilon_o)]$$

where $\delta^{18}O_{sw}$ is the oxygen isotopic ratio of water in the xylem of tree rings and $\delta^{18}O_{lw}$ is the oxygen isotopic ratio of water in the leaves (Roden et al., 1999). f_o represents the proportion of carbon-bound oxygen that exchanges with the source water. Both water and carbon dioxide provide oxygen atoms to the tree during carbohydrate metabolism, however, only a portion of CO_2 molecules undergo complete isotopic exchange with this source water prior to carbohydrate

synthesis. This portion of carbon bound oxygen has been empirically derived to be 0.42 at varying levels of humidity (Roden et al., 1999). ε_o is the net biological fractionation of oxygen that occurs when mediating formation of cellulose from sucrose in the leaf. The $\delta^{18}O$ of cellulose is known to be enriched with respect to leaf water due to the carbonyl-water interaction during photosynthesis and ε_o is empirically estimated to be 27‰ (Sternberg and DeNiro, 1983).

The enrichment of $\delta^{18}O$ leaf water is greatly reduced in tropical forests due to a low vapor pressure deficit. Diffusion through the stomata creates an equilibrium exchange between atmospheric water vapor and water within the leaf and has been effectively modeled by Flanagan et al. (1999). However, Roden and Ehleringer (1999) have shown that at high rates of transpiration, unfractionated xylem water is advected into the leaf, counteracting the leaf water enrichment during evapotranspiration at the leaf site. During the rainy season, evapotranspiration decreases, and the effect of leaf water enrichment on $\delta^{18}O$ becomes negligible (Evans and Schrag, 2004).

4.2.2 Carbon Isotopes

A model for how carbon isotopes are fractionated once they enter the tree has been developed (Farquhar, 1984) and is now thought to be well understood. The carbon isotopic ratio of tree ring cellulose is controlled by the carbon isotopic composition of the atmosphere and the biotic fractionation factors mediated by photosynthesis and stomatal conductance. This is modeled (Farquhar et al., 1989) as follows:

$$\delta^{13}C_{plant} = \delta^{13}C_{atm} - a - (b - a)\frac{c_i}{c_a} + \varepsilon_c$$

where "a" is the fractionation during CO_2 diffusion into the leaf through the stomata (a ~ 4.4‰), "b" is the fractionation during the carboxylation of CO_2 by rubisco during photosynthesis (b ~ -27.7‰), and c_i/c_a represents the ratio of intracellular to atmospheric partial pressure of CO_2 (Francey and Farquhar, 1982). This ratio is a function of the stomatal conductance of the individual tree. ε_c is the enrichment fractionation of sucrose when it is converted into cellulose (ε_c ~ 3.5‰). Thus, the $\delta^{13}C$ of the plant is mainly a function of the difference between $\delta^{13}C$ in the atmosphere and the ratio of partial pressures of intracellular and atmospheric CO_2 and can be used to solve for this ratio.

This partial pressure ratio can be used as a measure of water use efficiency in the plant, by the equation:

$$E/A = \frac{c_i}{c_a}$$

where "A" refers to the amount of carbon assimilated into the plant, and "E" is the water lost due to transpiration during photosynthesis. Under dry conditions, stomatal conductance will decrease in an attempt to minimize water loss (E) and the ratio of c_i/c_a will go down. This results in less discrimination between ^{12}C and ^{13}C and a reduction in the difference between $\delta^{13}C$ of the atmosphere and that due to biotic factors. Thus, $\delta^{13}C$ is largely a measure of response of the plant to water availability (Farquhar, 1989) with $\delta^{13}C$ values expected to increase in the plant during dry periods.

4.3 Study Area

Five trees of the species *Dipteryx micrantha* were collected in the summer of 2007 from the Madre de Dios department of southeastern Peru. *D. micrantha* is a dense fabaceae with distinct growth bands, making it an ideal choice for annual ring sampling. However its density and hardness make *in-situ* tree coring impossible, instead stem discs from each tree were collected. The stem discs were only cut from trees that had already been cut down by logging mills or farmers living on the edge of the forest. Four of the five trees come from logging concessions in and around the town of Inapari, Peru (12°3′0S, 69°24′0W). The fifth tree was taken from a private farm located just outside Puerto Maldonado (12°35′0S, 69°14′0W).

The town of Inapari sits at 238 meters above sea level while Puerto Maldonado is only 183 meters altitude. However, the average annual temperature for both regions is 26° C with little seasonal variation (+/- 1° C). The seasonality of rainfall, however, is strong, with monthly rainfall averages of >200 mm during the wet season and <75 mm during the dry season. The rainy season runs from October through April where it is defined as monthly rainfall >100mm. The dry season runs from May through September. Average annual rainfall for the entire region is ~1740 mm.

4.4 Climate Datasets

I compare the isotopic data from the trees of the Madre de Dios with three different instrumental datasets of precipitation and river discharge. The two precipitation datasets used in this study come from the Observational (OBS)

dataset from the Puerto Maldonado meteorological station and the Global Precipitation Climatology Center's (GPCC) rain gauge only 0.25°x0.25° resolution gridded dataset. Total wet season precipitation anomalies from October to April are computed for each year and compared with the isotope records. The PEM dataset spans 32 years from 1974-2006 and the GPCC dataset spans 36 years from 1970-2006. River discharge data come from the RIVDIS dataset. Because discharge measurements are in m^3/sec, average wet season anomalies are computed. Discharge data span 38 years from 1968-2006.

4.5 Materials & Methods

4.5.1 Laboratory Preparation

Tree samples were sawed, sanded and polished up to 400 sand grit and the rings were counted and measured on a Velmex measuring system. Once the rings were identified, samples from each ring were manually removed for isotope analysis using a non-electric flat-cutting rotary microtome. Samples were cut into sections and then sliced in 20 micron increments prior to powdering. The microtome blade was cleaned in ethanol between each sample. A coffee grinder followed by mortar and pestle were used to finely powder the sample prior to chemical extraction for α-cellulose.

Though it contains cellulose, bulk wood is composed of a variety of other compounds whose isotopic signatures do not remain fixed in time, making them unhelpful as environmental or climatic indicators. The Brendel method was developed by Brendel and colleagues in 2000 as a rapid way to process bulk

wood and remove these amorphous compounds, thus leaving pure α-cellulose for isotopic analysis. In this study, all samples were processed using the Modified Brendel Method which uses an acetic and nitric acid mixture followed by an NaOH rinse. For an evaluation and more detail on this extraction method, see Chapter 1 and Appendix I.

4.5.2 Isotope Analysis

One to two milligrams of α-cellulose were extracted from the tree rings of each of the five trees. Where possible, additional material was sampled for duplicate analyses. Both carbon and oxygen isotopic values are recorded for samples in all five trees. All isotope data are expressed using standard deltaic notation where

$$\delta^{18}O = \frac{\left(\frac{^{18}O}{^{16}O}\right)_{sample} - \left(\frac{^{18}O}{^{16}O}\right)_{standard}}{\left(\frac{^{18}O}{^{16}O}\right)_{standard}} \; x\ 1000$$

and

$$\delta^{13}C = \frac{\left(\frac{^{13}C}{^{12}C}\right)_{sample} - \left(\frac{^{13}C}{^{12}C}\right)_{standard}}{\left(\frac{^{13}C}{^{12}C}\right)_{standard}} \; x\ 1000$$

The values for both $\delta^{18}O$ and $\delta^{13}C$ are measured in parts per thousand (‰) or per mil. The standard for $\delta^{13}C$ measurements is the Vienna Peedee Belemnite (VPDB) and the standard for $\delta^{18}O$ is the Vienna Standard Mean Ocean Water (VSMOW).

Carbon isotopic measurements were made at the Duke University Environmental Stable Isotope Laboratory using a Finnigan MAT Delta Plus XL continuous flow mass spectrometer system interfaced with a thermochemical elemental analyzer. $\delta^{13}C$ samples (~1000 μg) were packed into tin capsules and thermally combusted to produce CO. Internal standards of *Duke sucrose*, *Duke cellulose* and *COSTECH Actenalide* are used to correct for the normal daily changes in instrument environment and parameters as well as any standard gas drift. For $\delta^{13}C$ values, internal standards are calibrated against NIST / IAEA Reference Material *NBS-22*, *Sucrose ANU*, and *PERFl foil*. Precision for $\delta^{13}C$ values is +/- 0.2 ‰.

Oxygen isotopic measurements were made at the University of Arizona's Mass Spectrometry Laboratory run by Professor Michael N. Evans. $\delta^{18}O$ samples (~550 μg) were packed into silver capsules and converted to CO in a Costech High Temperature Generator/Elemental Combustion System (HTG/ECS) and measured for their isotopic content. The HTG has a radio frequency of 1 Mhz that heats the reactor up to 1400+ °C in ~35 seconds. The reactor itself was designed by Evans (2008) and is composed of a quartz outer tube, boron nitride spacers, and a molybdenum foil crucible which work together to minimize the blank CO signal. All measurements were made on a Thermofinnigan Delta Plus XP with Conflo III continuous flow interface. Duplicate analyses results showed a mean error of less than .2‰ for $\delta^{13}C$ measurements and ~.3‰ for $\delta^{18}O$.

4.5.3 Establishing the chronology

The oldest of the five *Dipteryx micrantha* trees has been dated using the bomb ^{14}C signal. The analysis revealed that the growth rings are most likely annual and that they always form in response to the seasonal cycle of precipitation, but the ring boundaries are not always discrete or easily discernable, thus errors in ring counting occur especially low growth rates (see Chapter 3). It is therefore necessary to account for the error associated with ring counting. Typically this error is eliminated using cross-dating methods via programs like COFECHA, PRESS, etc. However, as a result of dating issues, this species is not readily cross-datable. Instead, I apply a correction function to each chronology to try to account for the error associated with missing or miscounted rings. This function assumes that miscounted rings are more frequent when the ring widths are narrow, hence, as the tree gets older.

In trees of the species *D. micrantha*, larger rings form in early life and smaller rings form near the outer edge of the stem disc, thus establishing a relationship between ring size or ring growth and age or location on the tree. The average growth rate of *D. micrantha* indicates decreased extension rates as the trees age (Figure 26).

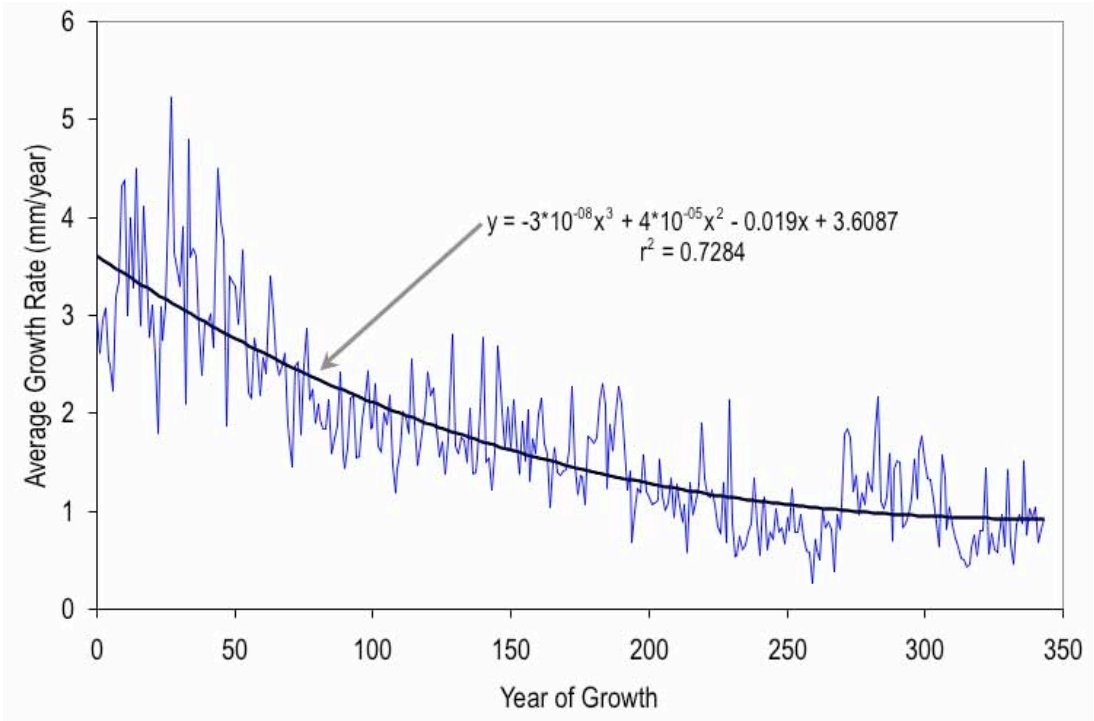

Figure 26. Average growth curve of the five *D. micrantha* tree specimens used in this study.

Younger trees generally have larger ring widths and rings near the outer edge of the stem disc have smaller rings relative to those rings closer to the pith. This relationship is quantified by the polynomial equation:

$$y = -0.00000003x^3 + 0.00004x^2 - 0.0191x + 3.611$$

where "y" is ring growth (mm a^{-1}) and "x" refers to the year of growth. A relationship between the width of a tree ring and its visibility has been documented in other species whose ring boundaries are defined by changes in vessel density. For example, Verheyden et al. (2005) showed that ring visibility in Kenyan mangrove trees decreased as a direct function of ring size and that tree rings below 0.5 mm were often missed in ring counting. Conversely, as ring

width increases, the likelihood that the ring will be visually detected also increases. A relationship between error and ring width can be assumed as:

$$z = \frac{A}{y}$$

where "z" is equal to the error (defined as percent rings missed) and "y" is ring width (in millimeters). "A" is a constant derived empirically for this species based on the ^{14}C dating of the oldest tree. By examining the oldest tree, I can establish an upper boundary for maximum possible error. The results of the ^{14}C measurements revealed the ring counting between 1959 and 2006 to be off by 13 rings, implying an error (% rings missed) of ~28% (13/47). I measured the average ring width of rings counted during this period (predicted years: 1972-2006; years of growth: 309-343) and obtained an average ring width value of 0.799 mm. Solving for "A":

$$z = 0.28 = \frac{A}{y}$$

where y = 0.799

solving for A,

A = 0.28 x 0.799 = 0.22372

I substitute "A" back into the equation to yield:

$$z = \frac{0.22372}{y}$$

The estimated error as a function of year of growth can be found by substituting this into the original polynomial equation above:

$$\frac{0.22372}{z} = -0.00000003x^3 + 0.00004x^2 - 0.0191x + 3.611$$

where z = error and x = year of growth. This equation allows me to estimate the number of actual rings present on a given tree versus the number identified visually by ring counting. By accounting for this estimated error, I can appropriately adjust the chronology of each tree.

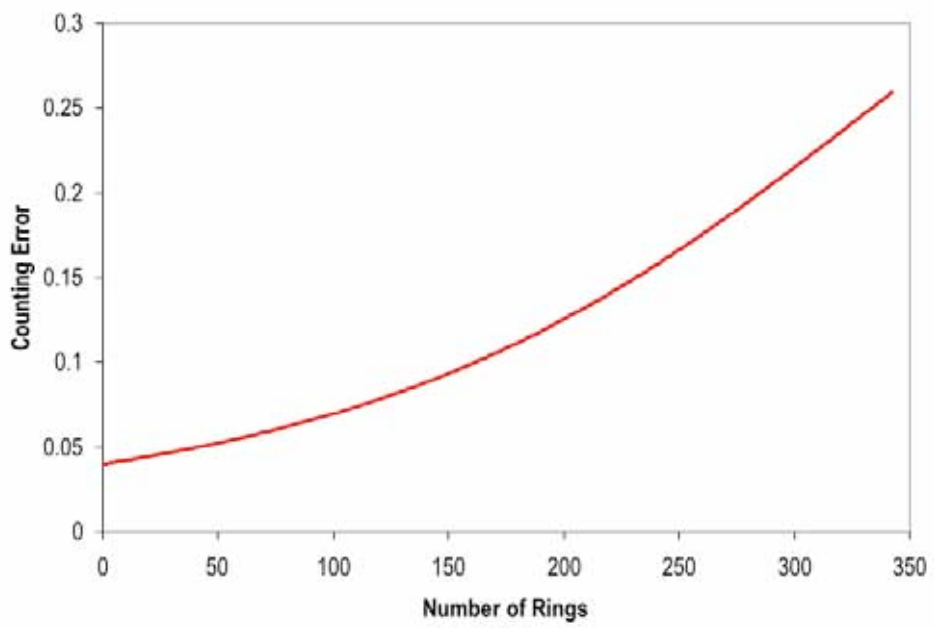

Figure 27. Estimated ring counting error (% of total rings missed) as a function of ring number.

Because the samples for isotopic analyses were taken continuously across the surface of the stem discs, any missing rings have been averaged into the samples for counted rings. This enables me to reconstruct this adjusted chronology without losing any information (i.e. missing rings are not identified by gaps in the isotope record). However, because there is an error correction associated with the chronology, I do not definitively assign rings to actual years. Thus, all analyses are run on the patterns of variability that emerge from the record, rather than on the annual variability tied to each specific year. I should

also note that all figures that follow are labeled as 'Year' but this is the error corrected year based on the procedure as explained.

4.5.4 MTM Analysis

I used the multi-taper method (MTM, Mann and Lees, 1996) to estimate the power spectra for both the carbon and oxygen isotopic data of individual trees. This method was employed to examine periodic behavior common to all trees. MTM has been used by many researchers (e.g. Pederson et al., 2000; D'Arrigo et al., 2001; Herweijer, et al., 2007) to evaluate periodic behavior in tree ring data, and is favored over single-taper methods because it reduces bias from data leakage and produces direct spectral estimates with multiple degrees of freedom (Percival and Walden, 1993; Ghil et al., 2002). The method reduces the variance of spectra by employing several tapers (2p – 1, where p equals the sampling resolution), rather than just one taper (i.e. spectral window) as is used in other methods (Thomson, 1982). For the carbon isotope data, the dataset for each tree was detrended by first removing the mean and then employing a 50-year highpass filter to remove possible non-climate related trends. The 50-year highpass filter was selected primarily to ensure the removal of the Seuss Effect which dominates the signal for the latter half of the 20th century. For the oxygen isotope data, a different highpass filter was used (80-years) in order to preserve all low frequency trends except those obviously unique to each tree. The frequency domain examined was from 0-0.5 and the number of tapers used for each analysis was 3.

4.5.5 Comparisons with SSTs

Once the patterns of variability were detected by the MTM analysis, I compared these patterns with sea surface temperature (SST) anomalies in both the Atlantic and Pacific basins as well as with a few standard climatic indices including the North Atlantic Oscillation (NAO) and the Pacific Decadal Oscillation (PDO). Because the individual trees showed variable responses in the spectral analysis, I compared each tree separately with the SST anomalies. Comparisons were made with yearly SST anomalies from a gridbox over the subtropical North Atlantic (5-20°North, 60-30°West) and were calculated between 1950 and 2008 using the observed Reynolds SST field (Reynolds and Smith, 1994). Anomalies from the Pacific basin were calculated using Nino 3.4 (5° North-5° South, 170-120° West). These anomalies were calculated using a July-June yearly average. The NAO index, defined as the difference in Sea Level Pressure (SLP) between Lisbon, Portugal, and Reykjavik, Iceland, is measured between 1865 and 2002 (Hurrell, 1995). The PDO index is defined as the leading principle component of monthly SST anomalies in the North Pacific, north of 20°N (Zhang et al., 1997). To compare the periodicity of each tree ring reconstruction with the SST anomalies, a bandpass filter of the selected frequency response (based on the MTM analysis) was passed over both the isotope reconstructions and the SST anomalies. The isotope reconstructions are then regressed onto the filtered SST anomalies and their patterns of variability are compared.

4.6 Results

4.6.1 Comparisons between Trees

The carbon isotope records for all 5 trees show a progressive depletion of ~1.61‰ between 1940 and 2006 (Figure 28). The strongest trend is observed in tree 67 where the depletion is 2.23‰. The average rate of depletion is ~.03‰ per year but the rate of depletion increases to .05‰ per year toward the end of the time series. This trend records the 'so-called' Suess effect (Keeling, 1979), the decrease of atmospheric $\delta^{13}C$ ($\delta^{13}C_{atm}$ ~ -7‰) due to the anthropogenic influence of fossil fuel CO_2 ($\delta^{13}C$ ~ -25‰).

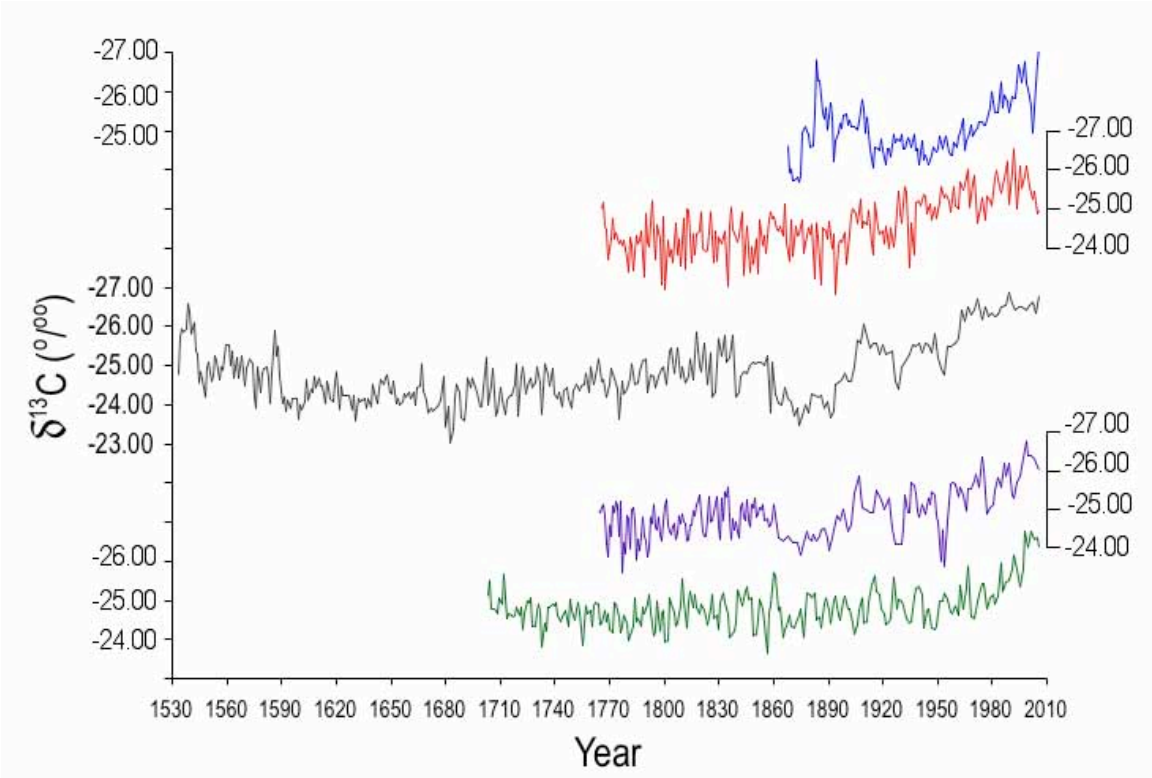

Figure 28. Unfiltered carbon isotope curves for five *D. micrantha* trees. Tree labels are as follow: Tree 20 (blue), tree 78 (red), tree 67 (gray), tree 88 (purple), tree 82 (green). Note that "Year' here is the error adjusted year.

Friedli et al. (1986) measured the $^{13}C/^{12}C$ ratio of atmospheric CO_2 using CO_2 bubbles trapped in an ice core at Siple Station, Antarctica. Their findings indicate a decrease in atmospheric $\delta^{13}C$ from -6.6‰ to -7.9‰ from 1900 to 1980. Keeling et al. (2005) directly measured a decrease of atmospheric $\delta^{13}C$ from –7.6‰ to –8.1‰ in 2002 (Figure 29). The five-tree mean $\delta^{13}C$ values record the Suess effect remarkably well.

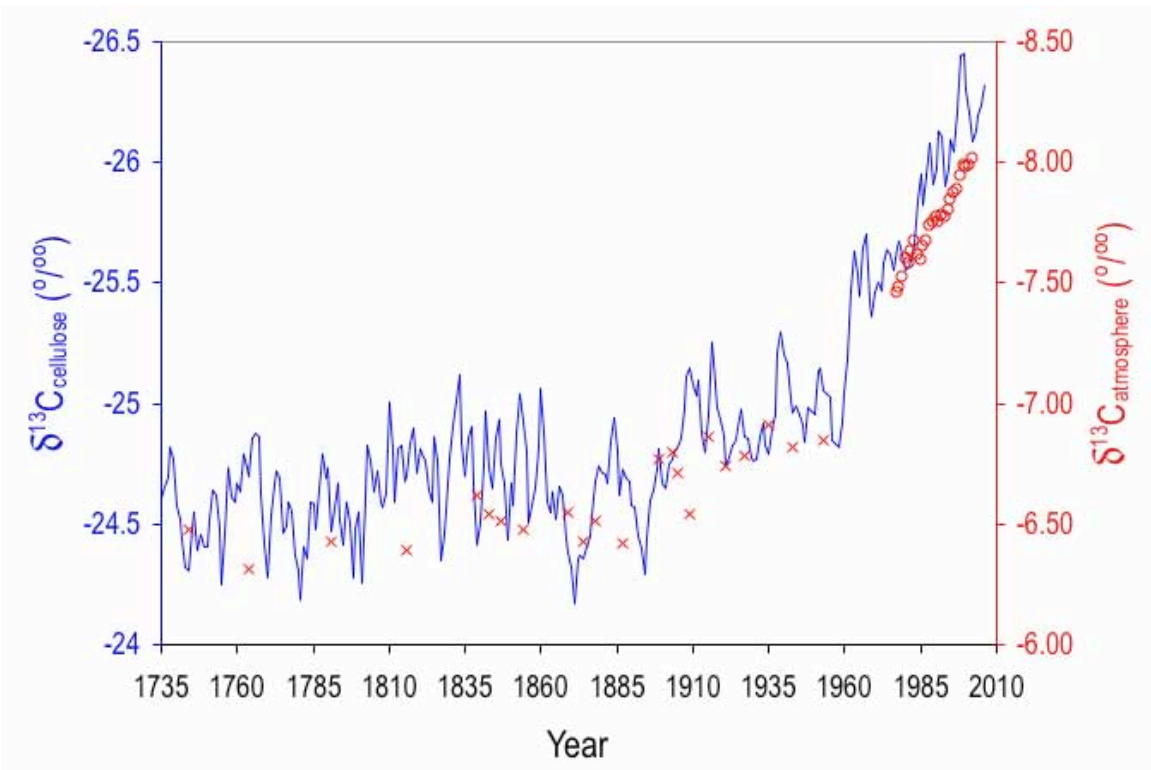

Figure 29. Average of all five carbon isotope records plotted against atmospheric measurements of $\delta^{13}C$ since 1735. Open circles are atmospheric measurements of $\delta^{13}C$ from American Samoa (15°S) roughly equivalent in latitude to the tree ring study site (12°S). X's are $\delta^{13}C$ values obtained from the ice core at Siple Station, Antarctica. All values are standardized to VPDB.

Numerous previous studies have detected the effect of atmospheric $\delta^{13}C$ on tree ring cellulose, but few of these were undertaken in the Southern Hemisphere. This study is one of the first to show the interhemispheric

reproducibility of the fossil fuel signal in tree ring cellulose. February and Stock (1999) found a decrease of nearly 2‰ between 1940 and 1980 in a *Widdringtonia cedarbergensis* tree from South Africa and Leavitt and Lara (1994) measured the $\delta^{13}C$ for 5 *Fitzroya cupressoides* trees in Chile, finding a 1.22‰ decrease since the turn of the century. This study affirms that this signal is recorded in trees much closer to the equator (12° S) and shows roughly the same magnitude change (1.75 ‰) since 1735.

There are no long-term trends apparent in the oxygen isotopic records of the individual trees (Figure 30). Instead, each series exhibits variability in the multi-decadal, decadal and higher frequency domains. Only one of the five trees (tree 67) displays a trend throughout the length of the record that is roughly sinusoidal with a period length equal to slightly less than half of the record (150 years). Because this trend is not observed in any of the other four trees (three of which are from roughly the same area), the pattern is attributed to local effects specific to the individual tree. Roden and Ehleringer (1999) noted that though the oxygen isotopic composition of cellulose varies linearly with the isotopic composition of meteoric water, this relationship can be affected by changes in relative humidity, source water, or root depth.

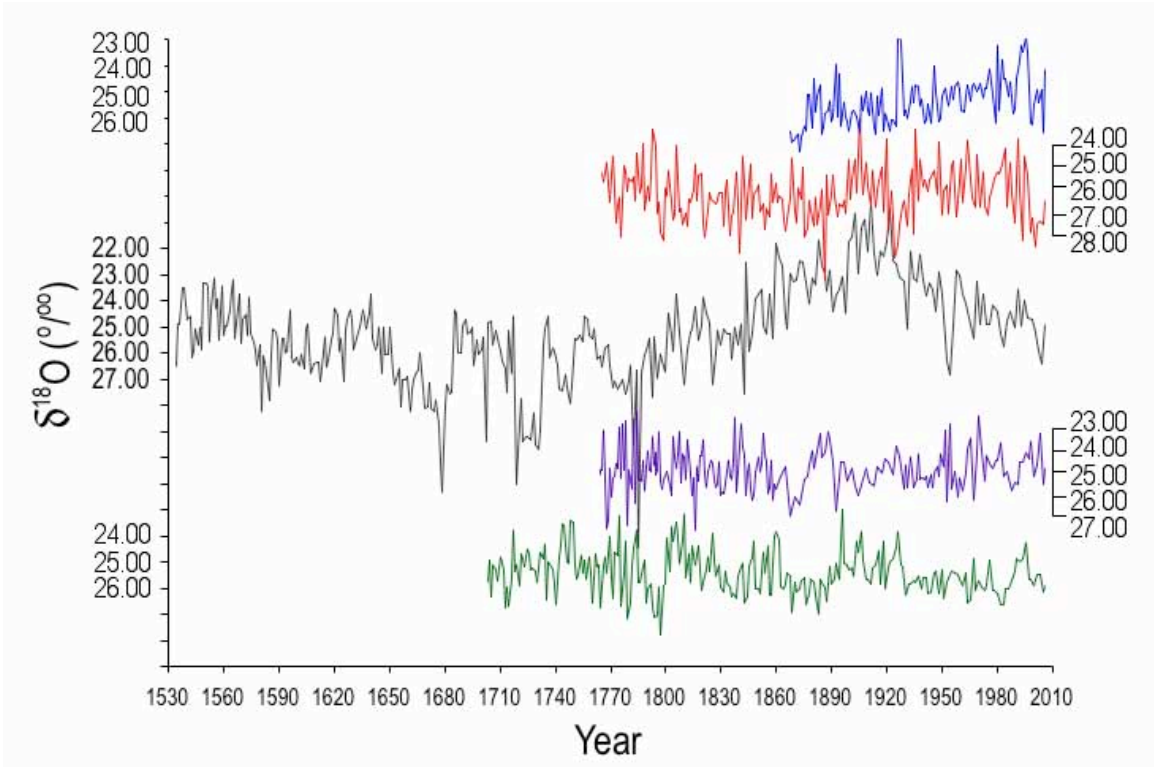

Figure 30. Stable Oxygen isotope data for five *D. micrantha* trees. Tree labels are as follows: Tree 20 (blue), tree 78 (red), tree 67 (gray), tree 88 (purple), tree 82 (green).

There is a large amount of inter-tree variation in the isotopic values for a given year. Of course, this is to be expected as the chronologies for each tree could easily be offset from each other by several years. Indeed, the average standard deviation between tree data points is 0.64‰ for the carbon isotopes and 1.24‰ for oxygen isotopic measurements. The mean correlation between the $\delta^{13}C$ of individual trees is strong (r = 0.46) though this is largely driven by the Suess effect. When the Suess effect is removed from the $\delta^{13}C$ records, the correlation between trees is reduced (r = .24). Eight-year running averages of each individual tree helps to minimize interannual imperfections in their chronologies and illustrates that lower frequency variation of $\delta^{13}C$ is partially coherent between specimens (r = .31, Figure 31). The mean correlation between the $\delta^{18}O$ of

individual trees is extremely low (r = .10) and an 8-year running average does not improve the relationship (r = .15) (Figure 32).

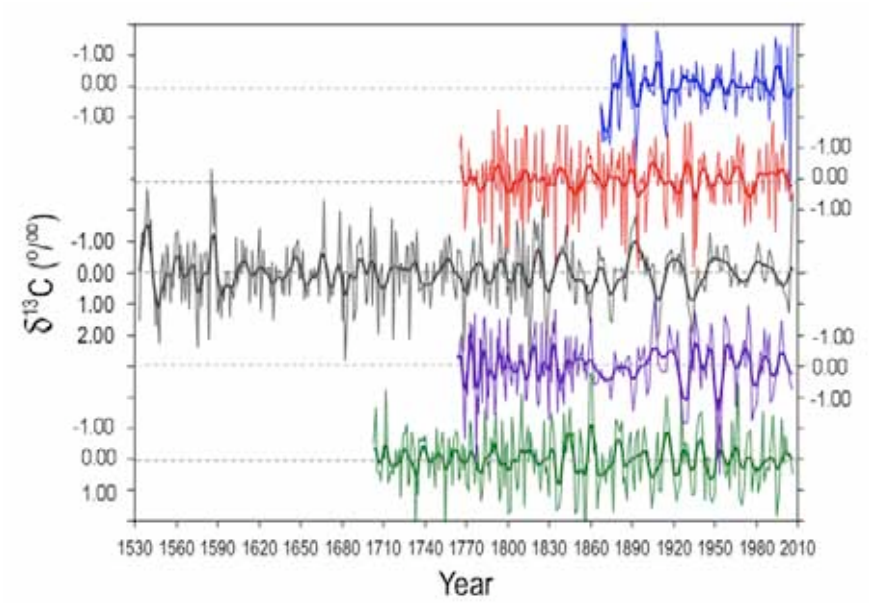

Figure 31. Detrended $\delta^{13}C$ records for each of the five trees. Records have been detrended using an 50 year highpass filter. An eight-year running average is plotted in bold.

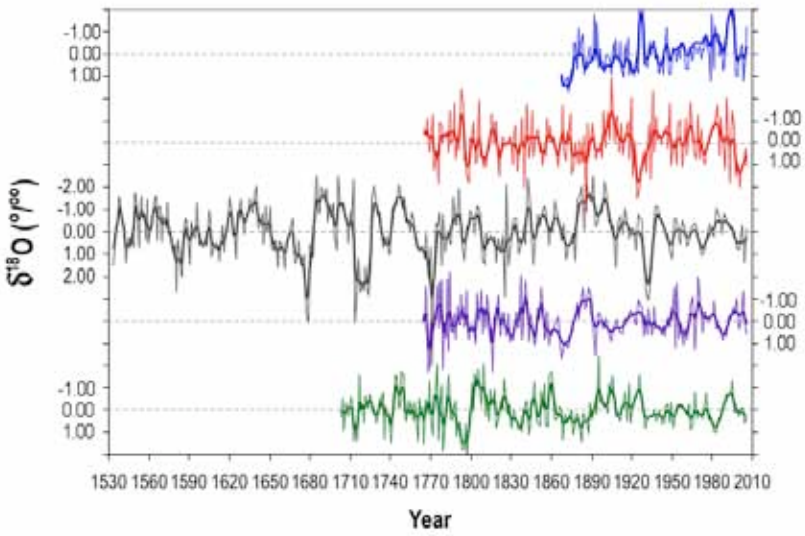

Figure 32. Detrended $\delta^{18}O$ records for each of the five trees. Records have been detrended using an 80 year highpass filter. An eight-year running average is plotted in bold.

4.6.2 Comparisons between Isotopes

If the oxygen isotopic signature of tree cellulose is, at least to a first approximation, a measure of precipitation (Feng and Epstein, 1994; Roden and Ehrlinger, 2001) and the carbon isotopic signature is a measure of water availability, these two proxies should contain some shared variability. However, the way in which both proxies record this climatic information is neither simple nor straightforward. A carbon-oxygen isotope correlation assumes that the amount of water being used by the tree is related to the mean annual precipitation or mean wet season precipitation and some studies have shown that root activity can disrupt this relationship, as some species draw on deeper groundwater reservoirs that do not depend only on precipitation from a given year (Thorburn and Walker, 1993; Valentini et al., 1992). Furthermore, humidity is known to have an effect on the $\delta^{18}O$ value of cellulose, though this value is often assumed to be constant in the very humid conditions of a tropical rainforest. Given this assumption, trees 82, 88, and 20 all exhibit significant agreement (at the 99% confidence level) between the two isotopes (Table 11) while trees 67 and 78 do not.

Table 11. Correlation Coefficients between $\delta^{13}C$ and $\delta^{18}O$ for each tree.

Specimen	r-value	p-value
Tree 67	0.12	0.0371
Tree 20	0.10	0.3200
Tree 82	0.21	0.0100
Tree 88	0.30	0.0008
Tree 20	0.26	0.0020

Although both the $\delta^{13}C$ and $\delta^{18}O$ were determined on the same sample of the same age, it is possible that one or both may have a lagged response to the same external (e.g. climate) forcing. In particular, it seems possible that $\delta^{18}O$ might lag the $\delta^{13}C$, that is that the biological responses of the tree to drought might be exhibited more immediately than the groundwater ($\delta^{18}O$ response). The rooting depth of tropical trees is poorly understood over much of the Amazon basin, but recent studies have suggested roots may extend to below 10 meters depth (Nepstad et al., 1994 and 2002). Excavation of soil profiles near Rio Branco has revealed roots up to a maximum depth of 8 meters (D. Nepstad, unpublished data). It is likely that since tropical trees can draw on water reserves from previous rainy seasons, a lag may exist between the $\delta^{18}O$ of tree cellulose and that of meteoric water. Because the $\delta^{13}C$ value of the tree records the interstitial partial pressure of CO_2 inside and outside the stomata during photosynthesis, this value may be dependent on more immediate environmental changes, thus should show little lag with environmental forcing. The lagged response ($\delta^{18}O$ lagged by one year) does not significantly improve the correlation between the two isotopes in four of the five trees, however tree 20 does show a significantly increased correlation (Table 12, Figure 33).

Table 12. Correlation Coefficients between $\delta^{13}C$ and $\delta^{18}O$ for each tree. $\delta^{18}O$ is lagged 1 year behind $\delta^{13}C$.

Specimen	r-value	p-value
Tree 67	0.11	0.0128
Tree 20	0.12	0.0887
Tree 82	0.08	0.1556
Tree 88	0.08	0.2152
Tree 20	0.34	0.00003

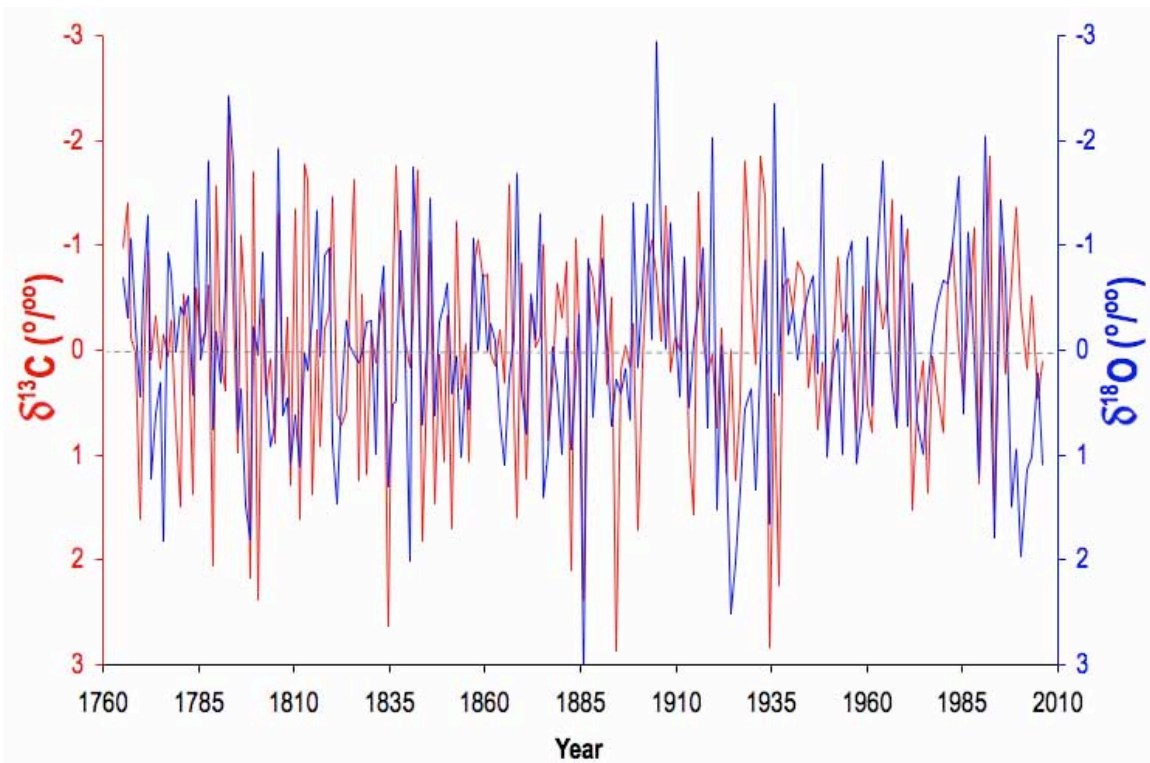

Figure 33. $\delta^{13}C$ (red) and $\delta^{18}O$ (blue) records for Tree 88. Axes are oriented such that an increase in the amount of ^{12}C in the cellulose should correlate with an increase in the amount of ^{16}O. The correlation between the two records is r = 0.3.

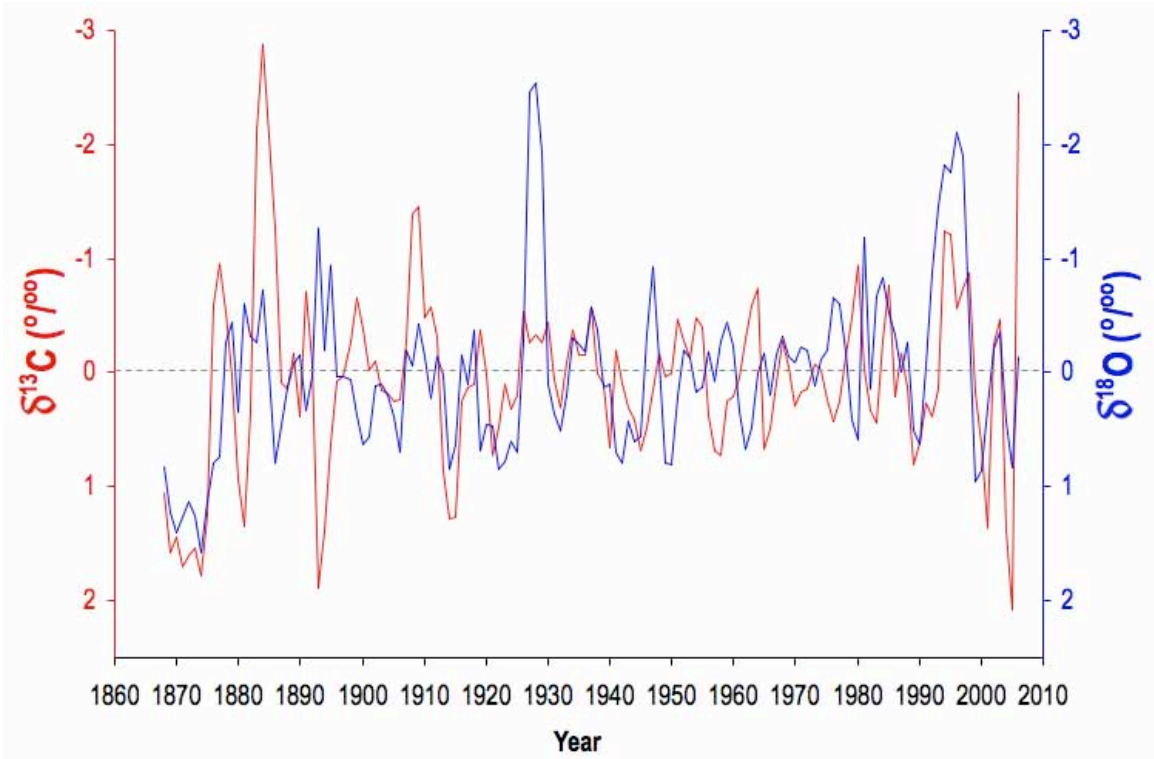

Figure 34. $\delta^{13}C$ (red) and $\delta^{18}O$ (blue) records for Tree 20. d18O was lagged by one year. An 8-year running average is also plotted in bold for both isotopic values.

4.6.3 Correlations with Climate

Because of the highly variable relationships of carbon and oxygen isotopes in each individual tree and because of the uncertain chronologies, climate-isotope correlations are undertaken with individual trees rather than compositing the specimens. Here, the tree ring records are compared with total wet season (October-April) precipitation (mm) using the GPCC and OBS datasets (1974-2006) as well with average wet season river discharge rates (m3/sec) from the RIVDIS dataset (1968-2006). Because the chronologies for each of the trees have been adjusted to account for counting error, I also compare 5-year running means of the tree ring records with the instrumental datasets (Figure 35). This

comparison allows me to examine lower frequency controls on isotopic partitioning.

Both tree 67 and tree 20 show statistically significant correlations (r = –0.51, and –0.37 respectively) between $\delta^{13}C$ and precipitation (Tables 13 and 14) while trees 78, 82, and 88 do not. None of the $\delta^{13}C$ records exhibit significant correlation with river discharge. When 5-year running means are compared, four of the five trees show significant correlations with wet season precipitation, the exception being tree 78. The sign of the correlation is negative because as precipitation increases, the $\delta^{13}C$ ratio decreases as relatively more ^{12}C is assimilated by the tree. Although the actual data do not exhibit an overall strong correlation with precipitation, 5 year moving averages significantly improve the correlation because the averaging process helps to account for random interannual errors in the chronology.

The $\delta^{18}O$ datasets show a slightly higher degree of correlation with climate (Table 15). Trees 67, 88, and 82 all show significant correlation with wet season precipitation while trees 20 and 78 do not. Centered five-year running means substantially improve the correlations between wet season precipitation and the oxygen isotopic records (Table 16).

Table 13. Correlation coefficients between $\delta^{13}C$ records from individual trees and precipitation and river discharge datasets. Correlations for the GPCC and OBS datasets are over the period 1974-2006, correlations for RIVDIS are between 1968-2006.

			$\delta^{13}C$		
DATASET	TREE 67	TREE 78	TREE 88	TREE 82	TREE 20
GPCC	**-0.38**	0.17	-0.2	-0.27	**-0.37**
OBS	**-0.51**	0.16	-0.16	-0.27	**-0.36**
RIVDIS	-0.05	-0.03	0.22	-0.22	-0.19

*Bolding denotes correlation coefficients significant at $p<0.05$

Table 14. Correlation coefficients between 5 year running averages of $\delta^{13}C$ records from individual trees and precipitation and river discharge datasets. Correlations for the GPCC and OBS datasets are over the period 1974-2006, correlations for RIVDIS are between 1968-2006.

			$\delta^{13}C$ SMOOTHED		
DATASET	TREE 67	TREE 78	TREE 88	TREE 82	TREE 20
GPCC	**-0.45**	0.21	**-0.51**	**-0.59**	**-0.42**
OBS	**-0.57**	0.22	**-0.34**	**-0.60**	**-0.43**
RIVDIS	-0.13	-0.04	0.28	-0.27	-0.21

*Bolding denotes correlation coefficients significant at $p<0.05$

Table 15. Correlation coefficients between raw $\delta^{18}O$ records from individual trees and precipitation and river discharge datasets. Correlations for the GPCC and OBS datasets are over the period 1974-2006, correlations for RIVDIS are between 1968-2006.

			$\delta^{18}O$		
DATASET	TREE 67	TREE 78	TREE 88	TREE 82	TREE 20
GPCC	**-0.48**	-0.05	**-0.46**	-0.33	-0.11
OBS	**-0.52**	-0.03	**-0.54**	**-0.36**	-0.11
RIVDIS	-0.15	0.26	-0.007	-0.13	-0.02

*Bolding denotes correlation coefficients significant at $p<0.05$

Table 16. Correlation coefficients between 5 year running averages of $\delta^{18}O$ records from individual trees and precipitation and river discharge datasets. Correlations for the GPCC and OBS datasets are over the period 1974-2006, correlations for RIVDIS are between 1968-2006.

	$\delta^{18}O$ SMOOTHED				
DATASET	TREE 67	TREE 78	TREE 88	TREE 82	TREE 20
GPCC	**-0.47**	-0.07	**-0.60**	**-0.47**	-0.13
OBS	**-0.56**	-0.01	**-0.78**	**-0.53**	-0.14
RIVDIS	-0.21	**-0.46**	-0.18	-0.18	**-0.3**

*Bolding denotes correlation coefficients significant at $p<0.05$

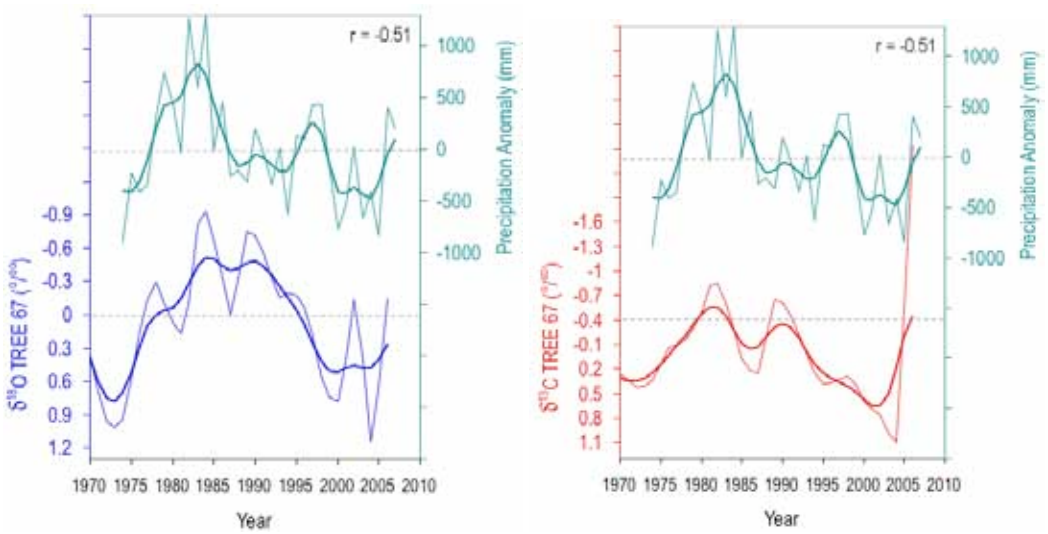

Figure 35. Time series of $\delta^{18}O$ (left panel) and $\delta^{13}C$ (right panel) and wet season precipitation for Tree 67. Bold lines are 5-year running means. Precipitation measurements derived from wet season anomalies (October-April) from the OBS dataset.

4.6.4 MTM Analysis

4.6.4.1 Comparisons Between Trees

Carbon Isotopes

The frequency spectra for carbon isotope reconstructions for all of the five trees show generally similar patterns, with multiple peaks appearing at both interannual (3-6 year) and decadal (8-10 year) time scales. All five of the carbon isotopic reconstructions exhibit periodicity in the 8-10 year band that is significant above the 99% confidence interval except tree 88, which only shows a peak significant at the 95% level (Figure 44). Trees 67 and 78 show strong power in this band, with tree 78 showing power between 8 and 10 year periodicity (Figures 37 and 39, respectively). Tree 67 shows a peak in the 28 year band that does not appear in any of the other reconstructions. Both tree 78 and tree 82 show power in the 11-14 year band, with tree 82 peaking well above the 99% confidence interval at ~12 year periodicity (Figure 40). With the exception of tree 88, all trees show strong periodicity in the 5-7 year band. There is an additional peak in most of the reconstructions around the 3-4 year band and this is recognized by tree 88. Trees 67, 88, and 82 all show power in this band, ranging from 3.5-4.3 year bands. Tree 78 does not show this period to be significant at the 99% confidence interval, though it is significant at the 95%. Tree 88 is the only tree to show a peak in the 2-3 year band and shows a spectral behavior somewhat different from the other reconstructions, with peaks in the 4.2, 4, and 2.8 year bands. In general there is a strong agreement between carbon isotope reconstructions with two peaks appearing in the 8-10 and 5-7 year bands and a smaller peak of 3-4 years appearing in 4 of 5 of the reconstructions.

Oxygen Isotopes

There are two emergent peaks that appear in common to all oxygen isotope reconstructions and these occur at 4-5 years and 3-3.5 years. The oxygen isotope spectra in general show peaks at higher frequencies than the carbon reconstructions, showing more peaks in the 2-6 year range. Tree 82 shows the highest frequency peak occurring in the 2.8 year band (Figure 43). Trees 82, 88, and 67 show multiple peaks occurring between the 2.8 and 5 year bands (Figures 37, 41, and 43). Tree 67 shows multiple low frequency peaks at 50, 18, 10, and 7.5 year bands, however, it is the only tree to do so. Tree 20 also shows a peak at the 9-11 year band. Tree 82 reveals a spectral peak in the 6-7 year band, though generally shows power at higher frequencies. There is slightly more disagreement between the spectral peaks of the oxygen isotopic reconstructions, though this is not unexpected given their low correlation. All peaks reported are significant at the 99% confidence level.

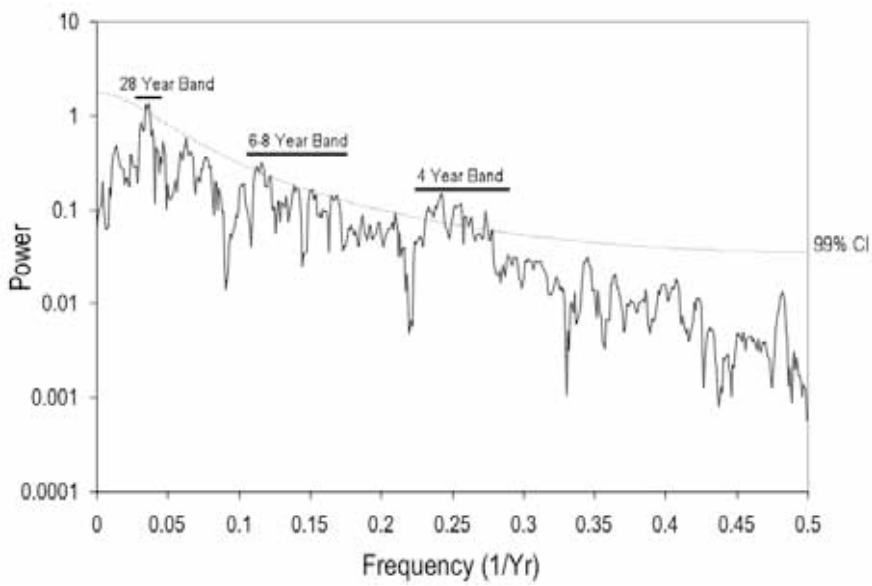

Figure 36. Spectral analysis of $\delta^{13}C$ reconstruction from Tree 67. Peaks that fall above the 99% confidence interval are labeled on the graph.

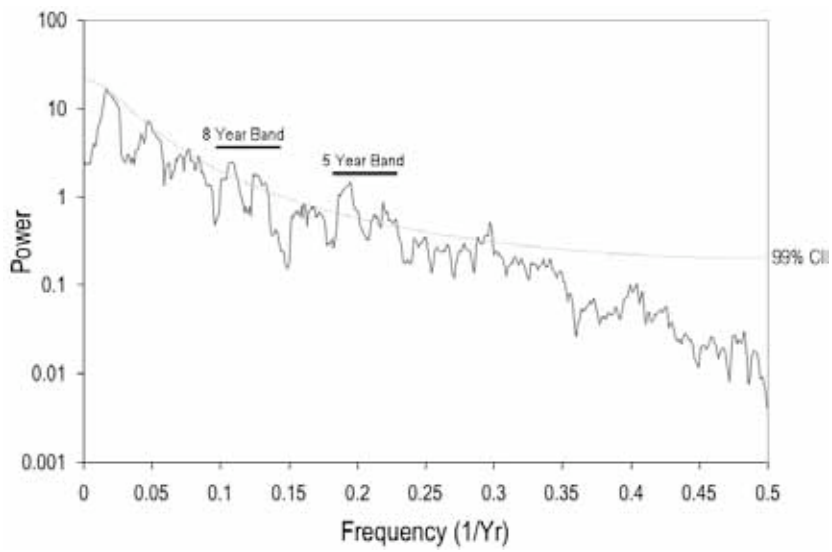

Figure 37. Spectral analysis of $\delta^{18}O$ reconstruction from Tree 67. Peaks that fall above the 99% confidence interval are labeled on the graph.

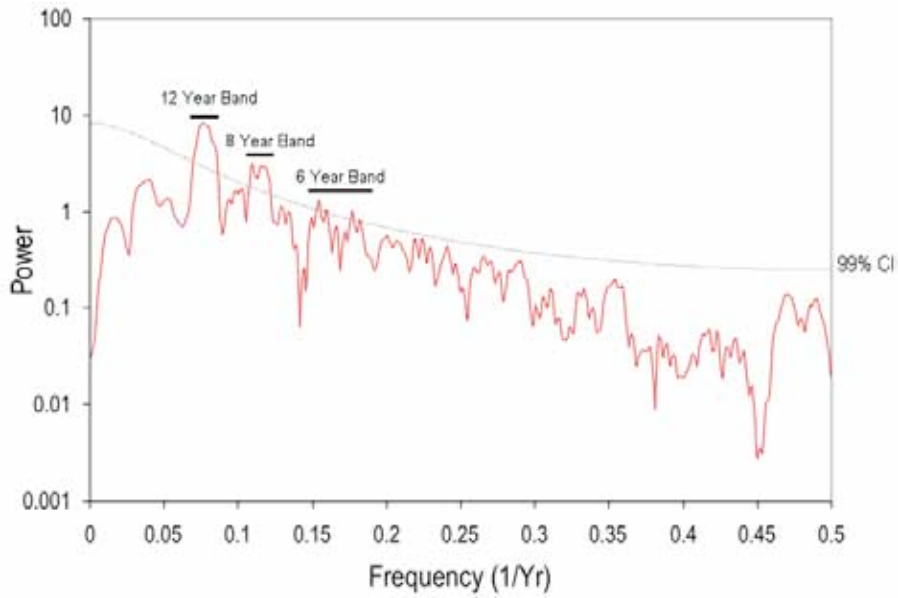

Figure 38. Spectral analysis of $\delta^{13}C$ reconstruction from Tree 78. Peaks that fall above the 99% confidence interval are labeled on the graph.

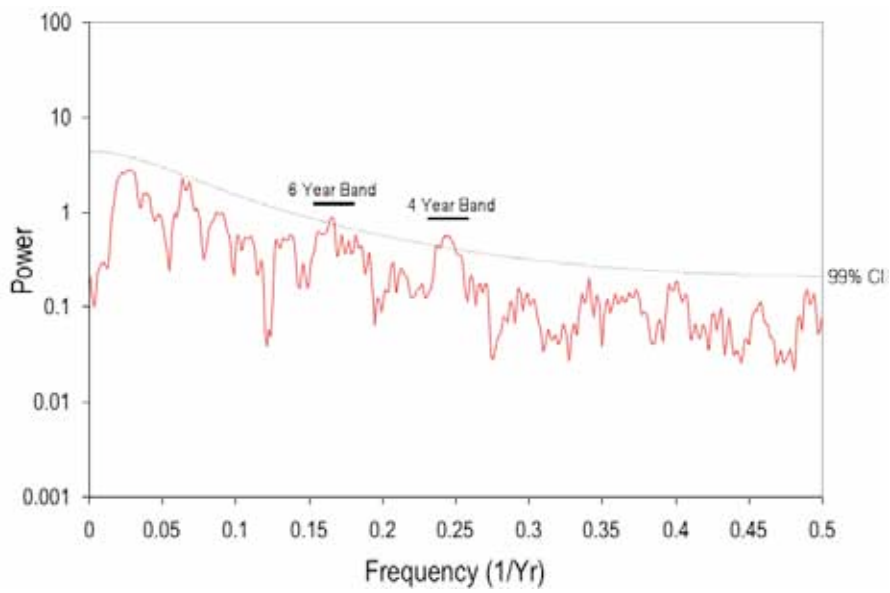

Figure 39. Spectral analysis of $\delta^{18}O$ reconstruction from Tree 78. Peaks that fall above the 99% confidence interval are labeled on the graph.

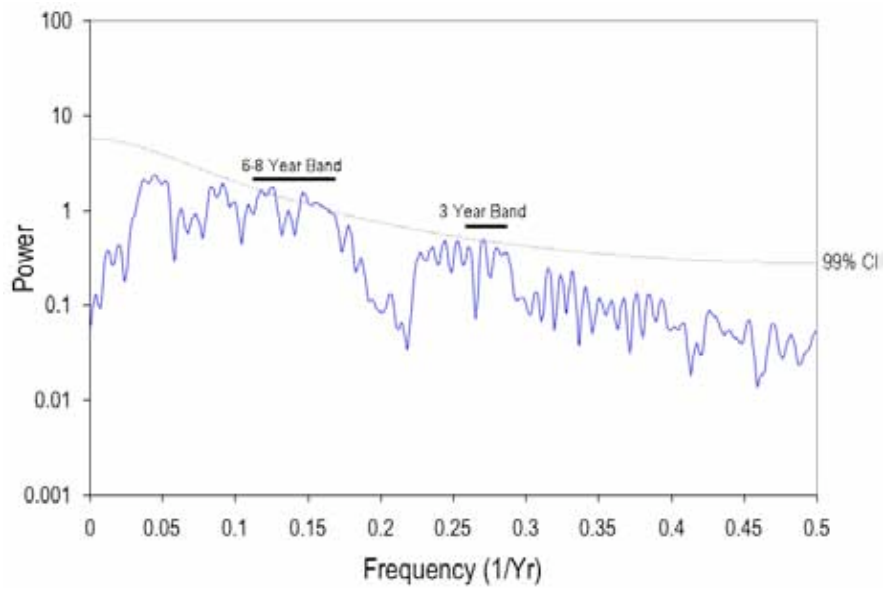

Figure 40. Spectral analysis of $\delta^{13}C$ reconstruction from Tree 20. Peaks that fall above the 99% confidence interval are labeled on the graph.

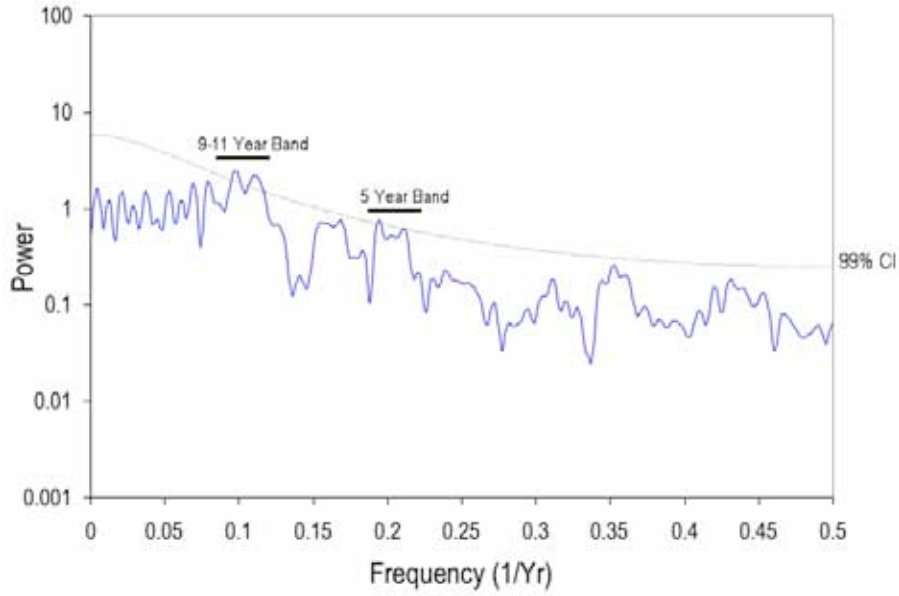

Figure 41. Spectral analysis of $\delta^{18}O$ reconstruction from Tree 20. Peaks that fall above the 99% confidence interval are labeled on the graph.

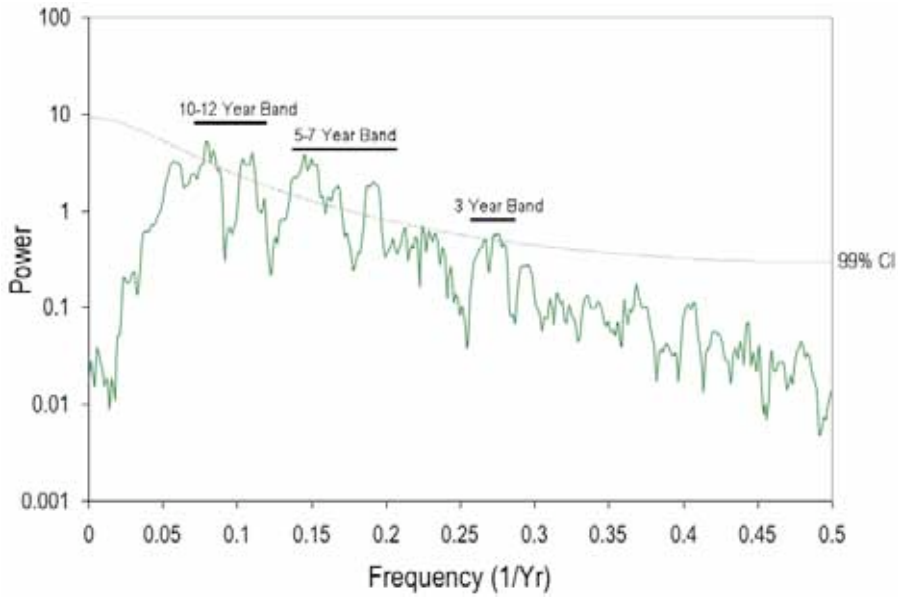

Figure 42. Spectral analysis of $\delta^{13}C$ reconstruction from Tree 82. Peaks that fall above the 99% confidence interval are labeled on the graph.

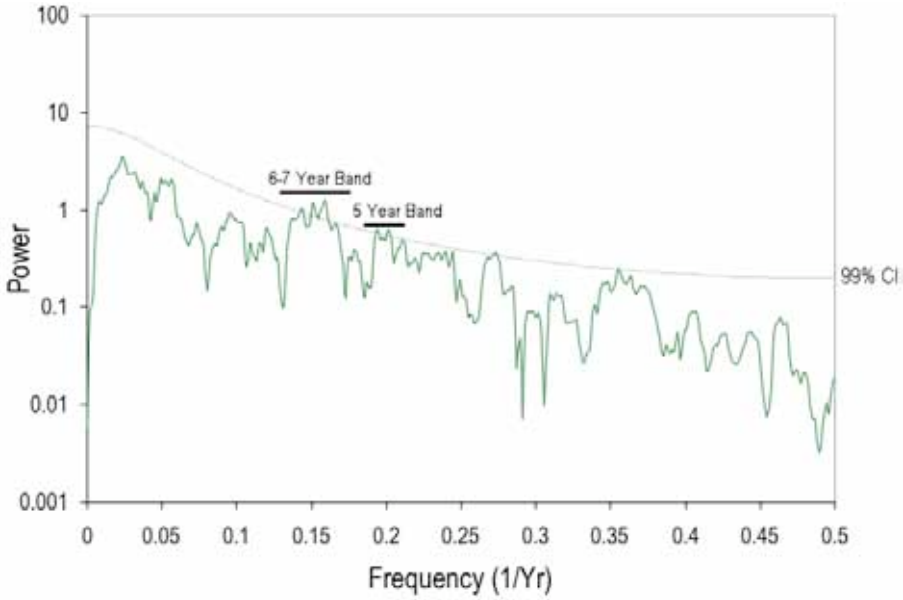

Figure 43. Spectral analysis of $\delta^{18}O$ reconstruction from Tree 82. Peaks that fall above the 99% confidence interval are labeled on the graph.

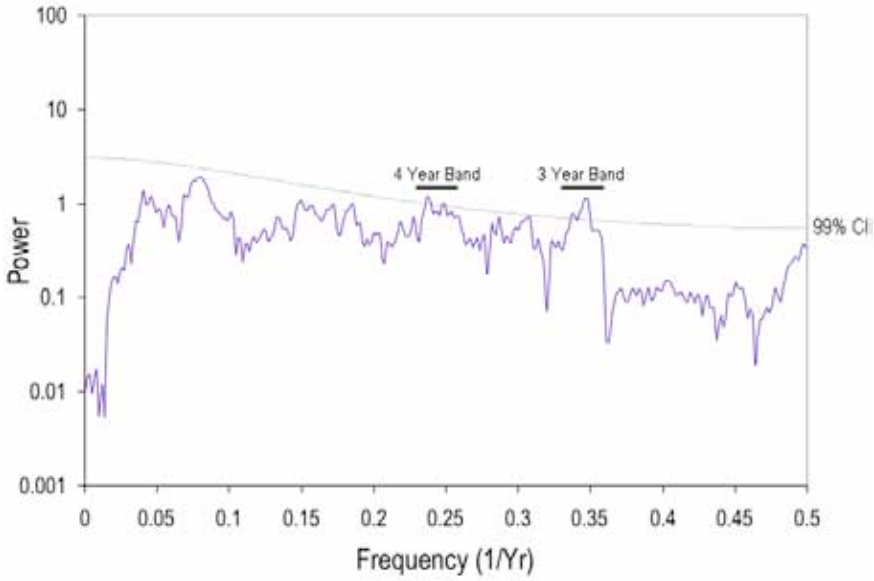

Figure 44. Spectral analysis of $\delta^{13}C$ reconstruction from Tree 88. Peaks that fall above the 99% confidence interval are labeled on the graph.

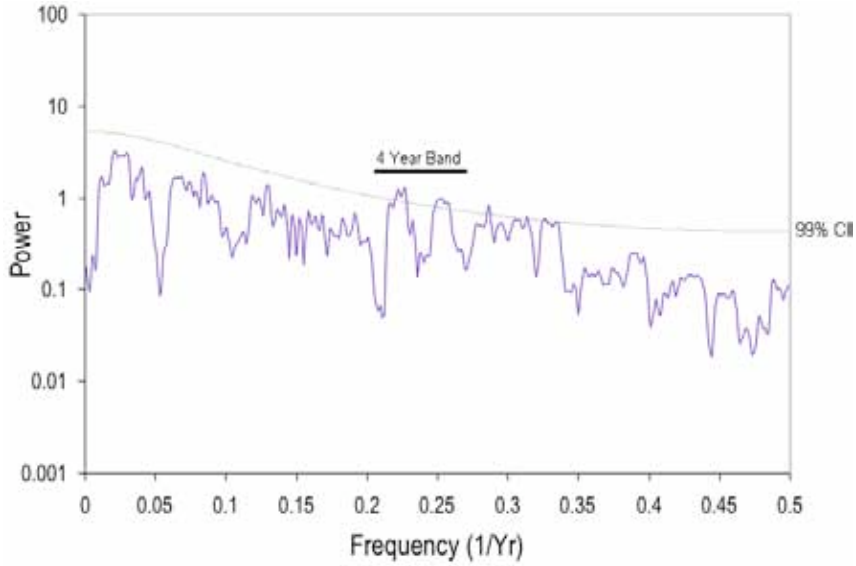

Figure 45. Spectral analysis of $\delta^{18}O$ reconstruction from Tree 88. Peaks that fall above the 99% confidence interval are labeled on the graph.

Because the carbon and oxygen isotopic measurements were taken from exactly the same place on each tree, they can be directly without accounting for any error between chronologies. Comparisons between the spectral plots for both isotopic reconstructions generally show coherency in both the 3-5 and 7-8.5 year bands (Figures 36 and 37). The lower frequency peaks are not, however, similar for both isotopes, showing 50 and 19 year bands in the oxygen and a 28 year band in the carbon. The reconstructions for tree 78 only show agreement in the 6 year band and then diverge, with the carbon reconstruction showing lower frequency (8-10, 11-14) power and the oxygen reconstruction showing higher frequency (4) year power (Figures 38 and 39). Both power spectra for tree 88 show high frequency power and generally good agreement, with peaks between and 3 and 4 year bands (Figures 44 and 45). This tree is the only one to show only higher (interannual) variability and no decadal or lower frequency pattern. For tree 82, both isotope reconstructions show strong periodicity in the 3.6, 5, and 6-7 year bands (Figures 42 and 43). However, the carbon isotope reconstruction also shows lower frequency (8-10, 12-12.5 years) variability that the oxygen reconstruction does not. In general, the oxygen isotopic reconstructions fail to capture much of the decadal and lower frequency variability as compared with the carbon isotopic reconstructions. However, both reconstructions identify interannual variability and there is good agreement between reconstructions for individual trees.

4.6.5 Spectral Analysis of SST Anomalies

To examine the relationship between sea surface temperature anomalies and the periodicity identified in the isotope reconstructions, I examine the relationship between proxy datasets and four indices; ENSO (Nino 3.4), tropical North Atlantic SST, PDO and NAO. A maximum entropy analysis reveals the dominant peaks within each of these datasets (Figure 46). The periodicities identified in each of these 4 forcings are compared with those identified in the tree ring records and correlations between SST anomalies and tree ring isotopes are calculated.

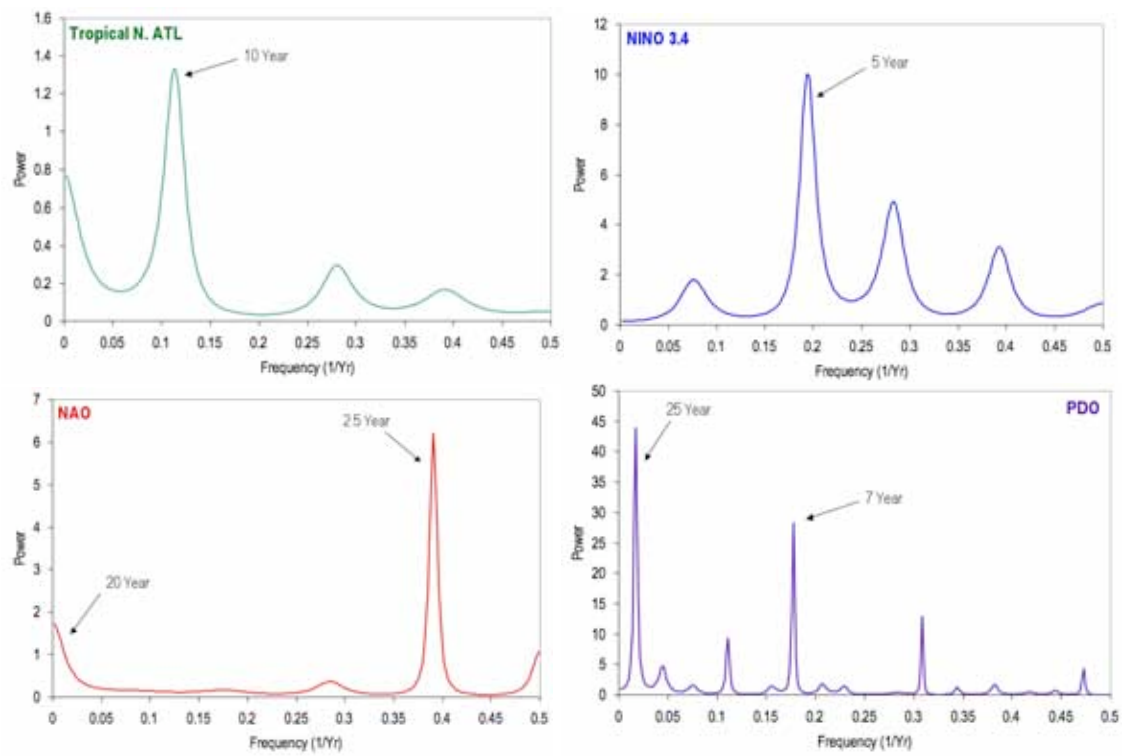

Figure 46. Maximum entropy analysis revealing spectral peaks in each of the four datasets (PDO, NAO, NINO 3.4, and Tropical N. Atlantic SST).

4.6.6 Comparisons with SST Anomalies

4.6.6.1 Carbon Isotopes & SST's

The strongest relationship emerges between the carbon isotopic reconstructions and the Pacific Decadal Oscillation (Figure 47). This is not surprising given that most of the tree reconstructions identified an 8-10 year periodicity in their spectra. The strongest relationship identified is between the carbon isotopic reconstruction of tree 88 and the PDO (r = 0.83). A bandpass filter over both datasets reveals a significantly similar pattern of variability (Figure 47). Trees 67, 82, and 20 also show statistically significant correlation with the PDO (Tables 17 and 18), however tree 88 by far shows the strongest correlation. However, when a 3-5 year bandpass filter is applied to the $\delta^{13}C$ record, only Tree 88 exhibits significant correlation with ENSO (Tables 19 and 20). The only tree to show any relationship with El Nino is tree 88, though the relationship is negative (such that positive SST anomalies are associated with a decreased $\delta^{13}C$) (Figure 48). The $\delta^{13}C$ of tree 88 is also correlated with tropical North Atlantic SST's in the 3-5 year period. Both tree 88 and tree 20 show a relationship with the NAO in the low frequency (8-10 year) domain.

Table 17. Table of correlation coefficients between 8-10 year bandpass filtered isotope reconstructions and SST anomalies. Note that 'TNA' represents SST anomalies from a gridbox (5-20°North, 60-30°West) in the tropical North Atlantic.

			$\delta^{13}C$		
DATASET	TREE 67	TREE 78	TREE 88	TREE 82	TREE 20
PDO	**0.38**	-0.16	**0.83**	**0.43**	**0.37**
TNA	-0.09	0.08	0.03	0.07	-0.02
NINO 3.4	0.06	-0.03	**0.54**	**0.52**	-0.13
NAO	0.08	0.08	**-0.25**	-0.05	**0.26**

Bolding Denotes r-values that are statistically significant at the $p<0.05$ value.

Table 18. P-values for correlation coefficients in Table 17.

			$\delta^{13}C$		
DATASET	TREE 67	TREE 78	TREE 88	TREE 82	TREE 20
PDO	0.0039	0.2224	0.0000	0.0008	0.0042
TNA	0.5266	0.5623	0.8187	0.5920	0.8926
NINO 3.4	0.6568	0.8121	0.00002	0.00004	0.3352
NAO	0.3227	0.3422	0.0030	0.5319	0.0082

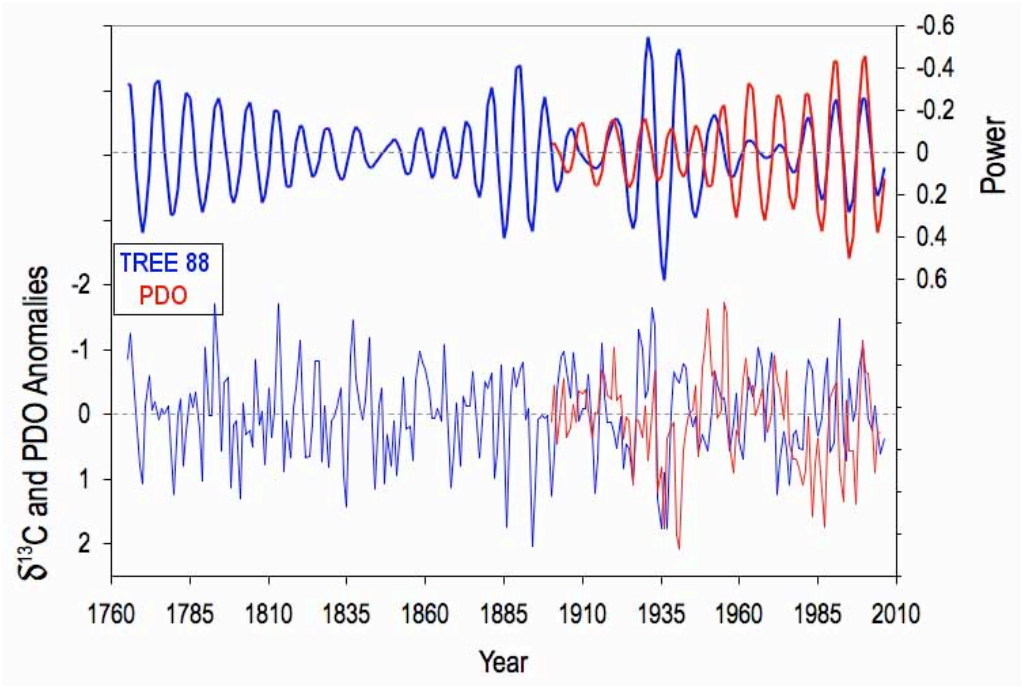

Figure 47. Unfiltered $\delta^{13}C$ data from tree 88 plotted against the PDO in the bottom panel. The top panel is a graph of the $\delta^{13}C$ and PDO passed through an 8-10 year bandpass filter to isolate this variability.

Table 19. Table of correlation coefficients between 3-5 year bandpass filtered isotope reconstructions and SST anomalies. Note that 'TNA' represents SST anomalies from a gridbox (5-20°North, 60-30°West) in the tropical North Atlantic.

			$\delta^{13}C$		
DATASET	TREE 67	TREE 78	TREE 88	TREE 82	TREE 20
PDO	-0.04	0.03	-0.11	0.12	0.05
TNA	-0.10	0.08	**-0.30**	0.05	0.12
NINO 3.4	0.02	0.15	**-0.38**	0.02	-0.05
NAO	0.05	-0.01	**0.25**	-0.08	0.08

Bolding denotes r-values that are statistically significant at the $p<0.05$ value.

Table 20. P-values for correlation coefficients in Table 19.

			$\delta^{13}C$		
DATASET	TREE 67	TREE 78	TREE 88	TREE 82	TREE 20
PDO	0.7562	0.8456	0.4136	0.3855	0.7370
TNA	0.4384	0.5495	0.0214	0.7391	0.3751
NINO 3.4	0.8772	0.2849	0.0036	0.8769	0.7127
NAO	0.5989	0.4941	0.0030	0.3757	0.3313

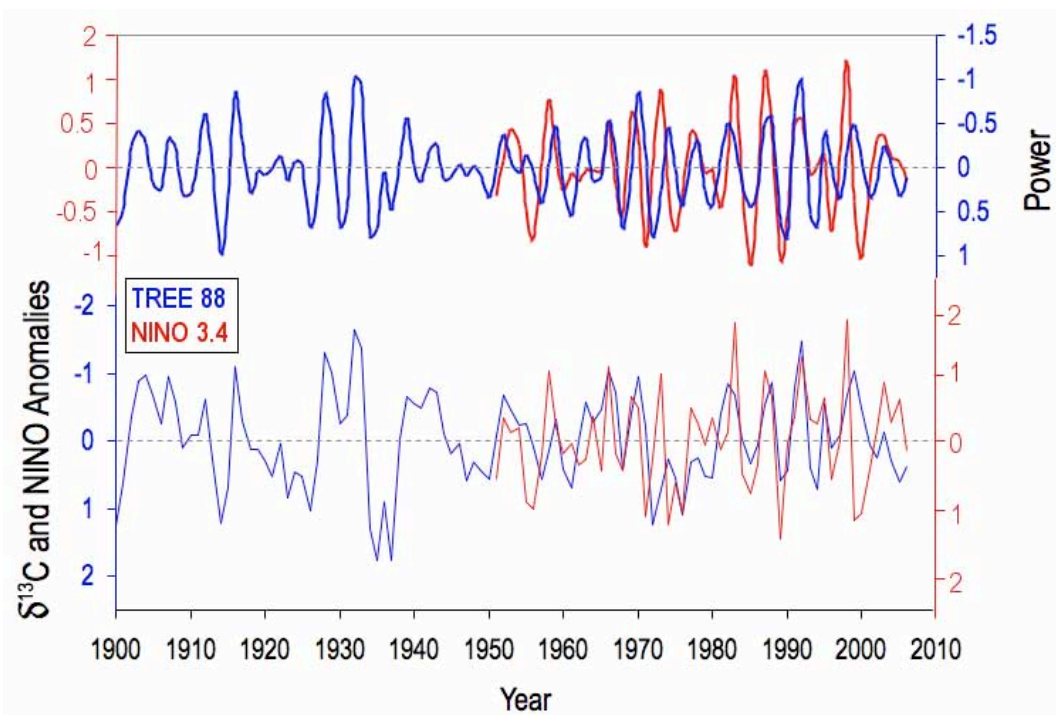

Figure 48. Unfiltered $\delta^{13}C$ data from tree 88 is plotted against the NINO 3.4 index in the bottom panel. The top panel is a graph of the $\delta^{13}C$ and NINO 3.4 passed through an 3-5 year bandpass filter to isolate this variability. The Nino 3.4 index is plotted on a reverse axis (red) as compared with the $\delta^{13}C$ record (blue) in both panels.

4.5.4.2. Oxygen Isotopes & SST's

With the exception of Tree 78, the bandpassed (8-10 years) $\delta^{18}O$ values of all trees are significantly correlated with the PDO. Tree 82 exhibits the strongest correlation (r = 0.64) (Figure 49). Although $\delta^{18}O$ reconstructions contain peaks of high frequency (3-5 year) variability, none of the trees show a significant correlation between $\delta^{18}O$ and ENSO (Tables 23 and 24). Tree 20 does yield a correlation with El Nino when an 8-10 year bandpass is passed over the two datasets, but does not show this correlation in the 3-5 year band (Tables 23 and 24). As for $\delta^{13}C$, the $\delta^{18}O$ records of trees 88 and 20 also show a significant correlation with both the PDO and the NAO indices.

Table 21. Table of correlation coefficients between 8-10 year bandpass filtered isotope reconstructions and SST anomalies. Note that 'TNA' represents SST anomalies from a gridbox (5-20°North, 60-30°West) in the tropical North Atlantic.

			$\delta^{18}O$		
DATASET	TREE 67	TREE 78	TREE 88	TREE 82	TREE 20
PDO	**0.45**	0.20	**0.25**	**0.64**	**0.40**
TNA	0.00	-0.09	-0.12	0.02	-0.05
NINO 3.4	-0.05	-0.07	0.15	-0.24	**-0.28**
NAO	0.05	0.14	-0.13	0.13	0.11

Bolding denotes r-values that are statistically significant at the $p<0.05$ value.

Table 22. P-values for correlation coefficients in Table 21.

			$\delta^{18}O$		
DATASET	TREE 67	TREE 78	TREE 88	TREE 82	TREE 20
PDO	0.0005	0.1445	0.0576	0.0000	0.0021
TNA	0.9851	0.5286	0.3733	0.8757	0.7020
NINO 3.4	0.7036	0.6062	0.2755	0.0801	0.0366
NAO	0.5529	0.1071	0.1450	0.1300	0.1842

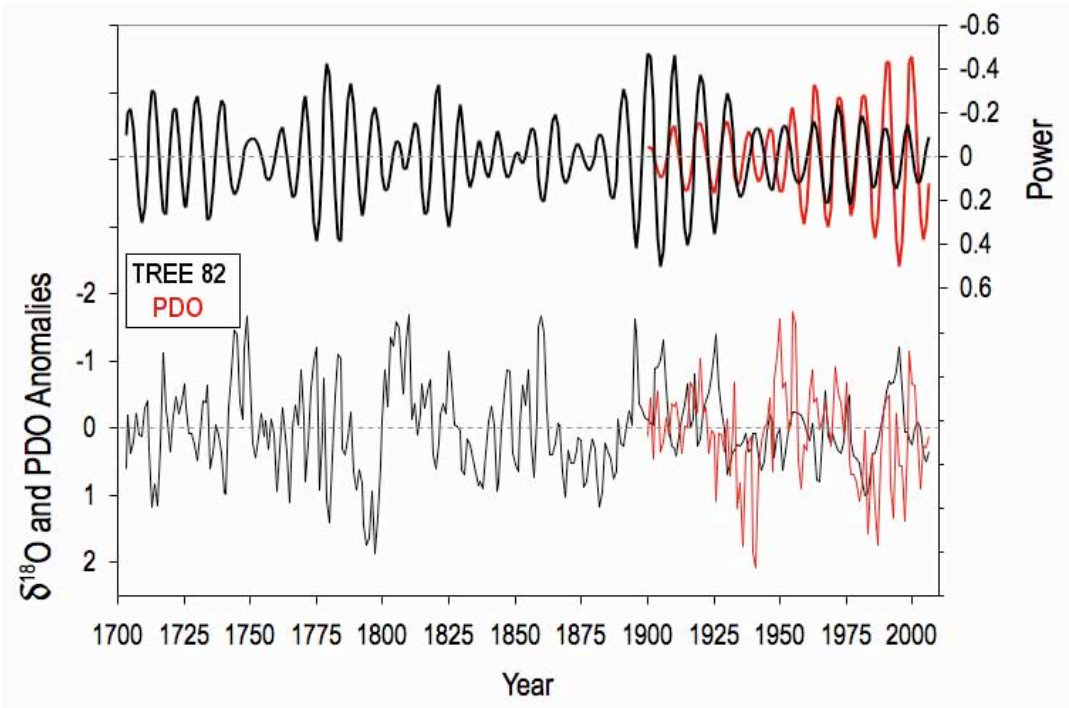

Figure 49. Unfiltered $\delta^{18}O$ data from Tree 82 is plotted against the PDO index in the bottom panel. The top panel is a graph of the $\delta^{18}O$ and PDO passed through an 8-10 year bandpass filter to isolate this variability.

Table 23. Table of correlation coefficients between 3-5 year bandpass filtered isotope reconstructions and SST anomalies. Note that 'TNA' represents SST anomalies from a gridbox (5-20°North, 60-30°West) in the tropical North Atlantic.

			$\delta^{18}O$		
DATASET	TREE 67	TREE 78	TREE 88	TREE 82	TREE 20
PDO	-0.29	-0.15	0.11	**0.29**	-0.15
TNA	0.00	0.00	-0.21	0.05	-0.09
NINO 3.4	-0.15	-0.11	-0.14	0.18	0.04
NAO	0.05	0.05	**0.26**	0.08	**0.27**

Bolding denotes r-values that are statistically significant at the $p<0.05$ value.

Table 24. P-values for correlation coefficients in Table 23.

			$\delta^{18}O$		
DATASET	TREE 67	TREE 78	TREE 88	TREE 82	TREE 20
PDO	0.0311	0.2553	0.4123	0.0284	0.2540
TNA	0.9773	0.9761	0.1129	0.6959	0.5197
NINO 3.4	0.2690	0.4347	0.2977	0.1950	0.7604
PDO	0.5556	0.5592	0.0021	0.3316	0.0014

4.6.6.2 Time-dependent Variability

Because Tree 67 is the oldest tree examined and contains the longest reconstruction, I examine the changing nature of its periodicity through time. As shown previously, both the carbon and oxygen isotopic reconstructions of this tree contain strong power in the 8-10 year frequency band and show moderate correlation with the PDO (r = 0.38 and 0.45, respectively). This decadal periodicity is enhanced in the earlier portion of the record (Figure 50) and is strongest between ~1530 and 1600 and between 1660 and 1720. Lower frequency (20-24 year) periodicity appears to be dominant after about 1810 A.D. The same patterns do not appear in the other trees, though their temporal ranges are short (<300 years). A wavelet analysis of the $\delta^{13}C$ record quantifies these impressions, showing that a lower frequency pattern is more dominant during the late 19th and all of the 20th century (Figure 51).

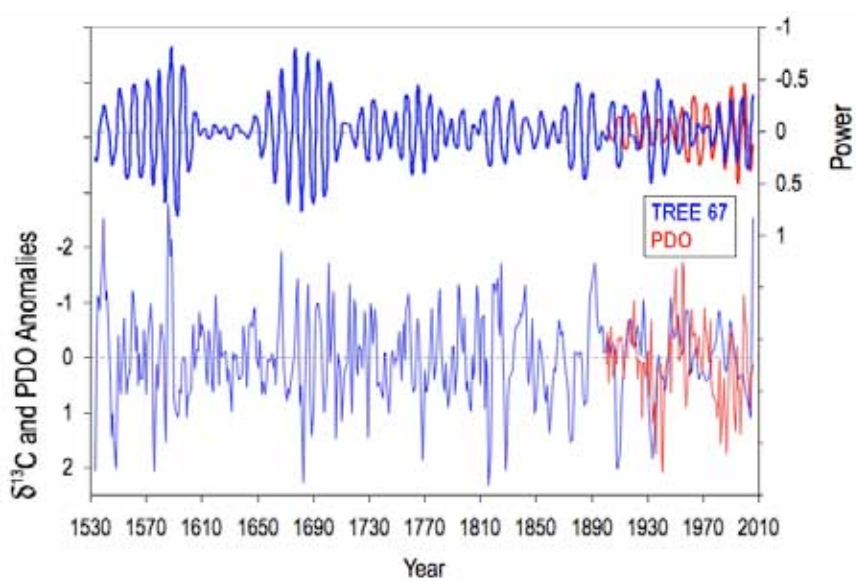

Figure 50. Unfiltered $\delta^{13}C$ data from tree 67 is plotted against the PDO index in the bottom panel. The top panel is a graph of the $\delta^{13}C$ and PDO passed through an 8-10 year bandpass filter to isolate this variability.

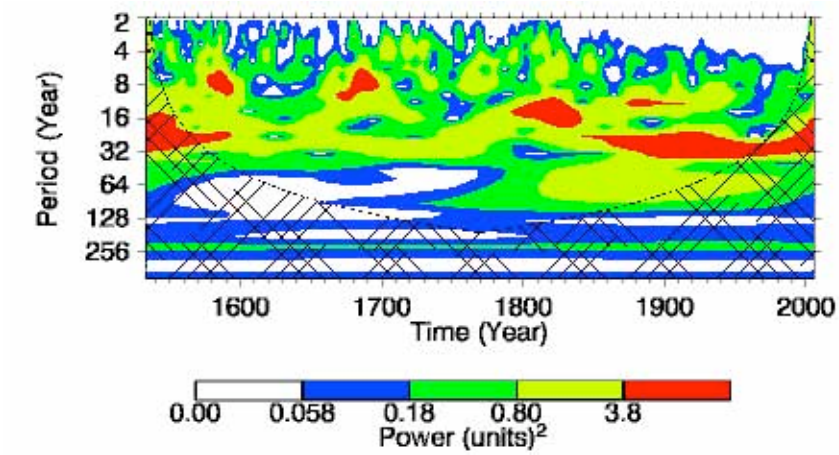

Figure 51. Wavelet of $\delta^{13}C$ record for tree 67. Power colored in red is significant.

4.7 Discussion

4.7.1 Evaluation of the Proxies

Carbon Isotopes

Because of the error corrections required in the chronologies for each of these 5 trees, as well as the serious imperfections of the instrumental climate records, evaluation of the fidelity of $\delta^{13}C$ and $\delta^{18}O$ as recorders of annual climate variability is impossible here. On longer time scales, however, such an assessment is possible. For example, I have clearly shown that all five $\delta^{13}C$ datasets faithfully record the Suess effect. This observation of a common trend, provides important confirmation for our corrected age model that was established using ^{14}C signals on only one of the five target trees. The low frequency (50 yr) inter-tree correlation is robust (r = 0.6), suggesting that despite internal canopy dynamics and variable settings with regard to local hydrology, there is a shared measure of climate variability between trees from different locations.

One of the most notable features of the isotopic time series is the inter-tree variability on higher frequency time-scales. Although some of the tree-to-tree differences can be ascribed to errors in the time-scale, some differences between trees should be expected. Leavitt and Long (1986) note that a variety of environmental influences such as tree shading and location within the canopy can result in scatter of up to 1-2‰ of $\delta^{13}C$ between trees. Saurer et al. (2000) found little inter-tree correlation of $\delta^{13}C$ on small time scales between *Abies alba* trees in montane Switzerland and attributed this observation to site-specific conditions. For example, when a tree is exposed to more light, photosynthetic capacity is increased while stomatal conductance remains unchanged. This results in a lower CO_2 concentration inside the leaf, resulting in less isotopic discrimination and a more positive $\delta^{13}C$. Thus, different degrees of shading would be expected to produce different $\delta^{13}C$ values. Broadmeadow and Griffiths (1993) exposed *Picea abies* trees to increased photon flux density and found a resulting increase in the $\delta^{13}C$ that correlated with increased growth. The effect of light on the $\delta^{13}C$ ratio in trees can also result in a 'juvenile effect' because younger trees are more shaded and show a progressive increase of as much as 2‰ in $\delta^{13}C$ within the first few years of tree life as they begin to emerge (Francey et al., 1985). Such site-specific conditions create inter-tree variability and can mask the climate signal. However, the standard deviation between carbon isotope records in the Madre de Dios is 0.64‰ which is actually quite robust given that internal canopy dynamics can result in changes of up to 3‰. However, no long term climatic trend is observed in the records, thus making it difficult to differentiate

between climate and internal dynamics. Comparisons between individual detrended tree ring records and climate revealed a significant correlation with wet season precipitation, such that a lower $\delta^{13}C$ value was associated with increased rainfall ($r = -0.50$) in 4 of the 5 trees. This suggests precipitation variability is being captured despite the presence of site-specific dynamics. However, this relationship is strongest when 5 year running means of the isotopic records are compared with precipitation, undoubtedly related to uncertainties in the chronologies of each tree.

Oxygen Isotopes

Despite low inter-tree correlation, regression of wet season precipitation against five year running averages of each of the five $\delta^{18}O$ tree records resulted in a significant correlation ($r = -0.6$, $p<.05$). This suggests that despite variability due to biologic and ecologic effects, some precipitation variability may be recorded by the $\delta^{18}O$ in these tree rings. The $\delta^{18}O$ in tree cellulose has previously been shown to be well correlated with the $\delta^{18}O$ in precipitation (Burk and Stuiver, 1981; Saurer et al., 2000; Evans and Schrag, 2004; Poussart et al., 2004; Poussart and Schrag, 2005; Anchukaitis et al., 2008; Evans, 2007; Liu et al., 2008) or water available during the growing season in both temperate and tropical tree species. However, the correlation of $\delta^{18}O$ between the individual tree records from this study is extremely low on annual time scales ($r = 0.10$) and is not greatly improved when using an eight-year running mean ($r = 0.15$). The combination of error adjustments to the isotope chronologies as well as tree-specific conditions (e.g. rooting depth), suppress the common climate signal on

annual and high frequency time scales. One way to overcome the error adjustments necessary in trees with poorly visible or even non-existent rings is to try to track the isotopic signal of the annual cycle of rainfall by making highly resolved intra-ring isotopic measurements. Evans and Schrag (2004) first proposed and confirmed the validity of this technique by reproducing 10 annual cycles in 10 trees rings of white pine in western Massachusetts. They also demonstrated the utility of this method to develop age models for tropical trees in multiple environs with no visible rings and related their age-constrained isotope records to climate. Subsequent studies have employed this technique (Poussart et al., 2004 and 2006; Anchukaitis et al., 2008) to examine the relationship between climate and isotopes from tree ring cellulose. However, there are several key places at which fractionation can occur to disjoint the relationship between these isotopes and climate. First, it is possible that soil water may not accurately reflect the isotopic composition of meteoric water, due to either the effect of evaporation which can create an isotopic gradient with increasing soil water depth or the fact that waters at depth may be older and possess a distinct isotopic signature (Saurer et al., 2000; Evans and Schrag, 2004). Second, isotopic enrichment can occur in the leaf water due to transpiration. This effect can be dramatic (up to 20‰) in places where relative humidity is low (Dongmann et al., 1974). Finally, some exchange can occur between xylem water that is isotopically depleted and leaf water during the formation of cellulose. This effect can actually work to reduce the effect incurred via transpiration at the leaf surface. These biologic effects can vary from tree to tree or with the age of a tree, thus masking the climate signal. Rooting depth could also affect the oxygen

isotopic ratio of trees, if for example, during drier years, trees with deep roots utilized water stored from the previous season. Nepstad et al. (2002) found that trees exposed to severe drought conditions in rainforest in central Brazil did not show a corresponding reduction in leaf drought stress during the first year. Soil water at depths greater than two meters was also unaffected, suggesting that trees may be drawing on the reserves at depth during times of drought. This observation, as well as the fact that in some species, photosynthates produced late in the season can be stored and utilized during the formation of earlywood in the following year, can serve to mix the climate signal from year-to year (Jacoby and D'Arrigo, 1990). Inter-tree variations may also be explained by the age differences in trees, such that older trees may utilize deeper root systems during times of drought until new rainfall can saturate the shallower roots.

Because the trees utilized in this analysis cannot be accurately dated to within 1 year, I cannot definitively conclude that a relationship exists between tree ring isotopes and climate on annual time scales. Because the error-adjusted chronology is only accurate to within approximately +/- 5 years, it is only meaningfully to discuss the relationship between climate and the isotope records at lower frequencies. Despite this error, there are several key points about the tree ring records that are certain; 1) rings formed near the pith are older than rings formed near the bark, 2) rings formed near the pith are thicker and better defined making ring counting more accurate near the pith, and 3) the outer rings on older trees are difficult to count leading to increasing counting error with increasing age of tree. By utilizing trees of different ages, I can minimize this problem, though it would of course be ideal to utilize perfectly dated trees as

seen in tree species *C. odorata* (see Chapter 3). Barring this, however, trends in the low frequency variability of the *D. micrantha* records may be discussed.

4.7.2 Evaluation of Low Frequency Trends

A dominant interannual and decadal periodicity persists in both the oxygen and carbon isotopic records from all five trees. The records of the five trees from the Madre de Dios identify a persistent 8-10 year periodicity present throughout the length of each record, though the inter-tree variability is still high at low frequencies, though this too could be a consequence of the error correction associated with the adjusted chronology. The oldest tree (473 adjusted years) identifies this decadal scale variability to be more dominant during the early part of the record, with a shift toward more multidecadal (20-24 year) variability during the 20th century. Zhou and Lau (2001) document a 24-28 year oscillation in rainfall over the Amazon basin beginning in 1980, showing a decrease in rainfall from the northwest to the southeast due to a southwards shift of the ITCZ. They link this mode to changes in the SST field from the tropical North Atlantic. However, this is accompanied by an observed trend of decreasing rainfall over tropical southeastern South America. Marengo (2004) also observed a general trend of decreasing precipitation over the Amazon basin between 1928 and 2000, though this is not observed in the isotopic records from this study. If precipitation did decrease significantly, I would expect an increase in the $\delta^{18}O$ of both precipitation and of the trees. Likewise, a drying trend would be expected

to produce a change in the $\delta^{13}C$. But such a trend would be masked by the $\delta^{13}C$ decrease due to the Suess effect between ~1900 and 2006.

Decadal scale variability has been linked to rainfall over parts of the Amazon basin in several studies (e.g. Nobre and Shukla, 1996; Dettinger et al., 2000; Robertson and Mechoso, 1998). A warm period beginning in 1976 and continuing through 2000 has been detected in the Pacific which resulted in more frequent El Nino events (Mantua et al., 1997). Though a relationship between decreased rainfall in the Amazon basin and El Nino has been identified in many studies (Liebmann and Marengo, 2001; Botta et al., 2002; Foley et al., 2002), rainfall in the northern part of the basin appears more sensitive to ENSO events than the southeastern basin.

Tropical Atlantic SST's also display decadal scale variability that is consistent with an 8-10 year periodicity. The contrast in temperature between the tropical North and South Atlantic drives meriodonal shifts in the location of the Intertropical Convergence Zone (ITCZ) which work to create this decadal scale variability (e.g. Nobre and Shukla, 1996; Marengo, 2004). An 8-10 year bandpass filter applied to both the carbon and oxygen isotopic records from each of the 5 trees results in a significant correlation with the decadal scale variability of the PDO. However, 2 of the 5 trees also show relationship with the variability identified in the tropical North Atlantic. This may suggest that variability from both the Atlantic and Pacific contribute to the patterns of periodicity recorded in the tree rings.

Conclusions, Outlook and Future Research

Each component of this study has investigated the utility of tree rings as a climate proxy in tropical South America. The presence of verifiably annual growth rings has been investigated using both bomb ^{14}C dating for tree species *Cedrela odorata* and *Dipteryx micrantha* and cross-dating for species *Hymenaea courbaril, Myroxylon balsamum, Tabuia serratifolia,* and *Ceiba pentandra*. Results from these analyses verify that annual growth rings form in all species and they therefore hold great significance as paleoclimatic indicators. Ring growth in *Ceiba pentrandra* and *Cedrela odorata* has shown a ($r = 0.37$, and 0.42, respectively) correlation with wet season precipitation, and *Hymenaea courbaril* shows a strong correlation ($r = 0.68$) with January river discharge. A 189 year (1817-2006) ring width record from species *Cedrela odorata* shows a sensitivity to extreme drought conditions such that historically documented drought years are associated with abnormally low growth in the trees. This suggests that trees from this region are dependent on rainfall during the current season to stimulate growth, and that, though reserves of photosynthate or water may be stored within the tree, the trigger for growth in these trees occurs during the current wet season.

The carbon and oxygen isotopic measurements in 5 trees from the species *Dipteryx micrantha* demonstrate that site-specific conditions can greatly influence the growth of this species. This is further demonstrated by a low inter-tree growth correlation ($r < 0.1$). The variability of the oxygen isotopic measurements in these trees may attributed to variations in rooting depth between older and younger trees and the preferential use of deeper roots during times of drought.

However, little information is available on the rooting behavior of this species and further data is necessary to definitively conclude that site-specific conditions dominate the isotopic signal. One reason for this is due to the error-adjustment necessary in the chronology for this species, such that 1 ring can only be attributed to 1 year +/- an error correction. This limits the degree to which I can compare the isotopic signals between trees on annual time scales, however long term trends may be compared. The Suess effect is clearly evident in the carbon isotopic records of all 5 trees, demonstrating a decrease of 1.6‰ between 1900 and 2006. There is a measure of inter-tree variability in carbon isotopic records as well, however, this is expected due to canopy and tree specific changes in light conditions that affect the photosynthetic capacity of trees. The correlation between trees is significant ($r = 0.46$), however, and a comparison between 5 year running averages of the isotope records and climate reveals a relationship between wet season precipitation and the $\delta^{13}C$ in tree rings ($r = -0.50$). The oldest tree is an error adjusted 478 year long record (1533-2006) and no long term trends in climate are detected over this period. However, periodicity in both oxygen and carbon isotopic data reveal dominant 8-10 year and 3-5 year peaks which can be related to both the PDO and tropical North Atlantic SST anomalies. The oldest tree does show a shift in variability such that multidecadal (20-24 year) frequencies are increasingly dominant during the 20th century.

These data collectively demonstrate that tropical trees may be used as sources of paleoclimatic information. Using a combination of ring width and isotopic measurements, I confirm that a relationship exists between climate and these variables and used this knowledge to extend our record of climate for this

region. However, the issues associated with the chronology of *Dipteryx micrantha* severely limit the resolution at which conclusions may be drawn about climate. This, combined with the high degree of isotopic variability between trees, prevents me from definitively assigning isotopic values to individual years. However, the clear annual rings of *Cedrela odorata* hold great promise for this type of reconstruction. Because the bomb ^{14}C dating accurately matched counted rings with absolute years, I am currently running isotopic measurements on trees from this species. Furthermore, the fact that the growth behavior of *Cedrela odorata* shows relatively strong inter-tree correlation ($r = 0.50$) is encouraging and suggests that growth during each year is well connected to precipitation. Furthermore, I have demonstrated that dendrochronologic reconstructions based on ring width measurements are possible in this region. The *Cedrela odorata, Ceiba pentandra*, and *Hymenaea courbaril* chronologies all demonstrate coherence between trees from different regions and a significant relationship with climate. This greatly enhances the possibilities for paleoclimatic reconstruction in this region, particularly because ring width counting is a relatively inexpensive and rapid process. Increasing the number of trees for each species would greatly enhance the validity of the chronologies and potentially enable a reconstruction of precipitation to be developed. The limiting factor in this process is finding locations where trees have already been cut, as *in-situ* coring is not viable for most of these species.

There are also numerous other species that show great promise for dendrochronologic reconstruction due to their clear ring structures. These species were examined and ring widths measured, but were not included in

these analyses because <5 trees of each species were collected. These include, but are not limited to, *Amburana cearensis, Bertholletia excelsa, Hura crepitans, Copaifera reticulata, Jacaranda copaia, Couratari guianensis, Clarisia racemosa, Parkia pendula,* and *Manilkara bidentata*. It is clear that tree ring study in the tropics is both possible and viable, and the results of this work show great potential for continued dendroclimatic exploration in this region.

References

Aceituno, P., 1988, On the functioning of the southern oscillation in the South American sector, part I: surface climate, *Monthly Weather Review*, v. 116, p. 505-524.

Alvarado, C. R . Alvarado, C.A. and Mendoza, O.O. 2003. *Ceiba pentandra*. Tropical tree seed manual. http://www.rngr.net/Publications/ttsm/Folder.2003-07-11.4726/.

Anchukaitis, K.J., Evans, M.N., Lange, T., Smith, D.R., Leavitt, S.W., and Schrag, D.P., 2008, Consequences of a rapid cellulose extraction technique for oxygen isotope and radiocarbon analyses, *Analytical Chemistry*, p. 6.8A-6.8G.

Anchukaitis, K.J., Evans, M.N., Wheelright, N.T., and Schrag, D.P., 2008, Stable isotope chronology and climate signal calibration in neotropical montane cloud forest trees, *Journal of Geophysical Research*, v. 113, doi:10.1029/2007JG000613.

Anderson, W.T., Bernasconi, S.M., McKenzie, J.A., and Saurer, M., 1998, Oxygen and carbon isotopic record of climate variability in tree-ring cellulose (*Picea abies*): An example from central Switzerland (1913-1995), *Journal of Geophysical Research*, v. 103, p. 31,625-31,636.

Argollo, J., Soliz, C., and Villalba, R., 2004, Potencialidad dendrocronologica de *Polylepis tarapacana* en los Andes Centrales de Bolivia, *Ecologia en Bolivia*, v. 39, p. 5-24.

Baldock, J.A., and Smernik, R.J., 2002, Chemical composition and bioavailability of thermally altered *Pinus resinosa* (Red pine) wood, *Organic Geochemistry*, v. 22, no. 9, p. 1093-1109.

Becker, P., Lee, L.W., Rothman, E.D., and Hamilton, W.D., 1985, Seed predation and the coexistence of tree species: Hubbell's model revisited, *Oikos*, v. 44, p. 382-390.

Benner, R., Fogel, M.I., Sprague, E.K., and Hodson, R.E., 1987, Depletion of ^{13}C in lignin and its implications for stable carbon isotope studies, *Nature*, v. 328, p. 708-710.

Borella, S., Leuenberger, M., Saurer, M., Siegwolf, R., 1998, Reducing uncertainties in $\delta^{13}C$ analysis of tree rings: Pooling, milling, and cellulose extraction, *Journal of Geophysical Research*, v. 103, no. D16, p. 19519-19526.

Botta, A., Ramankutty, N., and Foley, J.A., 2002, Long-term variations of climate and carbon fluxes over the Amazon Basin, *Geophysical Research Letters*, v. 29, no. 9, p. 3301-3304.

Brendel, P., Iannetta, P.P.M., and Stewart, D., 2000, A rapid and simple method to isolate pure alpha-cellulose, *Phytochemical Analysis*, v. 11 (1), p. 7-10.

Brienen, R.J.W., and Zuidema, P.A., 2005, Relating tree growth to rainfall in Bolivian rain forests: a test for six species using tree ring analysis, *Oecologia*, v. 146, p. 1-12.

Broadmeadow, M.S.J., and Griffiths, H., 1993, Carbon isotope discrimination and the coupling of CO_2 fluxes within forest canopies, in *Stable Isotopes and Plant Carbon-Water Relations*, eds, Ehleringer, J.R., Hall, A.E., and Farquhar, G.D., Academic Press, San Diego, p. 109-129.

Burk, R.L., and Stuiver, M., 1981, Oxygen isotope ratios in trees reflect mean annual temperature and humidity, *Science*, v. 27, no. 4489, p. 1417-1419.

Chen, M., Xie, P., Janowiak, J.E., and Arkin, P.A., 2002, Global land precipitation: A 50-yr monthly analysis based on gauge observations, *Journal of Hydrometeorology*, v. 3, p. 249-266.

Cherubini, P., Gartner, B., Tognetti, R., Braker, O.U., Schoch, W., and Innes, J.L., 2003, Identification, measurement and interpretation of tree rings in woody species from Mediterranean climates, *Biological Review*, v. 78, p. 119-148.

Chudnoff, M. 1984. Tropical timbers of the world. USDA Forest Service. Ag. Handbook No. 607. http://www2.fpl.fs.fed.us/TechSheets/Chudnoff/TropAmerican/html_files/zantho1new.html.

Cintra, R., 1997, A test of the Janzen-Connell model with two common tree species in Amazonian forest, *Journal of Tropical Ecology*, v. 13, p.641-658.

Cintra, R., 1997, Leaf litter effects on seed and seedling predation of the palm *Astrocaryum murumuru* and the legume tree *Dipteryx micrantha* in Amazonian forest, *Journal of Tropical Ecology*, v. 13, no. 5, p. 709-725.

Cook, E.R, and Peters, K., 1980, The smoothing spline: a new approach to standardizing forest interior tree-ring width series for dendroclimatic studies, *Tree-Ring Bulletin*, v. 41, p. 45-53.

Costa, M.H., and Foley, J.A., 1997, A comparison of precipitation datasets for the Amazon Basin, *Geophysical Research Letters*, v. 25, p. 155-158.

Czimczik, C.I., Preston, C. M., Schmidt, M.W.I., Werner, R.A., and Schulze, E.D., 2002, Effects of charring on mass, organic carbon, and stable carbon isotope composition of wood, *Organic Geochemistry*, v. 33, p. 1207-1223.

Dansgaard, W., 1964, Stable isotopes in precipitation, *Tellus*, v. 16, p. 436-468.

D'Arrigo, R., Villalba, R., and Wiles, G., 2001, Tree-ring estimates of Pacific decadal climate variability, *Climate Dynamics*, v. 18, p. 219-224.

D'Arrigo, R., Wilson, R., Palmer, J., Krusic, P., Curtis, A., Sakulich, J., Bijaksana, S., Zulaikah, S., and Ngkoimani, L.O., 2006, Monsoon drought over Java, Indonesia, during the past two centuries, *Geophysical Research Letters*, v. 33, doi: 10.1029/2005GL025465.

DaSilva, Samia, 2008, Personal communication, October 21.

Detienne, P., 1989, Appearance and periodicity of growth rings in some tropical woods, *IAWA Bulletin*, v. 10, p. 123-132.

Dettinger, M.D., Battisti, D.S., Garreaud, R.D., McCabe Jr., G.J., and Bitz, C.M., 2000, Interhemispheric effects of interannual and decadal ENSO-like climate variations on the Americas, *In Present and Past Interhemispheric Climate Linkages in the Americas and their Societal Effects*, ed. V. Markgraf, Cambridge University Press, Cambridge, U.K., p. 1-16.

Doan, T.M., 2004, Extreme weather events and the vertical microhabitat of rain forest anurans, *Journal of Herpetology*, v. 38, no. 3, p. 422-425.

Dongmann, G., 1976, The contribution of land photosynthesis to the stationary enrichment of ^{18}O in the atmosphere, *Radiation and Environmental Biophysics*, v. 11, no. 3, p. 219-225.

Dunisch, O., Ribeiro, M.V., and Bauch, J., 2003, Dendroecological investigations on *Swietenia macrophylla* King and *Cedrela odorata* (Meliaciae) in the central Amazon, *Trees*, v. 17, p. 244-250.

Emanuel, K., 2005, Increasing destructiveness of tropical cyclones over the past 30 years. *Nature*, v. 436, p. 686-688.

Enquist, B.J., and Leffler, A.J., 2001, Long-term tree ring chronologies from sympatric tropical dry-forest trees: individualistic responses to climatic variation, *Journal of Tropical Ecology*, v. 17, p. 41-60.

Epstein, S., 1995, The isotope climatic records in the Allerod-Bolling-Younger Dryas and post-Younger Dryas events, *Global Biogeochemical Cycles*, v. 9, p. 557-563.

Evans, M.N., 2007, Toward forward modeling for paleoclimatic proxy signal calibration: A case study with oxygen isotopic composition of tropical woods, *Geochemistry, Geophysics and Geosystems*, v. 8, no. 7, doi:10.1029/2006GC001406.

Evans, M.N., 2008, A reactor for high temperature pyrolysis and oxygen isotopic analysis of cellulose via induction heating, *Rapid Communications in Mass Spectrometry*, v. 22, p. 2211-2219.

Evans, M.N., 2008, High resolution tropical isotope dendroclimatology: prospects and challenges, *in*: G.H. Schleser (ed.), *Stable isotope dendroclimatology -- Physiology, Systematics, Chronologies and Instrumentation*, Elsevier.

Evans, M.E., and Schrag, D.P., 2004, A stable isotope-based approach to tropical dendroclimatology, *Geochimica et Cosmochimica* Acta, v. 68, no. 16, p. 3295-3305.

Farquhar, G.D., and Sharkey, T.D., 1982, Stomatal conductance and photosynthesis, *Annual Review of Plant Physiology*, v. 33, p. 317-345.

Farquhar, G.D., and Wong, S.C., 1984, An empirical model of stomatal conductance, *Australian Journal of Plant Physiology*, v. 11, p. 191–210.

Farquhar, G.D., Ehleringer, J.R., and Hubick, K.T., 1989, Carbon isotope discrimination and photosynthesis, *Annual Review of Plant Physiology and Plant Molecular Biology*, v. 40, p. 503-537.

February, E.C., and Stock, W.D., 1999, Declining trend in the $^{13}C/^{12}C$ ratio of atmospheric carbon dioxide from tree rings of South African *Widdringtonia cedarbergensis, Quaternary Research*, v. 52, i. 2, p. 229-236.

Feng X., and Epstein, S., 1994, Climatic implications of an 8000-year hydrogen isotope time series from bristlecone pine trees, *Science*, v. 265, p. 1079-1081.

Fichtler E., Trouet, V., Beeckman, H., Coppin, P., and Worbes, M., 2004, Climate signals in tree rings of *Burkea Africana* and *Pterocaprus angolensis* from semiarid forests in Namibia, *Trees-Structure and Function*, v. 18, no. 4, p. 442-451.

Flanagan, L.B., Phillips, S.L., Ehleringer, J.R., Lloyd, J., and Farquhar, G.D., 1994, Effect of changes in leaf water oxygen isotopic composition on discimination against $C^{18}O^{16}O$ during photosynthetic gas exchange, *Australian Journal of Plant Physiology*, v. 21, p. 221-234.

Foley, J.A., Botta, A., Coe, M.T., and Costa, M.H., El Nino-Southern oscillation and the climate, ecosystems and rivers of Amazonia, *Global Biogeochemical Cycles*, v. 16, no. 4, p. 7901-7916.

Francey, R.J., and Farquhar, G.D., 1982, An explanation of $^{13}C/^{12}C$ variations in tree rings, *Nature*, v. 297, p. 28-30.

Francey, R.J., Gifford, R.M., Sharkey, T.D., and Weir, B., 1985, Physiological influences on carbon isotope discrimination in huon pine (*Lagarostrobos franklinii*), *Oecologia*, v. 66, no. 2, p. 211-218.

Friedli, H., Lotscher, H., Oeschger, H., Siegenthaler, U., and Stauffer, B., 1986, Ice core record of the $^{13}C/^{12}C$ ratio of atmospheric CO_2 in the past two centuries, *Nature*, v. 324, p. 237-238.

Fritts, H.C., Mosimann, J.E., and Bottoff, C.P., 1969, A revised computer program for standardizing tree-ring series, *Tree-Ring Bulletin*, v. 29, p. 15-20.

Fritts, H.C., 1976, Tree rings and climate, Academic, London.

Fu, R., Zhu, B., and Dickinson, R.E., 1999, How do atmosphere and land surface influence seasonal changes of convection in the tropical Amazon? *Journal of Climate*, v. 12, i. 5, p. 1306-1321.

Garreaud, R.D., 1999, Cold air incursions over subtropical and tropical South America: a numerical case study, *Monthly Weather Review*, v. 127, p. 2823-2853.

Gat, J.R., 1996, Oxygen and hydrogen isotopes in the hydrologic cycle, *Annual Review of Earth and Planetary Science*, v. 24, p. 225-262.

Gaudinski, J.B., Dawson, T.E., Quideau, S., Schuur, E.A.G., Roden, J.S., Trumbore, S.E., Sandquist, D.R., Oh, S.W., and Wasylishen, R.E., Comparative analysis of cellulose preparation techniques for use with ^{13}C, ^{14}C, and ^{18}O isotopic measurements, *Analytical Chemistry*, v. 77, no. 22, p. 7212-7224.

Gebrekirstos, A., Worbes, M., Teketay, D., Fetene, M., Mitlohner, R., 2009, Stable carbon isotope ratios in tree rings of co-occurring species from semi-arid tropics in Africa: Patterns and climatic signals, *Global and Planetary Change*, v. 66, i. 3-4, p. 253-260.

Ghil, M., Allen, M.R., Dettinger, M.D., Ide, K., Kondrashov, D., Mann, M.E., Robertson, A.W., Saunders, A., Tian, Y., Varadi, F., and Yiou, P., 2002, Advanced spectral methods for climatic time series, *Review of Geophysics*, v. 40, p. 301-341.

Goldenberg, S.B., Landsea, C.W., Mestas-Nunez, A.M., and Gray, W.M., 2001, The recent increase in Atlantic hurricane activity: causes and implications, *Science*, v. 293, p. 474-479.

Green, J.W., 1963, Methods in carbohydrate chemistry, Academic Press: New York, v. 3, p. 9-21.

Grissino-Mayer, H. D., 2001, Evaluating crossdating accuracy: a manual and tutorial for the computer program COFECHA, *Tree Ring Research*, v. 57, i. 2, p. 209-221.

Harden, J.W., Neff, J.C., Sandberg, D.VF., Tertsky, M.R., Ottmar, R, Gleixner, G., Fries, T.L., and Manies, K.L., 2004, Chemistry of burning the forest floor during the FROSTFIRE experimental burn, interior Alaska, 1999, *Global Biogeochemical Cycles*, v. 18, p. 34-41.

Holmes, R.L., 1983, Computer-assisted quality control in tree-ring dating and measurement, *Tree Ring Bulletin*, v. 43, p. 69-78.

Helle, G., Schleser, G.H., and Brauning, A., 2002, Climate history of the Tibetan plateau for the last 1500 years as inferred from stable carbon isotopes in tree-rings, *Proceedings of the International Conference on the Study of Environmental Change Using Isotope Techniques*, IAEA CN-80-80, Vienna, p. 301-311.

Herweijer, C., Seager, R., Cook, E.R., and Geay, J.E., 2007, North American droughts of the last millennium from a gridded network of tree-ring data, *Journal of Climate*, p. 1-53.

Hoper, S.T., McCormac, F.G., Hogg, A.G., Higham, T.F.G., and Head, M.J., 1998, Evaluation of wood pretreatments on oak and cedar, *Radiocarbon*, v. 40, p. 45-50.

Hua, Q., and Barbetti, M., 2004, Review of tropospheric bomb ^{14}C data for carbon cycle modeling and age calibration purposes, *Radiocarbon*, v. 46, p. 1273-1298.

Hurrell, J.W., 1995, Decadal trends in the North Atlantic Oscillation: regional temperature and precipitation, *Science,* v. 269, no. 5224, p. 676-679.

Iwasa, Y., and Cohen, D., 1989, Optimal growth schedule of a perennial plant, *American Naturalist*, v. 133, p. 480-505.

Jacoby, G.C., 1989, Overview of tree-ring analysis in tropical regions, IAWA Bulletin, v. 10, p. 99-108.

Jacoby, G.C. and D'Arrigo, R.D., 1990, Teak (*Tectona grandis* L.F.), a tropical species of large-scale dendroclimatic potential. *Dendrochronologia*, v. 8, p. 83-98.

Jøker, D. and Salazar, R. 2000. *Ceiba pentandra*. Seed Leaflet, no. 22. http://www.dfsc.dk/seedleaflets.htm.

Keeling, C.D, A.F. Bollenbacher, and T.P. Whorf. 2005. Monthly atmospheric $^{13}C/^{12}C$ isotopic ratios for 10 SIO stations, in *Trends: A compendium of data on global change,* Carbon Dioxide Information Analysis Center, Oak Ridge National Laboratory, U.S. Department of Energy, Oak Ridge, Tenn., U.S.A.

Knoch, K., 1926, Die starke atmosphareische trubung im jahre 1926 in Venezuela*, Meterology Z.,* v. 43, p. 421.

Lang, G.E., and Knight, D. H., 1983, Tree growth, mortality, recruitment, and canopy gap formation during a 10-year period in a tropical moist forest, *Ecology*, v. 64, no. 5, p. 1075-1080.

Lara, A., and Villalba, R., 1993, A 3620-year temperature record from *Fitzroya cupressoides* tree rings in southern South America, *Science*, v. 260, p. 1104-1106.

Leavitt, S.W., and Long, A., 1986, Stable-carbon isotope variability in tree foliage and wood, *Ecology*, v. 67, no. 4, p. 1002-1010.

Leavitt, S.W., and Long, A., 1991, Seasonal stable-carbon isotope variability in tree rings: possible paleoenvironmental signals*, Chemical Geology*, v. 87, p. 59-70.

Leavitt, S.W., and Danzer, S.R., 1993, Methods for batch processing small wood samples to holocellulose for stable-carbon isotope analysis, *Analytical Chemistry*, v. 65, p. 87-89.

Leavitt, S.W., and Lara, A., 2002, South American trees show declining $\delta^{13}C$ trend, *Tellus B*, v. 46, i. 2, p. 152-157.

Liebmann,B., and Marengo, J.A., 2001, Interannual variability of the rainy season and rainfall in the Brazilian Amazon Basin, *Journal of Climate*, v. 14, i. 22, p. 4308-4318.

Lipp, J., and Trimborn, P., 1991, Long-term records and basin principles of tree ring isotope data with emphasis on local environmental conditions, *Palaoklimaforschung*, v. 6, p. 105-117.

Lisi, C.S., Pessenda, L.C.R., Tomazello, M., and Rozanski, K., 2001, ^{14}C bomb effect in tree rings of tropical and subtropical species of Brazil, *Tree-Ring Research*, v. 57, p. 191-196.

Liu, Y., Cai, Q., Liu, W., Yang, Y., Sun, J., Song, H., and Li, X., 2008, Monsoon precipitation variation recorded by tree-ring $\delta^{18}O$ in arid Northwest China since AD 1878, *Chemical Geology*, v. 252, i. 1-2, p. 56-61.

Loader, N.J., Robertson, I., Barker, A.C., Switzur, V.R., and Waterhouse, J.S., 2003, An improved technique for the batch processing of small wholewood samples to α–cellulose, *Chemical Geology*, v. 136, no. 3, p. 313-317.

Mann, M., and Lees, J., 1996, Robust estimation of background noise and signal detection in climatic time series, *Climate Change*, v. 33, p. 409-445.

Mann, M.E., Bradley, R.S., and Hughes, M.K., 1999, Northern hemisphere temperatures during the past millennium: inferences, uncertainties and limitations, *Geophysical Research Letters*, v. 26 (6), p. 759-762.

Mantua, N.J., and Hare, S.R., 2002, The Pacific Decadal Oscillation, *Journal of Oceanography*, v. 58, no. 1, p. 35-44.

Mauriax, A., 1967, Las cernes dans les bois tropicaux africains, nature et periodicite, *Bois et Forets des Tropiques*, v. 113, p. 3-14.

Marengo, J.A., 1984, Estudio sinoptico-climatico de los friajes (friagems) en la Amazonia peruana, *Revista Forestal del Peru*, v. 12, p. 55-80.

Marengo, J.A., 2004, Interdecadal variability and trends of rainfall across the Amazon basin, *Theoretical Applied Climatology*, v. 78, p. 79-96.

Marengo, J.A., 2005, Characteristics and spatio-temporal variability of the Amazon River Basin water budget, *Climate Dynamics*, v. 24, p. 11-12.

Marengo, J.A., 2006, On the hydrological cycle of the Amazon Basin: A historical review and current state-of-the-art, *Revista Brasileira de Meteorologia*, v. 21, p. 1-19.

Marengo, J.A., Cornejo, A., Satyamurty, P., Nobre, C., and Sea, W., 1997, Cold surges in tropical and extratropical South America: the strong event in June 1994, *Monthly Weather Review*, v. 125, p. 2759-2786.

Marengo, J.A., Nobre, C.A., Tomasella, J., Oyama, M.D., Sampaio de Oliveira, G., de Oliveira, R., Camargo, H., Alves, L., and Brown, I.F., 2008, The drought of Amazonia in 2005, *Journal of Climate*, v. 21, p. 495-516.

Marengo, J.A., Soares, W.R., and Saulo, C., 2002, Climatology of Low-Level Jet east of the Andes as derived from the NCEP reanalyses, *XII Congresso Brasileiro de Meteorologia*, Foz de Iguacu-PR, 6 p.

McCarroll, D., and Loader, N.J., 2004, Stable isotopes in tree rings, *Quaternary Science Reviews*, v. 23, i. 7-8, p. 771-801.

Meggers, B., 1994, Archaeological evidence for the impact of mega-Nino events on Amazonia during the past two millennia, *Climatic Change*, v. 28, p. 321-338.

Miller, D.L., Mora, C.I., Grissino-Mayer, H.D., Mock, C.J., Uhle, M.E., and Sharp, Z., 2006, Tree-ring isotope records of tropical cyclone, *Proceedings of the National Academy of Sciences of the United States of America (PNAS)*, v. 103, no. 39, p. 14294-14297.

Mooney, H.A., Field, C., Gulmon, S.L., and Bazzaz, F.A., 1981, Photosynthetic capacity in relation to leaf position in desert versus old-field annuals, *Oeceologia*, v. 50, p. 109-112.

Negron Juarez, R.I., Li, W., Fu, R., Fernandes, K., and Cardoso, A., 2009, Comparison of precipitation datasets over the tropical South American and African Continents, *Journal of Hydrometeorology*, v. 10, p. 289-299.

Nepstad, D.C., de Carvalho, C.R., Davidson, E., Jipp, P.H., Lefebvre, P.A., Negreiros, G.H., Da Silva, E.D., Stone, T.A., Trumbore, S.E., and Vieira, S., 1994, The role of deep roots in the hydrological and carbon cycles of Amazonian forests and pastures, *Nature*, v. 372, p. 666-669.

Nepstad, D.C., Verissimo, A., Alencar, A., Nobre, C., Lima, E., Lefebvre, P., Schlesinger, P., Potter, C., Moutinho, P., Mendoza, E., Cochrane, M., and Brooks, V., 1999, Large-scale impoverishment of Amazonian forests by logging and fire, *Nature*, v. 398, p. 505-508.

Nepstad, D.C., Moutinho, P., Dias-Filho, M.B., Davidson, E., Cardinot, G., Markewitz, D., Figueiredo, R., Vianna, N., Chambers, J., Ray, D., Guerreiros, J.B., Lefebvre, P., Sternberg, L., Moreira, M., Barros, L., Ishida, F.Y., Tohlver, I., Belk, E., Kalif, K., and Schwalbe, K., 2002, The effects of partial throughfall exclusion on canopy processes, aboveground production, and biogeochemistry of an Amazon forest, *Journal of Geophysical Research*, v. 107, no. D20, p. 5301-5318.

Ng, F.S.P., 1988, Forest tree biology, *Key Environments Malaysia*, Earl of Cranbrook, ed., Pergamon Press: Oxford, p. 102-125.

Nobre, P., and Shukla, J.,1996, Variations of sea surface temperature, wind stress, and rainfall over the Tropical Atlantic and South America, *Journal of Climate*, v. 9, p. 2464-2479.

Norton, D.A., Palmer, J.G., and Ogden, J., 1987, Dendroecological studies in New Zealand 1. An evaluation of tree age estimates based on increment cores, *New Zealand Journal of Botany*, v. 25, p. 373-383.

Nydal, R., and Lovseth, K., 1983, Tracing bomb ^{14}C in the atmosphere 1962-1980, *Journal of Geophysical Research*, v. 88, p. 3621-3642.

Pederson, N., Jacoby, G.C., D'Arrigo, R.D., Cook, E.R., Buckley, B.M., Dugarjav, C., Mijiddorj, R., 2000, Hydrometeorological reconstructions for Northeastern Mongolia derived from tree rings: 1651-1995*, *Journal of Climate*, v. 14, p. 872-880.

Percival, D.B., and Walden, A.T., 1993, Spectral analysis for physical applications, Cambridge University Press, New York, 583 p.

Phillips, O.L., Aragao, L., Lewis, S., Fisher, J., Lloyd, J., Lopez-Gonzales, G., Malhi, Y., Monteagudo, A., Peacock, J., Quesada, C.A., van der Heijden, G., Almeida, S., Amaral, I., Arroyo, L., Aymard, G., Baker, T., Banki, O., Blanc, L., Bonal, D., Brando, P., Chave, J., et al., 2009, Drought sensitivity of the Amazon rainforest, *Science,* v. 323, no. 5919, p. 1344-1347.

Poussart, P.F., Evans, M.E., and Schrag, D.P., 2004, Resolving seasonality in tropical trees: multi-decade, high-resolution oxygen and carbon isotope records from Indonesia and Thailand, *Earth and Planetary Sciences Letters*, v. 218, p. 301-316.

Poussart, P.F., and Schrag, D.P., 2005, Seasonally resolved stable isotope chronologies from northern Thailand deciduous trees, *Earth and Planetary Science Letters*, v. 235, i.3-4, p. 752-765.

Reinsch, C.H., 1967, Smoothing by spline functions, *Numerische Mathematik*, v. 10, no. 3, p. 177-183.

Rendle, B.J., 1969, World timbers, volume I (Europe and Africa), Ed. London: Ernest Benn Ltd. Publishers.

Reynolds, R.W., and Smith, T.M., 1994, Improved global sea surface temperature analyses using optimum interpolation, *Journal of Climate*, v. 7, p. 929-948.

Richey, J.E., Nobre, C., and Deser, C., 1989, Amazon river discharge and climate variability: 1903 to 1985, *Science*, v. 246, no. 4926, p. 101-103.

Richter, H.G., and Dallwitz, M.J., 2000, Commercial timbers: descriptions, illustrations, identification, and information retrieval, http://delta-intkey.com/wood/english/.

Ricker, M.. and Daly, D.C., 1997, Botánica económica en bosques tropicales. Editorial Diana, Mexico.

Robertson, I., Switsur, V.R., Carter, A.H.C., Barker, A.C., Waterhouse, J.S., Briffa, K.R., and Jones, P.D., 1997, Signal strength and climate relationships in $^{13}C/^{12}C$ ratios of tree ring cellulose from oak in east England, *Journal of Geophysical Research*, v. 102, p.19507-19519.

Robertson, A.W., and Mechoso, C.R., 2000, Interannual and interdecadal variability of the South Atlantic convergence zone, *Monthly Weather Review*, v. 128, p. 2947-2957.

Roden, J.S., Lin, G., and Ehleringer, J.R., 2000, A mechanistic model for the interpretation of hydrogen and oxygen isotope ratios in tree-ring cellulose, *Geochimica et Cosmochimica Acta*, v. 64, i. 1, p. 21-35.

Roden, J.S., and Ehleringer, J.R., 2007, Summer precipitation influences the stable oxygen and carbon isotopic composition of tree-ring cellulose in *Pinus ponderosa, Tree Physiology*, v. 4, p. 491-501.

Rozanski, K., Araguas-Araguas, L., and Gonfiantini, R., eds, 1993, Isotopic patterns in modern global precipitation, edited by P.K. Swart, K.C. Lohmann, J.A. McKenzie, and S. Savin, v. 78, *Climate change in continental isotopic records*: AGU Monographs.

Rudolf, B., and Schneider, U., 2005, Calculation of gridded precipitation data for the global land-surface using in-situ gauge observations, *Proceedings Second Workshop of the International Precipitation Working Group (IPWG),* Monterey, CA, EUMETSAT, p. 231-247.

Saleska, S.R., Didan, K., Huete, A.R., and da Rocha, H.R., 2007, Amazon forests green-up during 2005 drought, *Science*, v. 318, no. 5850, p. 612.

Saurer, M., Borella, S., Schweingruber, F., and Siegwolf, R., 1997, Stable carbon isotopes in tree rings of beech: climatic versus site-related influences, *Trees – Structure and Function*, v. 11, no. 5, p. 291-297.

Saurer, M., Cherubini, P., and Siegwolf, R., 2000, Oxygen isotopes in tree rings of *Abies alba*: the climatic significance of interdecadal variations, *Journal of Geophysical Research*, v. 105, p. 12,461-12,470.

SENAMHI, 2008, Servicio Nacional de Meteorologia e Hidrologia del Peru,

http://www.senamhi.gob.pe/.

Sheffield, J., Andreadis, K.M., Wood, E.F., and Lettenmaier, D.P., 2007, Global and continental drought in the second half of the 20th century: severity-area-duration analysis and temporal variability of large-scale events, *unpublished*, 50p.

Skomarkova, M.V., Vaganov, E.A., Mund, M., Knohl, A., Linke, P., Noerner, A., and Schulze, E.D., Inter-annual and seasonal variability of radial growth, wood density and carbon isotope ratios in tree rings of beech (*Fagus sylvatica*) growing in Germany and Italy, *Trees – Structure and Function*, v. 20, no. 5, p. 571-586.

Sombroek, W.G., 2001, Spatial and temporal patterns of Amazon rainfall, *Ambio*, v. 30, p. 388-396.

Stahle, D.W., Mushove, P.T., Cleaveland, M.K., Roig, F., and Haynes, G.A., Management implications of annual growth rings in *Pterocarpus anolensis* from Zimbabwe, *Forest Ecology and Management*, v. 124, i.2-3, p. 217-229.

Sternberg, H., 1968, Man and environmental change in South America, *Biogeography and Ecology in South America*, E.J., Fittkau et al., Eds., Junk, W., N.V. Publishers, p.413-445.

Sternberg, L., and DeNiro, M.J., 1983, Biogeochemical implications of the isotopic equilibrium fractionation factor between the oxygen atoms of acetone and water, *Geochimica et Cosmochimica Acta*, v. 47, p. 2271-2274.

Stuiver, M., and Polach, H.A., 1977, Discussion: reporting of ^{14}C data, *Radiocarbon*, v. 19, p. 353-363.

Stuiver, M., and Quay, P.D., 1981, Atmospheric ^{14}C changes resulting from fossil fuel CO_2 release and cosmic ray flux variability, *Earth & Planetary Science Letters*, v. 53, p. 349-363.

Taiz, L., and Zeiger, E., 1998, *Plant Physiology*, 2nd edition, Sinauer Associates, Inc: Sunderland, MA.

Thorburn, P.J., and Walker, G.R., 1993, The source of water transpired by *Eucalyptus camaldulensis*: soil, groundwater, or streams? In Ehleringer, J.R., Hall, A.E., Farquhar, G.D., Eds., *Stable Isotopes and Plant Carbon-Water Relations*, Academic Press, San Diego, p. 511-527.

Thomson, D.J., 1982, Spectrum estimation and harmonic analysis, *Proceedings of the IEEE*, v. 70, p. 1055-1096.

Trenberth, K.E., and Shea, D.J., 2006, Atlantic hurricanes and natural variability in 2005, *Geophysical Research Letters*, v. 33, p. L12704-L12708.

Tsuji, H., Nakatsuka, T., and Takagi, K., 2006, $\delta^{18}O$ of tree-ring cellulose in two species (spruce and oak) as proxies of precipitation amount and relative humidity in northern Japan, *Chemical Geology*, v. 231, i. 1-2, p. 67-76.

Turney, C.S.M., and Palmer, J.G., 2007, Does the El Nino-Southern Oscillaton control the interhemispheric radiocarbon offset?, *Quaternary Research*, v. 67, p. 174-180.

Valentini, R., Scarascia Mugnozza, G.E., and Ehleringer, J.R., 1992, Hydrogen and carbon isotope ratios of selected species of a Mediterranean macchia ecosystem, *Functional Ecology*, v. 6, p. 627-631.

Verheyden, A., Kairo, J.G., Beeckman, H., and Koedam, N., 2004, Growth rings, growth ring formation and age determination in the Mangrove *Rizophora mucronata*, *Annals of Botany*, v. 94, p. 59-66.

Villalba, R., and Veblen, T.T., 1996, A tree-ring record of dry spring-wet summer events in the forest-steppe ecotone, northern Patagonia, Argentina, *Tree Rings, Environment and Humanity*, eds. J.S. Dean, D.M. Meko, and T.W., Swetnam, Radiocarbon, University of Arizona, Tucson, Arizona, USA., p. 107-116.

Vogel, J.S., Southon, J.R., and Nelson, D.E., 1987, Catalyst and binder effects in the use of filamentous graphite for AMS, *Nuclear Instruments and Methods in Physics Research Section B*, v. 29, p. 50-56.

Vozzo, J.A., 2002, Tropical tree seed manual, Eds. USDA Forest Service, Washington DC, Agricultural Handbook Number 721, 899 p.

Vuille, M., and Bradley, M., Werner, R., Healy, R., and Keimig, F., 2003, Modeling $\delta^{18}O$ in precipitation over the tropical Americas: interannual variability and climatic controls, *Journal of Geophysical Research*, v. 108, no.6, p. 4175-4184.

Webster, P.J., Holland, G.J., Curry, J.A., and Chang, H.R., Changes in tropical cyclone number, duration, and intensity in a warming environment, *Science*, v. 309, no. 5742, p. 1844-1846.

White, J.W.C., Lawrence, J.R., and Broecker, W.S., 1994, Modeling and interpreting D/H ratios in tree rings: A test case of white pine in northeastern United States, *Geochimica et Cosmochimica Acta*, v. 58, p. 851-862.

Wigley, T.M.L., Briffa, K.R., and Jones, P.D., 1984, On the average value of correlated time series, with applications in dendroclimatology and hydrometeology, *Journal of Applied Meteology*, v. 23, p. 201-213.

Williams, E., Dall'Antonia, A., Dall'Antonia, V., de Almeida, J., Suarez, F., Liebmann, B., and Malhado, A., 2005, The drought of the century in the Amazon basin: An analysis of the regional variation of rainfall in South America in 1926, *Acta Amazonica*, v. 35, p. 231-238.

Willmot, C.J., Rowe, C.M., and Philpot, W.D., 1985, Small-scale climate maps: A sensitivity analysis of some common assumptions associated with grid-point interpolation and contouring, *American Cartography*, v. 12, p. 5-16.

Worbes, M., 1989, Growth rings, increment and age of trees in inundation forests, savannas and a mountain forest in the Neotropics, *IAWA Bulletin*, v. 10, p. 109-122.

Worbes, M., 1992, Occurrence of seasonal climate and tree-ring research in the tropics, tree rings and environment. *Proceedings of the International dendrological symposium*, Lund University, p. 338-342.

Worbes, M., 1995, How to measure growth dynamics in tropical trees – a review, *IAWA Journal*, v. 16, p. 337-351.

Worbes, M., 1999, Annual growth rings, rainfall-dependent growth and long-term growth patterns of tropical trees from the Caparo Forest Reserve in Venezuela, *Journal of Ecology*, v. 87, p. 391-403.

Worbes, M., and Junk, W.J., 1989, Dating tropical trees by means of ^{14}C from bomb tests, *Ecology*, v. 70, p. 503-507.

Worbes, M., Staschel, R., Roloff, A., and Junk, W.J., 2002, Tree ring analysis reveals age structure, dynamics and wood production of a natural forest stand in Cameroon, *Forest Ecology and Management*, v. 173, p. 105-123.

Xie, P., and Arkin, P.A., 1997, Global precipitation: A 17-year monthly analysis based on gauge observations, satellite estimates, and numerical model outputs, *Bulletin of the American Meteorological Society*, v. 78, p. 2539-2558.

Zhang, Y., Wallace, J.M., and Battisti, D.S., 1997, ENSO-like interdecadal variability, *Journal of Climate*, v. 10, p. 1004-1020.

Zhou, J., and Lau, K.M., 1998, Does a monsoon climate exist over South America? *Journal of Climate*, v. 11, p. 1020-1040.

Zhou, J., and Lau, K.M., 2001, Principle modes of interannual and decadal variability of summer rainfall over South America, *International Journal of Climatology*, v. 21, p. 1623-1644.

Appendix I

Brendel Method

Extraction of Pure α-cellulose
Procedure developed by Brendel et al. (2000)

Step1.
- Take 50-100 mg milled wood samples (dried) and place in centrifuge tube
- Add 2 ml 80% acetic acid
- Add 0.2 ml 69% nitric acid
- Cap and mix gently (avoid getting sample stuck high on the glass)
- Boil at 120°C for 20-30 min.

Step 2.
- Allow to cool (~5-10 min)
- Add 2.5 ml 99% ethanol

Step 3.
- Vortex
- Centrifuge for 5 min at highest speed (3500 rpm or higher).
- Decant supernatant

Step 4.
- Add 2x2.5 ml 99% ethanol (a total of 5 ml are added, but in two steps, the first is added and then mixed the second is added to wash down the sides of the glass to force sample back into the solution, also during the last addition try to match the volumes in the tube to balance the centrifuge).
- Repeat step 3

Step 5.
- Add 2x2.5 ml DDI
- Repeat step 3

Step 6.
- Add 2x2.5 ml DDI
- Repeat step 3

Step 7.
- Add 2x2.5 ml 99% ethanol

- Repeat step 3

Step 8.
- Add 2x2.5 ml acetone
- Repeat step 3

Allow sample to dry in the hood or a vacuum evaporator overnight then place in a drying oven at 50°C.

Modified Brendel Method

Cellulose extraction method as developed by Brendel et al. (2000) and modified by Gaudinski et al. (2005)

Step1.
- Take 50-100 mg milled wood samples (dried) and place in centrifuge tube
- Add 2 ml 80% acetic acid
- Add 0.2 ml 69% nitric acid
- Cap and mix gently (avoid getting sample stuck high on the glass)
- Boil at 120°C for 20-30 min.

Step 2.
- Allow to cool (~5-10 min)
- Add 2.5 ml 99% ethanol

Step 3.
- Vortex
- Centrifuge for 5 min at highest speed (3500 rpm or higher).
- Decant supernatant

Step 4.
- Add 2x2.5 ml 99% ethanol (a total of 5 ml are added, but in two steps, the first is added and then mixed the second is added to wash down the sides of the glass to force sample back into the solution, also during the last addition try to match the volumes in the tube to balance the centrifuge).
- Repeat step 3

Step 5.

- Add 2x2.5 ml DDI
- Repeat step 3

Step 6.

- Add 2x2.5 ml 17% (w/v) NaOH (17 g NaOH per 100 ml water) use only glass pipettes with this solution.
- Let sit for ~10 min
- Repeat step 3

Step 7.

- Add 2x2.5 ml DDI
- Repeat step 3

Step 8.

- Add 2.2 ml DDI + 0.6 ml acetic acid
- Vortex
- Add 2.2 ml DDI only (wash down the sides) and gently mix
- Repeat step 3

Step 9.

- Add 2x2.5 ml DDI
- Repeat step 3

Step 10.

- Add 2x2.5 ml 99% ethanol
- Repeat step 3

Step 11.

- Add 2x2.5 ml acetone
- Repeat step 3

Allow sample to dry in the hood or a vacuum evaporator overnight then place in a drying oven at 50°C.

Modified DeVries Pretreatment Method
Modified after Hoper et al., 1998.

Step 1.

- Place 3-6 milligrams of dilled or diced wood into individual culture tubes.

Step 2.

- Add ~3milliliters of 1N HCl and place samples on a heating block at 90°C for 20-30 minutes.

Step 3.

- Pipette off the supernatant and repeat Step 2.

Step 4.

- Add 3 milliliters of 1N NaOH to sample culture tubes. Place samples on heating block at 90°C for 20-30 minutes.

Step 5.

- Remove sample from heat, pipette off supernatant. Repeat step 4 a minimum of 3 times until supernatant runs clear. Note: this may require up to 10 rinses in NaOH for each sample (In tree species *Myroxylon balsamum* this process required 11 rinses of NaOH until supernatant ran clear).

Step 6.

- Soak sample in 10 milliliters of MQ/DI water. Pipette off supernatant.

Step 7.

- Repeat Step 2 two times to remove any acid-soluble 'activated' compounds.

Step 8.

- Pipette off remaining supernatant and store samples in MQ water with 1 drop of 1N Hcl. Screw top vials are preferable to snap caps and are less likely to leak.

Note:

This process should be conducted in a hood where there isn't a lot of foot traffic or the likelihood for a lot of dust flying around with excess ^{14}C that might affect the samples. Use a disposable liner of aluminum foil along the hood counter to prevent contamination.

Packing Procedure for $\delta^{18}O$ & $\delta^{13}C$

- Tin capsules are for the analysis of $\delta^{13}C$
- Silver capsules are for the analysis of $\delta^{18}O$.

- Tare the microbalance with the appropriate capsule.
- For the preparation of $\delta^{13}C$ add approximately 1000 μg to capsule and weigh sample.
- For the preparation of $\delta^{18}O$ add approximately 350-500 μg to capsule and weigh sample.
- Using the un-serrated forceps carefully pack samples so as not to tear the capsule (check that sample is sealed by bouncing several times on a clean flat surface).
- Record the sample identification code, the corresponding weight and the array number into a spreadsheet.
- Clean forceps and surface with Ethanol before proceeding to the next sample.

Note:

Sample weights may vary depending on the sensitivity of the analysis

Appendix II

Table 1. $\delta^{13}C$ measurements made on 10 Samples of *C. odorata* using multiple preparation techniques.

Cedrela odorata	$\delta^{13}C$		
SAMPLE NUMBER	HIGH SPEED	LOW SPEED	MICROTOME
1	-27.472	-26.410	-26.911
2	-27.196	-25.603	-26.055
3	-28.356	-26.471	-24.523
4	-27.454	-26.292	-24.160
5	-27.585	-26.368	-23.973
6	-27.689	-26.195	-23.321
7	-27.620	-26.238	-24.778
8	-27.093	-27.375	-24.445
9	-27.092	-26.119	-24.542
10	-27.123	-26.879	-24.518

Table 2. $\delta^{13}C$ measurements made on 10 Samples of *D. micrantha* using multiple preparation techniques.

Dipteryx micrantha	$\delta^{13}C$		
SAMPLE NUMBER	HIGH SPEED	LOW SPEED	MICROTOME
1	-27.195	-27.404	-24.555
2	-27.300	-25.998	-24.831
3	-27.534	-25.864	-24.599
4	-26.753	-26.825	-24.207
5	-26.902	-25.737	-24.111
6	-25.699	-26.335	-24.947
7	-27.684	-27.137	-24.046
8	-27.061	-26.180	-25.550
9	-28.406	-25.975	-24.999
10	-27.789	-26.286	-24.163

Table 3. $\delta^{18}O$ measurements made on 10 Samples of *D. micrantha* using multiple preparation techniques.

Dipteryx micrantha	$\delta^{18}O$		
SAMPLE NUMBER	HIGH SPEED	LOW SPEED	MICROTOME
1	26.382	25.185	28.210
2	25.282	26.912	27.659
3	26.813	25.125	27.140
4	25.662	26.524	26.913
5	24.750	24.837	25.037

Table 4. $\delta^{13}C$ measurements made on 10 Samples of *C. odorata* using multiple extraction techniques.

Cedrela odorata	$\delta^{13}C$		
SAMPLE NUMBER	BRENDEL	M.BRENDEL	BULK
1	-27.044	-25.921	-27.632
2	-27.137	-26.225	-27.661
3	-27.052	-25.498	-27.791
4	-27.099	-26.137	
5	-26.803	-26.228	
6	-26.925	-26.184	
7	-25.493	-27.274	
8	-27.015	-26.259	
9	-25.983	-26.134	
10	-26.012	-26.141	

Table 5. $\delta^{13}C$ measurements made on 10 Samples of *D. micrantha* using multiple extraction techniques.

Dipteryx micrantha	$\delta^{13}C$		
SAMPLE NUMBER	BRENDEL	M.BRENDEL*	BULK
1	-25.702	-24.555	-27.363
2	-25.112	-24.831	-27.415
3	-24.749	-24.599	-27.243
4	-25.312	-24.207	
5	-25.482	-24.111	
6	-26.187	-24.947	
7	-26.018	-24.046	
8	-25.871	-25.550	
9	-25.184	-24.999	
10	-24.883	-24.163	

*These values are the same measurements as those prepared using the microtome preparation method

Table 6. Standard chronologies developed using the program ARSTAN for tree species *Ceiba pentandra, Tabebuia serratifolia,* and *Hymenaea courbaril*.

YEAR	*Ceiba pentadra*	*Tabebuia serratifolia*	*Hymenaea courbaril*
2006	-0.2424577	-0.4479693	-0.9843595
2005	-1.1694054	-1.3382736	-0.9544791
2004	0.2357655	0.3002437	-1.5868719
2003	-0.9440565	1.6001633	-0.0315627
2002	0.2056174	0.6236794	0.9692946
2001	0.0829269	-0.5919946	2.7287263
2000	-0.0490553	-0.0135449	0.4707334
1999	-0.9729557	0.6718642	2.5395439
1998	-0.6573125	0.3190715	-0.1881197
1997	-0.1164702	-0.1739975	-0.3348665
1996	-0.1290589	-1.1560095	-0.1051387
1995	-0.6591108	-0.3483893	-1.0951959
1994	-0.0895692	-0.2277869	-1.1293063
1993	0.0031231	-0.2537786	1.3869447
1992	0.8300351	1.7397235	-1.1107660
1991	2.9704997	0.4092421	0.1892100
1990	0.3831589	1.6639495	1.5964673
1989	-1.3708256	-0.5803510	0.7185065
1988	0.4388592	-0.6355627	-0.9044835
1987	1.3187489	1.0777818	-0.4767982
1986	-1.1360602	0.7720768	-0.7831620
1985	-0.0095656	-0.1078130	0.0622634
1984	-0.1495406	0.0459582	-0.9872845
1983	-0.0244273	-1.3701598	-2.2508551
1982	1.2006543	-0.7601701	0.7691321
1981	0.1616316	-1.3712054	0.5718947
1980	0.3860064	-0.0148199	-0.6390702
1979	0.8206934	-1.3293586	0.1510945
1978	-0.2715068	0.3363058	-0.2366303
1977	-0.5120171	-0.8341561	-0.5342639
1976	-1.2010771	1.4748934	-0.4621731
1975	-1.1540941	-0.7096836	1.0306753
1974	0.7216318	0.2917665	-0.3158313
1973	0.8390770	1.6713504	-0.7354164
1972	3.3389958	0.1019256	-0.8793732
1971	1.6692361	-0.9194250	-1.0916408
1970	1.4278016	1.3249652	1.1176614
1969	0.3484899	0.1451252	-1.1376314
1968	0.0931428	0.2503772	0.9011637
1967	-1.6001959	-0.5151001	-0.0972636
1966	-1.5238141	0.7523911	0.1136990
1965	-1.3713252	0.0963905	0.9382442
1964	-0.0859724	-0.2846352	0.5662696
1963	1.0822100	-0.9035184	-0.2333002
1962	-0.4214230	-1.9355304	-0.1531092
1961	-0.7470074	-1.8535755	0.5622196
1960	0.3625773	-0.1578519	-0.1520742

YEAR	*Ceiba pentadra*	*Tabebuia serratifolia*	*Hymenaea courbaril*
1959	1.8387598	-1.5833974	-0.8604280
1958	-0.0807770	-0.6488277	-1.7371738
1957	1.5467454	0.8569159	0.2500507
1956	1.5770434	-0.2630031	-1.2099023
1955	0.1822382	2.1445655	0.1150491
1954	-0.6488950	-0.4084710	2.1199138
1953	0.1665522	1.7978146	1.4324833
1952	2.4325548	-0.9743726	0.9417302
1951	0.1685255	1.7928697	0.3261657
1950	1.1639371	0.4233952	-0.5787980
1949	1.8623887	-2.0566897	0.3270526
1948	0.3656995	-0.1500582	0.1911414
1947	0.7713125	-0.8821199	-0.6669777
1946	-1.4449095	-1.6650701	0.6922148
1945	0.8956765	1.4566634	1.6645294
1944	-1.2040245	0.2197159	-0.9884935
1943	-1.3713002	0.2153925	-0.5138122
1942	-0.3141437	-0.8508247	-1.6176303
1941	0.2532998	2.0822120	-0.5658170
1940	-0.6224685	-0.2793876	-0.3638449
1939	-0.5526059	-0.6345513	-0.4509764
1938	-0.0705112	-0.4851254	-0.4617805
1937	-0.9322421	1.4162724	0.6779706
1936	1.3956053	2.6847490	-1.2443785
1935	-1.1220726	0.3672484	-0.5470576
1934	-0.4610876	-0.0576585	-0.4835500
1933	0.1877084	-1.0595144	1.3581447
1932	-0.4592392	0.8889218	0.1362072
1931	-1.0727916	0.1823272	-1.0796295
1930	-0.2518743	0.0234613	0.3717203
1929	-1.4071182	1.9179983	0.7419889
1928	-0.8650520	-0.0450112	1.8531172
1927	-0.7957889	-0.1311723	0.4124372
1926	0.6503205	0.7405625	-0.7062970
1925	-0.9596926	-0.3008786	-1.4242048
1924	-0.7947148	-0.1372869	-1.6150502
1923	-0.6474463	-1.1301102	0.5160705
1922	0.0709126	-1.0995884	0.0796066
1921	-1.3099050	-1.0147724	-0.3515627
1920	-0.9407345	-0.9050306	0.8426389
1919	-0.1107253	-0.7337884	0.5104534
1918	0.1258386	-0.4114605	1.4836818
1917	0.4826451	0.6256246	2.6138382
1916	0.2367646	1.6050592	1.5407123
1915	-0.5328985	0.9394813	1.2184171
1914	-0.9283705	-0.2112884	0.3191780
1913	0.0078938	0.0004769	-0.8779531
1912	1.6773667	0.5030119	1.5568110
1911	0.9747913	0.0638404	-0.0856530
1910	1.1769999	-0.5440377	-0.3673388

YEAR	*Ceiba pentadra*	*Tabebuia serratifolia*	*Hymenaea courbaril*
1909	-0.1365452	-0.4526078	-0.0178452
1908	0.0803720	-0.1685325	0.9307649
1907	1.3296530	-0.4171317	0.8942137
1906	-0.8799747	-0.4988506	-0.0370346
1905	0.1344364	0.2004264	-0.2427155
1904	-0.8266389	-0.7111531	-0.8228576
1903	-0.5289207	2.0790884	-0.9698954
1902	-0.3235504	-0.3758256	-2.1300184
1901	-0.4754612	-0.3150472	-0.8800763
1900	0.8138904	-0.0924723	-1.9104427
1899	0.4008267	-0.6626901	-0.4500358
1898	2.2954845	1.3533670	-0.4603830
1897	-0.5772116	0.0798432	-0.2158934
1896	-0.5668881	0.2415100	0.9449822
1895	-0.7103586	0.9307179	-0.4618612
1894	-0.8669569	-0.9344634	-0.8678747
1893	0.2789241	-0.5928365	1.1600696
1892	-0.7769459	-0.3517523	0.1262362
1891	-1.0118433	-0.1269563	-0.8698366
1890	-1.0727946	-0.2196327	0.2536546
1889	-0.0792779	1.0891284	-0.3408661
1888	1.0670705	0.5263733	-0.1617117
1887	-0.4140425	0.4542510	-1.4328051
1886	-1.1056071	-0.1214607	0.5465477
1885	-0.7774132	-0.2657649	-0.8177512
1884	-0.7122418	0.3231009	1.9749996
1883	-0.9560469	-0.1143146	1.5597531
1882	-0.6681711	0.1091797	-0.3332388
1881	-0.9846393	-0.1504822	-0.2742508
1880	-1.0198024	-0.7451789	-0.6545157
1879	-0.0886529	-0.9498825	-0.6368046
1878	-0.1139737	-0.2512174	-0.3301004
1877	-0.5509561	-0.7765506	-1.1892982
1876	-0.6259698	-0.8150481	-0.8714350
1875	-0.3066699	-1.0978051	-1.0719279
1874	-1.0057399	-1.1213495	-0.3666604
1873	-1.0507454	-0.2998110	0.5526082
1872	-0.2236832	-1.2222224	-0.7606536
1871	-0.8097584	-0.4156761	0.0295719
1870	-0.8017855	-0.5171565	-0.9783070
1869	0.1218585	-0.0479936	-0.6711072
1868	-1.0685744	2.2327996	-0.7177066
1867	-0.8064730	0.1141822	0.5532506
1866	1.4707592	0.2068567	-1.0288157
1865	1.1505245	-0.8188170	0.6501200
1864	-0.2396290	-0.9723591	0.6584892
1863	0.4547536	-0.1647559	0.5512133
1862	-0.4032654	-0.6191208	1.4536335
1861	0.6244796	0.9093610	0.6565070

YEAR	*Ceiba pentadra*	*Tabebuia serratifolia*	*Hymenaea courbaril*
1860	2.2439083	0.1493586	2.0855974
1859	1.6456401	0.5050427	-1.1858844
1858	-0.6794156	0.4204725	-1.1565373
1857	-0.7750626	2.8723257	1.0332847
1856	-0.9185331	0.7777819	0.3592914
1855	-0.4806160	-0.8626898	-1.4112096
1854	-0.7136440	0.0659080	2.0500284
1853	1.7961488	-0.4355865	-1.4034644
1852	0.2597068	-0.6758329	1.1287226
1851	-0.6198665	-0.7451760	1.8860221
1850	-0.4993798	-0.3168795	2.0478994
1849	2.0816740	-0.5125408	0.7560377
1848	-0.5856518	1.9328144	0.5079726
1847	-0.6381628	3.4633317	0.6277472
1846	-0.8496090	4.3480489	1.4552302
1845	-0.5851707	-0.5063529	0.3217587
1844	1.5396833	0.6679527	0.2616695
1843	-0.2386942	0.6142281	1.7681930
1842	-0.9865225	-0.5951099	0.7269108
1841	-0.8561798	-0.0918916	0.5809643
1840	1.5181153	-1.4042570	-0.8180081
1839	2.5233438	-0.0879756	-1.3922505
1838	1.6794011	-0.7765791	0.1678100
1837	0.9128228	0.0914236	0.8526685
1836	1.3347942	-0.3215268	0.7620760
1835	2.6850970	-0.2471718	0.4535363
1834	1.3286908	0.1669545	0.1961294
1833	0.9564262	-0.6442093	-1.5312227
1832	1.1495897	-0.8148574	-0.6495419
1831	-0.3938766	-0.1084027	-0.7429976
1830	-0.0952237	0.7846523	-1.1113328
1829	0.2461116	0.9342032	-0.9770774
1828	-0.7755300	0.6605277	-0.7758136
1827	-1.0221530	-1.0945972	-0.5368335
1826	-0.5542277	-1.1761532	0.9054714
1825	-1.1365501	-0.9319517	0.3934472
1824	-0.8482069	-0.6682172	0.6537356
1823	-0.5931436		-0.6128167
1822	0.4134871		-0.5512776
1821	0.5185091		-0.2557873
1820	1.0877037		-0.6797700
1819	-0.3540260		

Table 7. Standard chronologies developed using the program ARSTAN for tree species *Myroxylon balsamum and Cedrela odorata*.

YEAR	*Myroxylon balsamum*	*Cedrela odorata*
2006	-0.4539619	-0.0020113
2005	-1.2995834	-1.3666348
2004	-0.7037704	-0.9445981
2003	0.3361949	-0.4874486
2002	0.1129792	0.5636307
2001	-0.5282083	-0.1441290
2000	-1.1234454	-0.0087922
1999	-0.2235402	0.9550578
1998	0.2960477	-0.9605832
1997	3.2577461	-1.1866845
1996	1.3344694	-0.2412425
1995	-0.7097977	2.9144251
1994	-0.5113784	2.3747886
1993	0.6985983	2.0425719
1992	0.6014368	1.6979835
1991	0.4813808	0.2379725
1990	-0.5521368	-0.6362369
1989	-1.1942940	-1.0281903
1988	0.6323245	-0.6491556
1987	-0.0020216	-1.3132259
1986	-0.0605589	0.6128651
1985	0.0504844	-0.2201652
1984	-0.9906288	0.5176778
1983	-0.3564070	-0.5239675
1982	-0.6128062	-0.7482459
1981	1.5125176	0.1039304
1980	3.6384339	1.3889060
1979	-0.9700114	0.2590751
1978	-1.4353696	1.4548492
1977	-0.7158727	-0.6998280
1976	-0.2016178	-0.6209407
1975	1.4441615	-1.1443207
1974	-0.4386593	-0.8070628
1973	0.3457501	0.7613256
1972	-0.5147394	0.7579442
1971	-0.4162477	0.4360970
1970	-0.0478169	0.5181817
1969	-0.4893649	-0.5064600
1968	-0.2337365	0.2085521
1967	-0.4136951	-0.4984007
1966	-0.4747104	-0.9059830
1965	0.6961573	-0.6451366
1964	0.3515587	1.4361979
1963	-1.2202669	-0.7283706
1962	-0.2477921	-0.9185223
1961	0.7046433	-0.5305824
1960	-0.6729298	-0.8991970

YEAR	*Myroxylon balsamum*	*Cedrela odorata*
1959	0.9901493	-0.6766908
1958	-1.1483274	0.7204068
1957	-0.3103104	-1.0489557
1956	1.2064597	0.2302225
1955	-0.2056974	0.1973464
1954	-1.5933439	1.1376186
1953	-0.0264215	-0.6246316
1952	1.2842985	-0.1580689
1951	1.5527017	-0.8077056
1950	0.5653039	-1.0607915
1949	-0.2538061	-1.1358927
1948	-1.1348120	-0.5777676
1947	-0.6387573	-0.3286056
1946	1.0940826	0.0284649
1945	0.1182128	-1.0938054
1944	0.8219876	-0.4301924
1943	0.6059442	-0.2725030
1942	1.1001136	-0.2988646
1941	-1.0632508	-0.7159498
1940	-0.1868249	-0.3133970
1939	1.6549386	0.4196347
1938	1.0802874	-0.4544551
1937	0.1562938	0.1163105
1936	-0.3894297	0.0043334
1935	-0.8525176	-0.1331043
1934	0.8875946	2.5397993
1933	-1.0277556	-0.3108590
1932	-0.8588490	1.2318298
1931	-0.6305784	0.9263287
1930	-0.1890933	0.3643993
1929	-0.2179408	-0.3147023
1928	0.6205071	1.3960200
1927	-0.9823472	0.3484877
1926	0.0309605	-0.3758870
1925	-0.6609104	0.4763790
1924	0.3973243	0.3104924
1923	-0.3900029	-0.2596548
1922	3.0118692	0.7382920
1921	-0.0928071	-0.8852401
1920	-0.9043755	-0.7851955
1919	-0.3008515	-0.8108114
1918	0.4764010	1.0162874
1917	1.0377453	-0.0987102
1916	0.6056322	-1.4948495
1915	-0.2656772	1.2424635
1914	-1.3335557	-0.7739327
1913	-0.5855900	-0.0942315
1912	0.1901188	-0.4287879
1911	0.4588637	2.1091119
1910	-1.2797227	-0.6368535

YEAR	*Myroxylon balsamum*	*Cedrela odorata*
1909	-0.1839764	-0.7728305
1908	0.5266045	0.9411412
1907	0.7781651	3.0282556
1906	-0.2283377	-0.6681319
1905	-0.9659788	-0.6305179
1904	-1.5044113	-0.4630914
1903	-0.1316153	2.0954300
1902	-0.5266961	-0.8887913
1901	-0.5071613	-0.6821628
1900	-0.6996915	-0.5921141
1899	-0.3706931	-0.6634414
1898	0.3993707	-0.5296142
1897	-0.3141893	1.3014337
1896	0.8621546	1.0728103
1895	-0.1927716	-0.5868047
1894	0.8681575	0.1385525
1893	-0.2781526	-0.2331162
1892	1.9780018	0.3267933
1891	0.5314856	0.0772986
1890	-1.1090795	-0.7143616
1889	-1.3889746	-0.5851109
1888	1.0432124	-0.6533844
1887	-0.1323950	1.3090070
1886	1.5844085	-0.5353960
1885	-1.9500794	-0.7477328
1884	-1.7330035	-0.6541255
1883	-1.6866383	-0.4984091
1882	-1.3047276	-0.5717722
1881	2.1280539	-0.7362590
1880	0.7673042	2.0706753
1879	2.1367909	-0.4375542
1878	-1.2227646	-0.5658928
1877	-0.8939238	-0.6367070
1876	-1.2806605	-0.7222933
1875	-1.3912498	0.7610679
1874	-1.3625874	-0.4576926
1873	1.4753063	-0.7092232
1872	0.1398619	-0.5764222
1871	-1.2858577	0.0359305
1870	1.2632772	0.5678434
1869	0.4997516	-0.1189390
1868	0.6470440	0.3483242
1867	-0.1980814	1.6336562
1866	2.1494933	1.7058874
1865	0.3446565	-0.0609750
1864	-0.6711243	-0.4033127
1863	3.2431430	0.1126301
1862	-0.2950505	0.6886462
1861	0.0844852	1.2534569

YEAR	*Myroxylon balsamum*	*Cedrela odorata*
1860	0.6751713	0.7538148
1859	-1.1747893	1.0294811
1858	0.6058004	-0.1421308
1857	-0.1172580	-0.1133615
1856	-0.6991523	-0.1899667
1855	-0.3899908	0.8218061
1854	-0.8822195	1.0292558
1853	1.0004529	-0.2965985
1852	0.4789270	0.5407894
1851	0.4404581	-0.5537848
1850	-0.6866630	-0.0058170
1849	-0.7800399	0.0097017
1848	-0.6483522	-0.1361484
1847	-0.2733345	0.1665922
1846	-0.3264658	0.4676803
1845	-0.5570432	-0.3203139
1844	-0.0100396	-0.4500324
1843	0.4509849	-1.1880317
1842	1.3254961	-1.0805495
1841	0.6265240	-0.8778513
1840	0.4215297	-0.2782623
1839	-0.5208003	-0.7435713
1838	-0.3488672	0.3675349
1837	-0.0195829	-1.0529770
1836	0.6646490	-0.8841946
1835		-1.0558291
1834		-0.7644200
1833		-0.4310424
1832		-0.0815331
1831		-0.4629314
1830		-0.0053270
1829		0.2021976
1828		-0.4712490
1827		-0.8752578
1826		-0.5031380
1825		-0.7296725
1824		0.2942966
1823		-0.3000918
1822		-0.5556632
1821		-0.7482820
1820		-0.4520203
1819		-0.1460796

Table 7. Oxygen Isotope Measurements for Trees 67 and 78.

	$\delta^{18}O$			
	TR EE 67		TR EE 78	
YEAR	RAW MEASURE	ERROR ADJUSTED	RAW MEASURE	ERROR ADJUSTED
2006	24.914	24.910	25.017	24.400
2005	24.483	25.693	24.395	24.808
2004	25.933	26.292	23.073	24.414
2003	25.188	26.128	24.318	23.348
2002	24.710	25.846	24.733	23.830
2001	24.658	25.462	23.374	24.423
2000	23.976	25.116	24.074	24.618
1999	24.993	24.860	23.795	23.966
1998	23.559	24.700	24.209	23.540
1997	25.058	24.673	24.196	23.950
1996	24.446	24.473	25.052	23.923
1995	24.802	24.121	24.962	23.877
1994	25.766	24.318	25.255	24.133
1993	25.289	24.815	24.761	24.205
1992	24.435	24.422	24.564	24.352
1991	24.162	23.766	24.736	24.878
1990	24.881	24.252	23.459	25.007
1989	24.914	24.917	24.147	25.011
1988	23.762	24.738	24.119	25.182
1987	24.897	24.509	24.433	25.022
1986	23.283	24.658	24.217	24.743
1985	25.447	24.937	23.942	24.606
1984	24.686	25.445	24.885	24.643
1983	24.150	25.667	23.787	24.527
1982	23.773	25.416	22.396	23.743
1981	23.048	25.054	23.889	23.784
1980	22.841	24.596	25.647	24.125
1979	25.024	24.336	23.299	24.131
1978	26.840	24.213	23.708	24.271
1977	26.332	24.466	24.593	24.384
1976	23.772	24.819	25.261	24.253
1975	22.911	24.895	24.784	24.077
1974	24.405	24.803	25.504	24.137
1973	23.550	24.237	24.543	24.691
1972	23.352	23.948	25.217	24.287
1971	23.814	24.522	22.741	23.476
1970	23.223	24.549	25.687	22.660
1969	22.262	23.681	22.976	23.274
1968	23.292	23.924	24.361	24.365

	$\delta^{18}O$			
	TR EE 67		TR EE 78	
YEAR	RAW MEASURE	ERROR ADJUSTED	RAW MEASURE	ERROR ADJUSTED
1967	23.122	25.070	23.900	25.306
1966	22.104	25.157	24.744	24.150
1965	25.066	24.751	24.346	23.434
1964	23.267	24.433	24.586	23.757
1963	23.070	24.151	25.176	24.325
1962	22.613	23.934	24.637	24.850
1961	22.497	23.679	25.122	25.163
1960	20.501	23.293	24.728	24.902
1959	21.775	23.007	24.874	25.111
1958	22.279	22.893	24.792	25.308
1957	22.139	23.515	24.851	24.731
1956	23.002	24.708	23.853	24.908
1955	22.152	25.766	24.879	24.603
1954	20.255	26.651	25.126	23.246
1953	22.136	26.579	24.470	24.857
1952	20.918	26.081	23.973	24.045
1951	21.196	24.749	25.143	23.647
1950	22.961	23.640	24.306	24.188
1949	20.687	23.146	25.205	24.129
1948	21.565	23.329	23.917	24.621
1947	21.787	24.135	23.587	24.420
1946	24.491	24.074	24.672	24.580
1945	23.085	23.626	24.190	25.012
1944	23.571	23.449	24.039	24.837
1943	23.811	23.406	24.586	24.895
1942	24.447	23.635	24.374	24.957
1941	22.847	23.695	25.081	24.779
1940	23.617	23.375	24.990	24.847
1939	22.944	22.934	24.446	24.805
1938	22.697	22.430	24.865	24.738
1937	21.710	22.692	24.092	24.092
1936	23.364	23.197	25.067	24.629
1935	23.133	23.198	24.397	25.041
1934	24.123	22.988	24.895	24.750
1933	23.322	22.436	24.182	24.231
1932	22.524	22.807	24.174	24.420
1931	22.464	24.448	26.076	24.872
1930	23.184	24.411	24.153	24.545
1929	23.295	23.457	23.318	25.021
1928	22.997	23.170	23.040	24.498

	$\delta^{18}O$			
	TR EE 67		TR EE 78	
YEAR	RAW MEASURE	ERROR ADJUSTED	RAW MEASURE	ERROR ADJUSTED
1927	25.110	23.028	23.813	23.946
1926	24.670	22.778	24.001	23.746
1925	22.694	22.589	23.075	23.681
1924	22.370	22.519	23.773	24.131
1923	21.830	21.811	24.437	24.571
1922	25.477	20.785	23.779	24.442
1921	23.766	21.119	24.325	24.222
1920	25.246	21.766	24.753	24.122
1919	24.963	22.093	24.870	24.073
1918	23.587	22.247	25.792	24.277
1917	23.747	22.175	25.536	24.525
1916	23.947	22.447	26.233	24.500
1915	25.272	22.870	24.384	24.412
1914	25.910	22.567	24.705	24.648
1913	22.534	21.949	25.239	24.983
1912	27.562	20.888	25.056	25.046
1911	24.918	20.716	25.630	24.996
1910	25.677	21.771	24.117	24.796
1909	25.056	21.649	25.166	24.539
1908	26.221	21.037	25.391	24.592
1907	25.255	21.078	24.210	24.796
1906	25.271	21.486	23.873	25.057
1905	25.062	22.484	23.077	25.343
1904	25.668	22.246	24.268	25.327
1903	25.165	21.018	24.516	25.137
1902	26.000	21.112	23.995	24.859
1901	27.220	21.549	24.578	24.531
1900	24.853	21.711	25.480	24.551
1899	24.494	22.457	25.621	24.791
1898	23.884	23.983	25.211	24.675
1897	24.987	23.894	24.262	24.323
1896	25.495	23.215	24.636	24.177
1895	24.215	23.376	25.459	24.176
1894	25.118	23.615	23.903	24.738
1893	25.219	23.761	23.617	25.684
1892	25.892	24.053	22.754	25.481
1891	27.228	24.295	23.605	24.479
1890	25.870	23.540	24.537	23.755
1889	25.200	23.012	25.352	23.283
1888	23.783	23.431	22.475	23.113

	$\delta^{18}O$			
	TR EE 67		TR EE 78	
YEAR	RAW MEASURE	ERROR ADJUSTED	RAW MEASURE	ERROR ADJUSTED
1887	25.920	23.377	24.183	23.485
1886	25.342	22.994	24.871	23.861
1885	24.482	22.807	24.733	23.907
1884	26.701	22.535	24.130	23.363
1883	26.308	21.960	24.547	23.344
1882	26.054	22.296	25.010	23.834
1881	26.990	23.185	25.380	24.285
1880	25.381	23.231	25.340	24.103
1879	27.693	23.311	25.434	23.913
1878	25.481	23.883	24.187	24.274
1877	25.909	23.821	25.046	24.593
1876	26.080	23.336	25.170	24.791
1875	26.812	22.850	24.828	24.930
1874	33.444	22.516	24.213	25.302
1873	26.664	22.479	24.106	25.683
1872	29.498	22.758	24.559	25.713
1871	26.484	23.144	25.169	25.615
1870	27.088	23.256	24.655	25.617
1869	27.560	23.225	23.353	25.875
1868	27.042	23.097	23.963	26.128
1867	27.158	24.002	23.910	25.726
1866	27.397	24.972	24.912	24.997
1865	27.063	24.799	24.376	24.451
1864	27.348	24.032	26.787	24.525
1863	26.462	22.893	24.795	24.652
1862	25.713	22.511	25.428	24.831
1861	25.838	22.271	24.602	25.045
1860	26.573	21.979	23.931	25.194
1859	26.119	23.360	23.321	25.154
1858	26.240	25.096	24.830	25.308
1857	25.063	24.344	23.991	24.464
1856	25.479	24.199	23.889	25.195
1855	25.345	25.050	24.999	24.948
1854	24.714	25.094	23.044	24.060
1853	24.634	24.714	23.869	23.444
1852	25.553	23.886	24.401	23.839
1851	25.345	23.658	24.012	24.425
1850	25.534	23.763	23.194	24.150
1849	25.479	23.887	25.471	24.598
1848	27.267	24.365	25.091	25.411

	$\delta^{18}O$			
	TR EE 67		TR EE 78	
YEAR	RAW MEASURE	ERROR ADJUSTED	RAW MEASURE	ERROR ADJUSTED
1847	27.922	25.163	24.807	25.511
1846	27.331	25.642	24.564	24.914
1845	26.872	25.150	24.734	24.428
1844	27.480	23.223	24.827	25.061
1843	27.406	24.979	25.231	24.489
1842	26.504	27.004	24.889	23.663
1841	25.935	25.565	23.038	23.004
1840	25.848	25.226	24.466	23.606
1839	26.175	25.570	24.661	24.622
1838	24.586	25.256	23.803	24.491
1837	25.082	25.438	24.319	23.173
1836	26.045	26.045	23.229	24.515
1835	28.948	25.631	24.562	24.777
1834	29.683	25.266	24.476	24.326
1833	29.509	25.260	23.749	24.503
1832	28.302	25.154	24.428	25.002
1831	29.314	25.192	25.260	25.342
1830	29.235	25.553	24.111	25.370
1829	29.224	25.420	24.924	24.899
1828	29.388	25.327	24.820	24.663
1827	27.778	25.843	24.868	25.119
1826	29.822	26.559	22.232	24.865
1825	31.038	26.826	25.763	24.292
1824	24.586	25.413	22.550	24.214
1823	26.774	24.697	25.205	24.731
1822	25.124	24.428	24.869	24.941
1821	27.522	24.044	24.502	23.932
1820	26.596	24.326	26.625	23.762
1819	26.292	24.989	22.619	24.005
1818	25.923	25.355	24.511	24.693
1817	25.460	25.004	22.743	25.003
1816	24.396	24.396	24.782	26.016
1815	25.704	24.863	22.856	25.107
1814	24.790	25.158	24.407	24.902
1813	24.838	25.288	24.251	24.068
1812	29.398	25.702	24.735	23.611
1811	25.418	26.409	24.768	24.514
1810	25.852	26.996	25.542	23.990
1809	26.045	26.240	24.447	24.396
1808	25.492	25.600	26.422	23.843

	$\delta^{18}O$			
	TR EE 67		TR EE 78	
YEAR	RAW MEASURE	ERROR ADJUSTED	RAW MEASURE	ERROR ADJUSTED
1807	26.477	25.054	26.756	23.671
1806	25.022	24.154	24.781	24.261
1805	25.183	24.694	22.943	23.874
1804	25.298	25.749	24.501	23.963
1803	24.750	25.463	24.485	25.277
1802	24.975	24.943	24.647	24.914
1801	26.000	24.884		24.636
1800	25.976	26.256		24.717
1799	24.467	26.503		24.917
1798	24.371	26.263		25.096
1797	27.535	26.124		23.952
1796	27.577	26.577		23.989
1795	27.191	26.574		24.540
1794	28.066	25.707		23.996
1793	31.358	26.824		23.975
1792	30.174	26.989		23.822
1791	28.718	25.702		24.500
1790	27.813	25.781		23.989
1789	28.245	25.977		24.439
1788	28.093	26.172		24.914
1787	27.127	26.729		24.447
1786	28.084	30.011		24.865
1785	28.098	31.939		24.728
1784	27.316	27.834		23.132
1783	25.992	28.312		24.727
1782	26.645	28.624		23.592
1781	26.751	26.816		25.021
1780	27.038	26.901		24.708
1779	27.436	27.276		25.765
1778	28.254	27.462		23.415
1777	26.939	27.151		23.830
1776	27.051	27.102		23.778
1775	27.032	27.217		23.551
1774	28.076	27.350		24.091
1773	26.633	27.178		24.370
1772	27.035	27.167		24.729
1771	27.238	27.214		25.167
1770	26.642	26.642		24.883
1769	25.040	26.073		26.108
1768	26.078	25.750		26.262

	$\delta^{18}O$			
	TR EE 67		TR EE 78	
YEAR	RAW MEASURE	ERROR ADJUSTED	RAW MEASURE	ERROR ADJUSTED
1767	26.087	25.875		24.117
1766	25.057	26.331		23.813
1765	26.788	26.392		24.496
1764	25.047	26.158		24.649
1763	25.681	26.183		
1762	25.870	25.569		
1761	25.477	25.189		
1760	23.771	25.433		
1759	24.493	25.377		
1758	25.120	25.041		
1757	24.680	24.702		
1756	24.376	24.701		
1755	25.017	25.254		
1754	25.222	25.467		
1753	25.443	25.389		
1752	25.860	25.500		
1751	24.738	25.499		
1750	24.362	26.138		
1749	24.726	27.288		
1748	25.128	27.782		
1747	27.070	27.569		
1746	25.445	27.174		
1745	25.937	26.981		
1744	24.559	27.358		
1743	24.311	27.439		
1742	25.278	27.109		
1741	25.545	26.474		
1740	26.314	26.040		
1739	26.560	25.883		
1738	25.396	25.959		
1737	26.591	25.919		
1736	27.080	24.897		
1735	26.367	24.889		
1734	26.343	25.334		
1733	26.399	26.283		
1732	26.599	28.482		
1731	26.814	29.426		
1730	24.928	29.609		
1729	25.093	29.263		
1728	26.616	28.522		

	$\delta^{18}O$			
	TR EE 67		TR EE 78	
YEAR	RAW MEASURE	ERROR ADJUSTED	RAW MEASURE	ERROR ADJUSTED
1727	26.033	29.016		
1726	26.513	29.276		
1725	26.448	29.235		
1724	26.179	29.240		
1723	26.388	29.317		
1722	26.182	28.471		
1721	24.357	28.489		
1720	25.970	29.931		
1719	25.979	30.509		
1718	25.467	26.698		
1717	25.474	25.585		
1716	27.295	26.321		
1715	25.498	25.524		
1714	25.203	26.965		
1713	25.078	26.981		
1712	26.118	26.485		
1711	27.797	26.229		
1710	27.258	25.933		
1709	26.393	25.584		
1708	26.091	25.302		
1707	28.241	25.334		
1706	25.697	25.525		
1705	26.503	24.933		
1704	25.864	24.851		
1703	25.572	27.092		
1702	25.297	28.179		
1701	23.903	25.724		
1700	25.329	25.790		
1699	24.542	25.977		
1698	24.731	25.770		
1697	25.608	25.793		
1696	23.786	26.195		
1695	24.284	25.254		
1694	25.458	25.133		
1693	23.191	25.242		
1692	23.637	25.117		
1691	24.346	24.814		
1690	24.945	25.021		
1689	24.989	25.736		
1688	25.360	25.989		

	$\delta^{18}O$			
	TR EE 67		TR EE 78	
YEAR	RAW MEASURE	ERROR ADJUSTED	RAW MEASURE	ERROR ADJUSTED
1687	23.453	25.392		
1686	25.543	24.485		
1685	23.948	24.739		
1684	24.312	26.914		
1683	23.167	27.565		
1682	24.312	27.393		
1681	25.580	27.464		
1680	23.426	28.597		
1679	23.318	30.835		
1678	23.364	30.437		
1677	25.897	29.304		
1676	25.045	28.334		
1675	25.690	27.942		
1674	25.120	28.197		
1673	25.934	28.052		
1672	26.204	27.405		
1671	24.612	27.677		
1670	24.714	28.088		
1669	24.094	27.895		
1668	23.520	27.176		
1667	23.520	26.234		
1666	24.910	26.478		
1665	24.907	26.709		
1664	26.538	26.876		
1663		27.151		
1662		27.557		
1661		28.034		
1660		27.239		
1659		27.011		
1658		27.040		
1657		27.396		
1656		27.721		
1655		26.806		
1654		26.976		
1653		27.175		
1652		26.953		
1651		25.984		
1650		25.382		
1649		26.039		
1648		25.969		

	$\delta^{18}O$			
	TR EE 67		TR EE 78	
YEAR	RAW MEASURE	ERROR ADJUSTED	RAW MEASURE	ERROR ADJUSTED
1647		25.337		
1646		26.277		
1645		25.755		
1644		25.337		
1643		25.737		
1642		25.778		
1641		25.289		
1640		24.089		
1639		24.326		
1638		24.891		
1637		24.896		
1636		24.567		
1635		24.557		
1634		25.018		
1633		25.220		
1632		25.420		
1631		25.723		
1630		25.177		
1629		24.555		
1628		24.496		
1627		24.826		
1626		25.448		
1625		26.678		
1624		25.770		
1623		25.779		
1622		25.062		
1621		24.430		
1620		24.704		
1619		25.349		
1618		25.703		
1617		26.283		
1616		26.425		
1615		25.694		
1614		26.252		
1613		26.889		
1612		26.721		
1611		26.359		
1610		26.359		
1609		26.442		
1608		26.617		

	$\delta^{18}O$			
	TR EE 67		TR EE 78	
YEAR	RAW MEASURE	ERROR ADJUSTED	RAW MEASURE	ERROR ADJUSTED
1607		26.599		
1606		25.292		
1605		25.087		
1604		26.088		
1603		26.290		
1602		26.250		
1601		26.486		
1600		26.376		
1599		26.236		
1598		26.342		
1597		26.031		
1596		24.793		
1595		25.562		
1594		25.972		
1593		25.681		
1592		25.470		
1591		26.207		
1590		26.701		
1589		25.480		
1588		25.195		
1587		25.231		
1586		26.127		
1585		27.446		
1584		27.371		
1583		26.666		
1582		26.214		
1581		27.208		
1580		27.132		
1579		26.002		
1578		26.299		
1577		25.820		
1576		25.543		
1575		25.148		
1574		24.229		
1573		25.010		
1572		24.740		
1571		24.686		
1570		25.274		
1569		24.596		
1568		24.026		

	$\delta^{18}O$			
	TR EE 67		TR EE 78	
YEAR	RAW MEASURE	ERROR ADJUSTED	RAW MEASURE	ERROR ADJUSTED
1567		24.761		
1566		24.675		
1565		23.368		
1564		23.782		
1563		24.408		
1562		24.890		
1561		25.021		
1560		25.161		
1559		23.963		
1558		24.937		
1557		24.468		
1556		24.168		
1555		23.678		
1554		23.726		
1553		24.846		
1552		24.792		
1551		23.432		
1550		23.334		
1549		23.897		
1548		25.569		
1547		25.222		
1546		25.547		
1545		25.277		
1544		25.780		
1543		26.076		
1542		25.074		
1541		24.669		
1540		24.330		
1539		23.774		
1538		23.520		
1537		24.132		
1536		24.904		
1535		25.461		
1534		26.505		
1533		26.540		

Table 8. Oxygen Isotope Measurements for Trees 82 and 88.

	$\delta^{18}O$			
	TR EE 82		TR EE 88	
YEAR	RAW MEASURE	ERROR ADJUSTED	RAW MEASURE	ERROR ADJUSTED
2006	25.91	25.910	27.06	26.180
2005	26.13	26.052	26.18	26.804
2004	25.49	25.944	26.97	27.022
2003	25.48	25.564	27.08	26.992
2002	25.89	25.484	27.91	27.088
2001	25.64	25.578	26.87	27.557
2000	25.69	25.820	27.41	27.599
1999	24.27	25.757	25.20	27.009
1998	24.90	25.654	24.47	27.249
1997	24.98	25.652	27.67	26.403
1996	24.90	24.994	25.84	25.104
1995	25.37	24.413	23.82	24.732
1994	25.73	24.767	27.05	26.483
1993	26.04	24.937	25.88	27.019
1992	26.04	24.965	24.71	25.661
1991	26.64	24.923	26.42	24.312
1990	26.67	25.104	24.15	25.574
1989	26.19	25.399	24.79	26.704
1988	26.12	25.642	25.15	25.871
1987	26.06	25.860	25.11	25.036
1986	24.92	26.026	25.34	25.525
1985	25.89	26.043	25.63	25.872
1984	26.09	26.289	26.09	24.464
1983	25.95	26.615	26.73	24.590
1982	25.72	26.660	26.39	24.944
1981	26.08	26.469	25.08	25.132
1980	24.89	26.202	26.43	25.128
1979	26.44	26.137	24.42	25.261
1978	26.55	26.094	26.42	25.456
1977	25.43	25.895	26.04	25.703
1976	25.92	25.190	25.31	26.050
1975	25.65	25.366	23.88	26.501
1974	25.47	25.894	24.93	26.597
1973	25.43	26.047	26.22	26.169
1972	25.39	26.021	24.61	25.348
1971	25.49	25.908	26.24	25.953
1970	25.79	25.770	26.77	25.623
1969	26.40	25.914	24.65	24.864
1968	25.32	25.799	24.83	26.113

	$\delta^{18}O$			
	TR EE 82		TR EE 88	
YEAR	RAW MEASURE	ERROR ADJUSTED	RAW MEASURE	ERROR ADJUSTED
1967	26.21	25.125	26.69	26.164
1966	25.35	25.810	25.59	25.725
1965	25.44	26.467	25.80	25.020
1964	26.13	26.459	26.73	24.129
1963	26.22	25.813	23.94	24.633
1962	25.60	25.601	25.94	25.549
1961	25.61	25.858	25.02	25.789
1960	26.02	25.722	25.17	24.921
1959	25.52	25.573	25.38	25.861
1958	25.79	25.470	25.83	26.530
1957	25.71	25.437	25.37	26.088
1956	25.83	25.409	25.62	24.797
1955	25.83	25.413	24.61	24.872
1954	26.30	25.491	26.20	26.010
1953	25.20	25.675	23.43	26.239
1952	25.14	25.984	27.45	25.664
1951	23.84	26.246	24.95	25.850
1950	24.42	25.625	25.95	26.449
1949	24.85	25.703	27.14	25.277
1948	25.01	26.034	26.19	24.568
1947	25.24	25.510	26.39	25.686
1946	26.00	25.400	27.17	25.188
1945	24.22	25.626	27.86	25.118
1944	25.85	26.067	28.36	25.262
1943	24.58	26.191	26.85	25.485
1942	25.11	25.971	25.81	25.740
1941	25.27	25.627	27.39	25.479
1940	25.85	25.619	23.84	25.518
1939	25.66	25.836	26.61	25.234
1938	25.64	25.881	24.91	24.969
1937	24.92	25.591	25.45	25.783
1936	23.86	25.710	25.82	24.196
1935	24.64	25.756	26.45	25.680
1934	24.22	25.734	25.02	26.550
1933	25.55	25.811	26.36	25.236
1932	25.24	25.830	25.66	25.920
1931	25.31	25.986	24.72	26.817
1930	25.12	26.135	25.92	26.610
1929	25.07	25.450	24.91	26.263
1928	25.169	25.169	23.01	26.539

	$\delta^{18}O$			
	TR EE 82		TR EE 88	
YEAR	RAW MEASURE	ERROR ADJUSTED	RAW MEASURE	ERROR ADJUSTED
1927	25.65	24.804	25.85	27.140
1926	25.05	24.019	24.58	27.703
1925	25.66	24.255	25.38	28.153
1924	25.84	24.614	26.15	27.764
1923	25.16	24.874	24.59	26.649
1922	26.54	25.002	26.67	26.081
1921	25.97	25.163	26.20	26.945
1920	25.90	25.547	26.45	25.121
1919	25.65	25.655	26.33	25.105
1918	26.99	24.575	26.78	26.096
1917	26.30	25.247	26.02	25.098
1916	25.82	25.374	25.21	25.390
1915	25.66	24.721	25.96	25.722
1914	26.19	25.025	26.73	26.165
1913	26.66	25.209	25.24	25.921
1912	25.59	25.482	29.20	25.358
1911	25.73	25.793	25.79	26.154
1910	26.05	25.692	26.35	25.763
1909	26.16	25.648	27.10	25.042
1908	25.78	25.370	26.04	25.311
1907	26.93	24.767	27.16	25.584
1906	25.57	24.065	26.52	24.587
1905	25.43	24.363	26.16	23.494
1904	25.84	24.470	27.19	25.188
1903	26.01	24.493	27.60	25.036
1902	25.95	25.351	24.90	24.963
1901	24.14	25.338	26.10	25.621
1900	23.85	25.272	25.68	25.817
1899	24.05	25.264	27.01	24.968
1898	26.29	25.135	26.59	26.214
1897	26.26	25.058	24.54	26.361
1896	24.39	23.996	26.11	26.326
1895	25.42	23.806	26.50	26.407
1894	24.65	25.393	27.32	26.433
1893	26.24	25.187	26.90	26.647
1892	26.05	25.421	26.14	26.113
1891	26.05	25.729	25.98	25.456
1890	24.23	25.703	26.23	25.635
1889	24.84	25.343	25.51	26.279
1888	25.16	26.132	26.23	26.303

	$\delta^{18}O$			
	TR EE 82		TR EE 88	
YEAR	RAW MEASURE	ERROR ADJUSTED	RAW MEASURE	ERROR ADJUSTED
1887	26.31	26.258	25.16	25.999
1886	26.56	25.955	26.79	28.400
1885	25.04	25.873	26.47	26.556
1884	25.21	25.744	27.25	26.165
1883	25.55	26.486	26.28	26.741
1882	26.42	26.707	26.63	26.698
1881	26.18	26.211	25.59	26.349
1880	26.31	25.857	25.78	26.985
1879	25.95	25.709	25.95	26.577
1878	25.76	25.959	26.84	26.275
1877	25.37	26.357	24.77	26.843
1876	26.17	26.442	26.17	27.406
1875	25.99	25.740	26.91	26.547
1874	25.11	25.695	25.50	25.275
1873	25.53	25.900	24.46	25.958
1872	24.93	26.086	28.21	25.861
1871	23.89	26.089	26.27	26.727
1870	25.35	25.910	25.06	26.690
1869	24.81	26.592	26.68	25.399
1868	25.28	26.209	26.70	25.246
1867	25.82	25.527	27.49	26.226
1866	26.11	25.510	25.39	26.671
1865	24.38	25.799	25.84	27.194
1864	24.78	25.964	27.17	26.901
1863	25.09	25.977	25.90	26.306
1862	24.38	25.285	25.90	26.034
1861	25.80	24.138	26.19	26.119
1860	24.67	23.900	26.28	25.917
1859	25.59	24.064	26.20	25.748
1858	23.21	25.424	26.11	25.963
1857	24.19	26.277	25.86	25.483
1856	25.08	25.773	26.53	26.539
1855	24.04	24.667	27.60	26.570
1854	23.49	25.204	27.02	27.002
1853	24.22	24.899	25.15	26.674
1852	23.70	25.475	25.21	26.447
1851	25.34	26.170	26.16	26.248
1850	24.09	26.057	24.77	25.663
1849	25.86	25.875	25.76	25.802
1848	25.92	24.647	26.27	26.042

	$\delta^{18}O$			
	TR EE 82		TR EE 88	
YEAR	RAW MEASURE	ERROR ADJUSTED	RAW MEASURE	ERROR ADJUSTED
1847	27.77	24.618	26.10	26.551
1846	25.96	24.989	27.16	25.302
1845	27.06	25.504	26.67	25.728
1844	27.13	26.294	27.11	26.598
1843	26.73	26.404	26.48	26.246
1842	25.88	25.410	26.63	25.123
1841	26.04	25.145	24.08	25.520
1840	26.56	25.363	26.70	27.638
1839	24.94	25.803	26.90	26.280
1838	25.48	26.332	26.26	25.370
1837	25.79	26.221	25.02	26.345
1836	25.77	26.270	25.98	26.709
1835	23.78	26.082	25.70	27.190
1834	24.50	25.860	27.72	26.370
1833	25.18	25.636	27.38	25.585
1832	26.55	25.545	26.26	26.291
1831	27.18	26.067	26.66	26.804
1830	24.20	25.988	24.09	25.969
1829	25.42	25.392	23.44	25.939
1828	26.69	25.336	25.25	26.157
1827	23.27	25.298	26.15	26.258
1826	24.79	24.678	25.65	26.219
1825	24.65	24.183	26.57	26.139
1824	26.42	25.102	24.01	25.968
1823	25.59	24.952	25.62	26.179
1822	24.03	25.110	25.88	26.943
1821	25.42	25.546	24.35	27.406
1820	24.81	25.920	26.21	26.594
1819	25.19	25.699	25.27	25.280
1818	26.77	24.573	25.44	25.325
1817	25.10	24.741	25.36	25.902
1816	25.16	24.995	25.79	25.100
1815	24.70	24.644	25.04	25.515
1814	26.58	25.086	24.84	26.100
1813	25.40	25.386	27.59	26.171
1812	24.84	24.926	26.08	26.642
1811	25.66	25.157	26.37	26.949
1810	24.93	23.613	27.00	26.829
1809	25.40	24.007	24.49	26.922
1808	24.76	24.783	25.20	26.540

	$\delta^{18}O$			
	TR EE 82		TR EE 88	
YEAR	RAW MEASURE	ERROR ADJUSTED	RAW MEASURE	ERROR ADJUSTED
1807	25.50	24.507	26.22	26.182
1806	25.64	23.809	25.54	24.677
1805	25.14	23.717	24.72	26.337
1804	23.51	24.082	25.48	26.825
1803	23.42	23.955	25.10	26.376
1802	25.04	24.991		25.415
1801	25.03	24.447		25.622
1800	23.62	25.237		25.824
1799	23.57	25.892		26.675
1798	24.41	26.669		27.577
1797	24.84	27.209		26.998
1796	26.62	26.265		26.398
1795	25.85	26.968		26.053
1794	25.30	27.090		24.139
1793	25.20	26.795		23.755
1792	24.97	26.159		25.110
1791	26.44	25.970		25.962
1790	24.33	26.273		25.801
1789	24.86	26.007		26.254
1788	24.64	25.119		24.841
1787	25.27	25.497		25.020
1786	25.79	25.752		25.766
1785	25.39	25.656		25.117
1784	25.24	24.310		25.158
1783	25.33	24.254		25.849
1782	24.68	24.873		25.338
1781	24.50	25.783		25.414
1780	25.17	26.754		25.459
1779	24.89	26.408		25.625
1778	24.67	24.598		25.081
1777	25.89	25.444		25.173
1776	25.09	26.240		27.034
1775	25.35	24.109		26.388
1774	23.76	24.319		26.329
1773	25.65	24.708		26.761
1772	26.71	25.539		25.311
1771	25.99	26.083		24.941
1770	26.76	25.109		25.784
1769	25.31	24.413		25.868
1768	24.80	25.223		25.162

	$\delta^{18}O$			
	TR EE 82		TR EE 88	
YEAR	RAW MEASURE	ERROR ADJUSTED	RAW MEASURE	ERROR ADJUSTED
1767	25.22	24.921		25.031
1766	25.71	25.246		25.338
1765	25.30	26.351		24.988
1764	25.09	25.591		
1763	26.35	25.136		
1762	24.94	24.913		
1761	25.81	25.536		
1760		26.146		
1759		25.266		
1758		25.042		
1757		25.481		
1756		25.067		
1755		25.276		
1754		24.933		
1753		25.291		
1752		25.587		
1751		25.358		
1750		24.358		
1749		23.478		
1748		23.948		
1747		24.992		
1746		24.745		
1745		23.729		
1744		23.669		
1743		24.305		
1742		24.831		
1741		26.119		
1740		26.100		
1739		25.520		
1738		25.247		
1737		25.096		
1736		25.530		
1735		25.752		
1734		24.530		
1733		24.787		
1732		24.759		
1731		25.265		
1730		25.678		
1729		25.456		
1728		25.279		

	$\delta^{18}O$			
	TR EE 82		TR EE 88	
YEAR	RAW MEASURE	ERROR ADJUSTED	RAW MEASURE	ERROR ADJUSTED
1727		25.290		
1726		24.901		
1725		24.574		
1724		24.857		
1723		25.039		
1722		24.802		
1721		25.093		
1720		25.631		
1719		25.182		
1718		25.017		
1717		24.192		
1716		25.581		
1715		26.492		
1714		26.171		
1713		26.523		
1712		25.665		
1711		24.962		
1710		25.077		
1709		25.511		
1708		25.488		
1707		25.198		
1706		25.631		
1705		25.811		
1704		25.245		
1703		26.037		

Table 8. Oxygen Isotope Measurements for Tree 20.

	$\delta^{18}O$	
	TR EE 20	
YEAR	RAW MEASURE	ERROR ADJUSTED
2006	24.152	24.150
2005	25.455	26.015
2004	26.571	25.499
2003	24.949	25.201
2002	24.965	25.281
2001	25.571	25.106
2000	26.247	25.586
1999	26.200	26.118
1998	23.515	26.195
1997	22.942	24.761
1996	23.484	23.297
1995	23.260	23.086
1994	23.821	23.408
1993	24.534	23.331
1992	25.688	23.688
1991	25.841	24.251
1990	24.628	25.058
1989	25.188	25.727
1988	24.529	25.593
1987	24.532	24.816
1986	23.767	25.053
1985	25.739	24.726
1984	23.260	24.530
1983	26.218	24.206
1982	25.112	24.362
1981	24.638	25.175
1980	24.128	23.845
1979	24.863	25.607
1978	24.850	25.428
1977	25.240	24.836
1976	24.688	24.412
1975	24.885	24.368
1974	25.025	24.830
1973	24.701	24.902
1972	24.792	25.141
1971	25.392	24.832
1970	24.769	24.813
1969	25.186	24.952
1968	25.782	24.895

	$\delta^{18}O$	
	TR EE 20	
YEAR	RAW MEASURE	ERROR ADJUSTED
1967	25.744	24.731
1966	24.955	24.896
1965	24.645	25.257
1964	24.809	24.904
1963	25.328	25.091
1962	24.820	25.561
1961	25.525	25.760
1960	25.213	25.432
1959	24.883	24.875
1958	25.212	24.688
1957	26.051	24.859
1956	26.151	25.211
1955	24.975	24.963
1954	24.038	25.286
1953	25.357	25.346
1952	26.186	25.062
1951	25.506	24.995
1950	26.061	25.411
1949	26.184	26.015
1948	25.304	26.008
1947	25.540	25.116
1946	24.804	24.309
1945	24.733	24.924
1944	25.434	25.829
1943	24.844	25.878
1942	25.359	25.710
1941	26.001	26.080
1940	25.703	26.002
1939	25.931	25.414
1938	23.144	25.443
1937	22.828	24.951
1936	22.921	24.763
1935	26.305	25.170
1934	26.079	25.113
1933	26.091	25.068
1932	26.525	25.579
1931	26.013	25.904
1930	25.834	25.761
1929	26.513	25.514
1928	24.852	23.486

	$\delta^{18}O$	
	TR EE 20	
YEAR	RAW MEASURE	ERROR ADJUSTED
1927	25.884	22.894
1926	25.184	22.993
1925	26.642	25.186
1924	26.305	26.170
1923	25.044	26.085
1922	25.913	26.267
1921	25.701	26.347
1920	24.992	25.977
1919	25.715	25.974
1918	25.181	26.210
1917	26.579	25.167
1916	25.962	25.651
1915	25.841	25.398
1914	25.740	26.198
1913	25.815	26.420
1912	26.523	25.603
1911	26.146	25.450
1910	25.975	25.825
1909	25.441	25.474
1908	26.307	25.197
1907	24.310	25.565
1906	25.985	25.440
1905	23.979	26.345
1904	25.980	26.050
1903	26.132	25.860
1902	25.378	25.768
1901	25.722	25.797
1900	25.867	26.245
1899	26.329	26.319
1898	26.617	26.065
1897	24.776	25.758
1896	25.183	25.739
1895	25.796	25.731
1894	24.506	24.774
1893	26.366	25.508
1892	25.140	24.450
1891	25.147	25.740
1890	26.529	26.048
1889	26.338	25.554
1888	26.752	25.638

	$\delta^{18}O$	
	TR EE 20	
YEAR	RAW MEASURE	ERROR ADJUSTED
1887	27.308	25.832
1886	26.653	26.165
1885	26.693	26.495
1884	26.847	25.672
1883	26.965	24.961
1882	26.523	25.421
1881		25.359
1880		25.071
1879		26.004
1878		25.213
1877		25.372
1876		26.358
1875		26.407
1874		26.721
1873		27.159
1872		26.815
1871		26.682
1870		26.797
1869		26.916
1868		26.713
1867		26.297

Table 9. Carbon Isotope Measurements for Trees 67 and 78.

	$\delta^{13}C$			
	TR EE 67		**TR EE 78**	
YEAR	**RAW MEASURE**	**ERROR ADJUSTED**	**RAW MEASURE**	**ERROR ADJUSTED**
2006	-26.776	-26.780	-25.349	-25.351
2005	-26.327	-26.543	-25.430	-25.403
2004	-26.602	-26.375	-25.626	-25.492
2003	-26.549	-26.486	-25.696	-25.614
2002	-26.417	-26.587	-25.682	-25.673
2001	-26.510	-26.568	-26.049	-25.695
2000	-26.486	-26.528	-25.599	-25.698
1999	-26.404	-26.461	-25.176	-25.888
1998	-26.562	-26.440	-24.997	-25.945
1997	-26.839	-26.487	-24.587	-25.660
1996	-26.550	-26.505	-24.688	-25.380
1995	-26.508	-26.494	-25.505	-25.152
1994	-26.309	-26.460	-25.168	-25.024
1993	-26.271	-26.416	-25.490	-24.797
1992	-26.323	-26.464	-24.885	-24.617
1991	-26.240	-26.553	-25.136	-24.683
1990	-26.505	-26.689	-24.818	-25.076
1989	-26.178	-26.802	-24.440	-25.422
1988	-26.696	-26.687	-24.363	-25.244
1987	-26.421	-26.557	-24.215	-25.319
1986	-26.283	-26.526	-25.313	-25.384
1985	-26.475	-26.481	-25.661	-25.023
1984	-26.124	-26.377	-24.879	-25.006
1983	-26.397	-26.303	-25.209	-25.080
1982	-25.674	-26.281	-25.070	-24.883
1981	-25.561	-26.284	-24.866	-24.641
1980	-25.467	-26.310	-24.855	-24.437
1979	-25.496	-26.292	-24.273	-24.374
1978	-24.767	-26.257	-24.691	-24.292
1977	-24.932	-26.351	-24.907	-24.423
1976	-25.205	-26.461	-24.662	-25.113
1975	-25.796	-26.339	-24.974	-25.489
1974	-25.327	-26.243	-25.016	-25.495
1973	-25.541	-26.484	-24.987	-25.019
1972	-25.570	-26.649	-24.011	-25.060
1971	-25.316	-26.513	-22.878	-25.174
1970	-25.571	-26.391	-23.788	-25.081
1969	-25.489	-26.315	-23.009	-24.953
1968	-25.543	-26.339	-23.996	-24.865

	$\delta^{13}C$			
	TR EE 67		TR EE 78	
YEAR	RAW MEASURE	ERROR ADJUSTED	RAW MEASURE	ERROR ADJUSTED
1967	-25.289	-26.442	-24.172	-24.815
1966	-25.073	-26.341	-24.672	-24.480
1965	-24.974	-26.169	-24.777	-24.406
1964	-24.396	-26.253	-24.425	-24.676
1963	-24.601	-26.326	-24.602	-24.843
1962	-25.366	-25.985	-24.211	-24.813
1961	-25.338	-25.672	-24.316	-24.713
1960	-25.267	-25.597	-24.432	-24.896
1959	-25.509	-25.541	-24.133	-24.993
1958	-25.301	-25.492	-24.276	-25.013
1957	-25.552	-25.479	-24.737	-24.969
1956	-25.571	-25.483	-24.918	-24.459
1955	-25.449	-25.201	-25.025	-23.740
1954	-25.729	-24.844	-24.249	-23.081
1953	-26.033	-24.852	-24.256	-23.534
1952	-25.566	-24.953	-24.704	-23.317
1951	-25.634	-25.103	-23.844	-23.488
1950	-24.978	-25.314	-23.453	-24.058
1949	-24.598	-25.638	-23.421	-24.296
1948	-24.598	-25.669	-23.426	-24.659
1947	-24.801	-25.415	-23.825	-24.729
1946	-24.628	-25.412	-24.605	-24.495
1945	-24.545	-25.521	-24.343	-24.544
1944	-24.501	-25.555	-24.579	-24.351
1943	-23.848	-25.543	-24.807	-24.268
1942	-23.660	-25.415	-24.256	-24.366
1941	-24.051	-25.369	-24.246	-24.333
1940	-23.928	-25.504	-24.313	-24.175
1939	-24.240	-25.546	-24.365	-24.344
1938	-24.210	-25.504	-25.175	-24.704
1937	-24.244	-25.511	-24.714	-24.894
1936	-24.270	-25.521	-23.925	-24.980
1935	-23.776	-25.404	-23.777	-24.510
1934	-24.001	-25.267	-24.320	-24.256
1933	-23.724	-25.142	-24.049	-24.470
1932	-23.456	-25.047	-24.174	-24.369
1931	-23.901	-24.987	-23.583	-23.736
1930	-23.702	-24.761	-23.253	-23.458
1929	-24.082	-24.470	-23.601	-23.423
1928	-24.155	-24.500	-23.843	-23.425

	$\delta^{13}C$			
	TR EE 67		TR EE 78	
YEAR	RAW MEASURE	ERROR ADJUSTED	RAW MEASURE	ERROR ADJUSTED
1927	-24.421	-24.675	-23.790	-23.463
1926	-24.001	-25.089	-23.632	-23.641
1925	-24.021	-25.359	-23.514	-23.862
1924	-24.284	-25.347	-23.664	-24.221
1923	-25.097	-25.316	-23.511	-24.543
1922	-23.773	-25.287	-23.587	-24.482
1921	-25.244	-25.387	-23.764	-24.372
1920	-24.985	-25.477	-23.470	-24.449
1919	-25.073	-25.377	-23.168	-24.565
1918	-25.067	-25.354	-23.456	-24.679
1917	-25.037	-25.494	-23.455	-24.770
1916	-25.069	-25.557	-23.640	-24.585
1915	-24.994	-25.563	-23.529	-24.326
1914	-24.803	-25.509	-23.576	-24.256
1913	-24.825	-25.488	-24.460	-24.252
1912	-24.734	-25.636	-24.066	-24.272
1911	-24.303	-25.803	-23.913	-24.302
1910	-24.204	-25.968	-23.873	-24.332
1909	-25.783	-25.845	-24.089	-24.368
1908	-25.214	-25.611	-24.053	-24.647
1907	-25.087	-25.604	-24.440	-25.032
1906	-25.782	-25.521	-24.330	-25.016
1905	-25.253	-25.155	-24.358	-24.787
1904	-25.674	-24.860	-24.206	-24.458
1903	-24.316	-24.650	-24.116	-24.074
1902	-24.179	-24.600	-24.612	-23.883
1901	-25.326	-24.623	-24.346	-23.811
1900	-24.527	-24.732	-24.427	-23.946
1899	-25.563	-24.758	-23.885	-24.213
1898	-24.825	-24.659	-24.053	-24.238
1897	-24.998	-24.592	-24.555	-24.105
1896	-25.838	-24.543	-24.053	-24.086
1895	-24.516	-24.516	-24.135	-24.144
1894	-25.158	-24.368	-24.489	-23.994
1893	-24.705	-23.991	-24.383	-23.700
1892	-24.571	-23.778	-23.604	-23.478
1891	-24.970	-23.701	-23.744	-23.312
1890	-24.697	-23.882	-23.990	-23.417
1889	-25.447	-24.023	-23.788	-23.640
1888	-24.788	-23.960	-24.077	-23.800

	$\delta^{13}C$			
	TR EE 67		TR EE 78	
YEAR	RAW MEASURE	ERROR ADJUSTED	RAW MEASURE	ERROR ADJUSTED
1887	-25.448	-24.041	-23.571	-23.811
1886	-25.376	-24.208	-24.119	-23.745
1885	-24.503	-24.223	-24.907	-23.636
1884	-24.977	-24.216	-24.639	-23.548
1883	-24.917	-24.233	-24.776	-23.569
1882	-24.707	-24.251	-24.027	-23.632
1881	-24.424	-24.240	-24.607	-23.544
1880	-24.717	-23.996	-23.557	-23.551
1879	-24.747	-23.827	-23.936	-23.628
1878	-24.308	-23.947	-24.631	-23.722
1877	-25.152	-23.895	-24.225	-23.576
1876	-25.113	-23.727	-24.042	-23.366
1875	-24.848	-23.567	-24.011	-23.210
1874	-24.570	-23.553	-24.660	-23.306
1873	-24.534	-23.807	-24.094	-23.427
1872	-25.037	-23.817	-23.647	-23.457
1871	-24.691	-23.747	-23.627	-23.453
1870	-23.941	-23.941	-23.745	-23.470
1869	-24.273	-24.099	-24.216	-23.542
1868	-24.612	-24.153	-24.682	-23.615
1867	-23.624	-24.283	-24.516	-23.610
1866	-24.409	-24.356	-24.457	-23.567
1865	-24.684	-24.124	-24.167	-23.537
1864	-24.914	-24.006	-24.265	-23.553
1863	-24.496	-24.031	-23.907	-23.575
1862	-24.205	-24.165	-23.938	-23.794
1861	-24.619	-24.434	-23.563	-24.142
1860	-24.613	-24.914	-23.528	-24.370
1859	-25.149	-24.542	-23.966	-24.097
1858	-24.899	-23.995	-23.983	-23.920
1857	-24.509	-24.747	-24.194	-23.923
1856	-24.972	-25.167	-23.971	-24.070
1855	-24.296	-25.025	-24.156	-24.196
1854	-24.784	-25.033	-23.737	-24.388
1853	-24.495	-25.069	-23.550	-24.346
1852	-24.487	-25.070	-23.934	-24.263
1851	-24.342	-25.057	-23.954	-24.167
1850	-24.508	-25.045	-23.891	-24.484
1849	-24.350	-25.060	-23.687	-24.400
1848	-23.898	-25.045	-23.773	-24.326

	$\delta^{13}C$			
	TR EE 67		TR EE 78	
YEAR	RAW MEASURE	ERROR ADJUSTED	RAW MEASURE	ERROR ADJUSTED
1847	-24.171	-24.988	-23.915	-23.963
1846	-24.414	-24.880	-24.546	-24.207
1845	-24.352	-24.806	-24.402	-24.337
1844	-23.932	-24.815	-23.994	-24.093
1843	-24.299	-24.776	-23.500	-24.351
1842	-24.171	-24.666	-23.678	-24.378
1841	-24.255	-24.404	-24.141	-23.776
1840	-24.919	-24.260	-23.781	-23.754
1839	-24.489	-24.368	-23.871	-23.927
1838	-24.764	-25.280	-24.426	-23.882
1837	-25.038	-25.594	-23.970	-23.881
1836	-23.765	-25.257	-24.133	-23.842
1835	-24.549	-25.136	-23.293	-24.593
1834	-24.973	-25.271	-23.108	-24.726
1833	-24.548	-25.665	-23.502	-24.685
1832	-24.433	-25.487	-23.635	-24.218
1831	-24.688	-25.346	-24.132	-24.329
1830	-24.468	-25.565	-23.620	-23.719
1829	-24.272	-24.994	-23.290	-24.231
1828	-24.959	-24.327	-23.558	-24.409
1827	-24.731	-24.224	-23.044	-24.103
1826	-23.694	-24.707	-24.047	-24.065
1825	-25.034	-25.171	-24.358	-24.485
1824	-24.496	-24.728	-24.326	-24.047
1823	-24.235	-24.968	-23.313	-23.661
1822	-24.231	-25.417	-24.070	-23.681
1821	-24.120	-25.015	-24.148	-24.015
1820	-23.739	-24.892	-23.209	-24.526
1819	-24.130	-25.088	-23.456	-24.550
1818	-24.416	-25.604	-22.719	-24.424
1817	-23.811	-25.372	-24.545	-24.213
1816	-23.724	-24.761	-23.636	-24.134
1815	-24.904	-25.008	-24.463	-23.925
1814	-24.478	-24.984	-24.325	-23.704
1813	-23.986	-24.714	-24.532	-23.565
1812	-25.185	-24.608	-24.227	-23.898
1811	-24.399	-24.725	-24.410	-24.024
1810	-23.969	-24.916	-23.653	-24.111
1809	-23.951	-24.776	-23.926	-24.058
1808	-24.311	-25.002	-23.104	-23.906

	$\delta^{13}C$			
	TR EE 67		TR EE 78	
YEAR	RAW MEASURE	ERROR ADJUSTED	RAW MEASURE	ERROR ADJUSTED
1807	-24.444	-25.329	-23.494	-23.624
1806	-24.679	-24.962	-24.165	-23.867
1805	-24.439	-25.072	-24.449	-23.935
1804	-24.666	-25.413	-24.353	-23.827
1803	-23.939	-25.386	-24.224	-23.729
1802	-23.588	-24.974	-24.281	-23.875
1801	-23.652	-24.607		-24.376
1800	-24.332	-24.884		-24.367
1799	-24.498	-24.950		-23.907
1798	-24.163	-24.878		-23.579
1797	-23.328	-24.734		-23.913
1796	-23.015	-24.547		-23.906
1795	-23.957	-24.498		-23.902
1794	-23.414	-24.685		-24.281
1793	-24.728	-24.739		-24.041
1792	-24.119	-24.611		-23.763
1791	-24.029	-24.422		-23.190
1790	-23.963	-24.897		-23.404
1789	-23.861	-25.134		-23.686
1788	-23.811	-25.076		-23.967
1787	-23.921	-24.906		-23.505
1786	-23.781	-24.715		-23.432
1785	-24.099	-24.568		-23.247
1784	-24.556	-24.556		-23.902
1783	-24.827	-24.827		-24.325
1782	-24.470	-24.938		-23.968
1781	-24.435	-24.698		-23.706
1780	-23.985	-24.476		-24.085
1779	-24.311	-24.336		-23.421
1778	-24.161	-24.325		-23.279
1777	-24.311	-24.520		-23.378
1776	-24.174	-24.095		-24.078
1775	-24.279	-23.821		-24.187
1774	-24.089	-24.331		-24.371
1773	-24.001	-24.587		-24.445
1772	-24.145	-24.765		-24.304
1771	-24.016	-24.842		-24.012
1770	-24.577	-24.585		-23.803
1769	-24.254	-24.345		-23.298
1768	-24.307	-24.306		-23.618

	$\delta^{13}C$			
	TR EE 67		TR EE 78	
YEAR	RAW MEASURE	ERROR ADJUSTED	RAW MEASURE	ERROR ADJUSTED
1767	-24.755	-24.571		-24.262
1766	-24.664	-24.614		-24.392
1765	-24.517	-24.824		-24.260
1764	-24.636	-25.088		-24.280
1763	-24.405	-24.935		
1762	-24.048	-24.678		
1761	-24.320	-24.649		
1760	-24.510	-24.864		
1759	-23.942	-24.477		
1758	-24.151	-24.532		
1757	-23.915	-24.708		
1756	-24.171	-24.533		
1755	-24.129	-24.493		
1754	-24.078	-24.428		
1753	-24.155	-24.376		
1752	-23.593	-24.476		
1751	-24.246	-24.410		
1750	-23.849	-24.185		
1749	-24.217	-23.963		
1748	-24.129	-24.129		
1747	-24.223	-24.313		
1746	-24.227	-24.389		
1745	-24.487	-24.294		
1744	-23.872	-24.023		
1743	-24.832	-24.145		
1742	-24.548	-24.256		
1741	-24.084	-24.190		
1740	-24.156	-24.261		
1739	-24.422	-24.646		
1738	-24.612	-24.773		
1737	-24.049	-24.553		
1736	-24.457	-24.720		
1735	-24.455	-24.931		
1734	-24.681	-24.572		
1733	-24.435	-23.956		
1732	-24.734	-24.447		
1731	-24.317	-24.824		
1730	-24.392	-24.795		
1729	-24.120	-24.536		
1728	-24.635	-24.463		

	$\delta^{13}C$			
	TR EE 67		TR EE 78	
YEAR	RAW MEASURE	ERROR ADJUSTED	RAW MEASURE	ERROR ADJUSTED
1727	-24.059	-24.613		
1726	-23.874	-24.583		
1725	-23.977	-24.419		
1724	-23.634	-24.362		
1723	-24.137	-24.800		
1722	-24.138	-24.829		
1721	-24.155	-24.369		
1720	-23.896	-23.962		
1719	-24.117	-24.795		
1718	-23.826	-24.672		
1717	-24.186	-24.381		
1716	-24.045	-24.241		
1715	-24.725	-24.219		
1714	-25.501	-24.135		
1713	-25.224	-23.897		
1712	-25.903	-23.885		
1711	-24.810	-24.172		
1710	-24.023	-24.338		
1709	-24.673	-23.977		
1708	-24.978	-23.763		
1707	-24.937	-24.099		
1706	-24.813	-24.771		
1705	-24.328	-24.517		
1704	-24.953	-24.148		
1703	-23.907	-24.578		
1702	-24.191	-24.939		
1701	-25.048	-24.383		
1700	-25.147	-24.039		
1699	-25.057	-23.958		
1698	-24.920	-24.127		
1697	-24.484	-24.347		
1696	-25.251	-24.470		
1695	-24.972	-24.629		
1694	-24.663	-24.513		
1693	-25.210	-24.559		
1692	-24.690	-24.427		
1691	-25.365	-23.909		
1690	-25.014	-23.640		
1689	-25.521	-23.646		
1688	-25.522	-24.041		

	$\delta^{13}C$			
	TR EE 67		TR EE 78	
YEAR	RAW MEASURE	ERROR ADJUSTED	RAW MEASURE	ERROR ADJUSTED
1687	-25.200	-24.396		
1686	-24.865	-24.417		
1685	-24.971	-24.097		
1684	-24.636	-23.482		
1683	-25.114	-23.123		
1682	-25.259	-23.465		
1681	-24.726	-23.784		
1680	-24.576	-23.667		
1679	-25.088	-24.509		
1678	-24.974	-24.270		
1677	-24.180	-24.066		
1676	-24.434	-24.000		
1675	-24.822	-23.934		
1674	-24.567	-23.859		
1673	-25.284	-23.825		
1672	-25.366	-23.888		
1671	-26.073	-23.839		
1670	-25.790	-23.911		
1669	-26.372	-24.157		
1668	-26.591	-24.429		
1667	-25.944	-24.904		
1666	-25.864	-24.622		
1665	-25.936	-24.446		
1664	-25.722	-24.235		
1663		-24.081		
1662		-24.266		
1661		-24.192		
1660		-24.272		
1659		-24.220		
1658		-24.225		
1657		-24.213		
1656		-24.076		
1655		-24.027		
1654		-24.117		
1653		-24.065		
1652		-24.354		
1651		-24.431		
1650		-24.272		
1649		-24.399		
1648		-24.704		

	$\delta^{13}C$			
	TR EE 67		TR EE 78	
YEAR	RAW MEASURE	ERROR ADJUSTED	RAW MEASURE	ERROR ADJUSTED
1647		-24.670		
1646		-24.561		
1645		-24.591		
1644		-24.531		
1643		-24.288		
1642		-24.121		
1641		-24.321		
1640		-24.441		
1639		-24.088		
1638		-24.073		
1637		-24.028		
1636		-24.009		
1635		-24.154		
1634		-24.124		
1633		-24.094		
1632		-24.116		
1631		-23.762		
1630		-23.991		
1629		-24.056		
1628		-23.986		
1627		-24.212		
1626		-24.220		
1625		-24.221		
1624		-24.243		
1623		-24.407		
1622		-24.100		
1621		-24.371		
1620		-24.716		
1619		-24.411		
1618		-24.116		
1617		-24.191		
1616		-24.401		
1615		-24.546		
1614		-24.220		
1613		-24.301		
1612		-24.460		
1611		-24.548		
1610		-24.604		
1609		-24.514		
1608		-24.645		

	$\delta^{13}C$			
	TR EE 67		TR EE 78	
YEAR	RAW MEASURE	ERROR ADJUSTED	RAW MEASURE	ERROR ADJUSTED
1607		-24.379		
1606		-24.362		
1605		-24.203		
1604		-24.450		
1603		-24.311		
1602		-23.973		
1601		-23.911		
1600		-23.880		
1599		-23.752		
1598		-24.097		
1597		-24.141		
1596		-24.134		
1595		-23.970		
1594		-24.045		
1593		-23.951		
1592		-24.008		
1591		-24.133		
1590		-24.267		
1589		-24.894		
1588		-25.402		
1587		-25.338		
1586		-25.706		
1585		-24.976		
1584		-24.239		
1583		-24.465		
1582		-24.857		
1581		-24.959		
1580		-24.883		
1579		-24.639		
1578		-24.519		
1577		-24.688		
1576		-24.029		
1575		-24.272		
1574		-24.936		
1573		-25.126		
1572		-25.077		
1571		-24.956		
1570		-24.647		
1569		-24.909		
1568		-25.115		

	$\delta^{13}C$			
	TR EE 67		TR EE 78	
YEAR	RAW MEASURE	ERROR ADJUSTED	RAW MEASURE	ERROR ADJUSTED
1567		-24.844		
1566		-24.850		
1565		-25.052		
1564		-24.864		
1563		-25.253		
1562		-25.114		
1561		-25.453		
1560		-25.497		
1559		-25.254		
1558		-24.954		
1557		-24.930		
1556		-24.768		
1555		-24.901		
1554		-25.183		
1553		-25.036		
1552		-24.679		
1551		-24.739		
1550		-25.043		
1549		-24.808		
1548		-24.281		
1547		-24.458		
1546		-24.743		
1545		-24.666		
1544		-25.140		
1543		-25.373		
1542		-25.861		
1541		-25.891		
1540		-26.144		
1539		-26.492		
1538		-26.267		
1537		-25.905		
1536		-25.891		
1535		-25.865		
1534		-25.447		
1533		-24.565		

Table 10. Carbon Isotope Measurements for Trees 82 and 88.

	$\delta^{13}C$			
	TR EE 82		TR EE 88	
YEAR	RAW MEASURE	ERROR ADJUSTED	RAW MEASURE	ERROR ADJUSTED
2006	-26.372	-26.370	-25.957	-25.960
2005	-26.612	-26.525	-25.896	-25.919
2004	-26.572	-26.598	-26.436	-26.130
2003	-26.754	-26.584	-26.227	-26.386
2002	-26.343	-26.675	-26.582	-26.278
2001	-26.760	-26.651	-27.100	-26.431
2000	-25.788	-26.416	-26.848	-26.733
1999	-25.360	-26.564	-26.513	-27.032
1998	-25.780	-26.560	-27.096	-26.916
1997	-26.157	-25.960	-25.987	-26.695
1996	-25.805	-25.579	-27.533	-26.637
1995	-25.488	-25.442	-26.946	-26.960
1994	-25.449	-25.696	-26.124	-26.402
1993	-25.211	-25.954	-27.202	-26.538
1992	-25.945	-26.094	-26.784	-27.367
1991	-25.109	-25.890	-26.415	-27.053
1990	-24.896	-25.671	-26.566	-26.499
1989	-25.144	-25.498	-26.960	-26.428
1988	-25.062	-25.459	-26.765	-27.065
1987	-24.776	-25.349	-26.071	-26.889
1986	-25.436	-25.316	-26.205	-26.604
1985	-25.408	-25.749	-26.319	-26.453
1984	-25.137	-25.596	-25.707	-26.578
1983	-24.746	-25.122	-26.271	-26.837
1982	-24.516	-24.955	-26.060	-26.879
1981	-24.587	-25.001	-25.640	-26.637
1980	-25.864	-25.118	-26.865	-26.177
1979	-25.292	-25.078	-26.647	-26.162
1978	-24.776	-24.938	-26.043	-26.254
1977	-25.384	-24.888	-27.027	-26.206
1976	-24.604	-25.290	-26.616	-25.831
1975	-24.843	-25.426	-26.482	-26.069
1974	-24.667	-25.366	-26.704	-26.188
1973	-24.709	-25.188	-26.005	-25.993
1972	-25.006	-24.947	-26.100	-25.764
1971	-25.180	-24.713	-26.577	-26.429
1970	-24.992	-24.562	-25.932	-26.776
1969	-24.963	-24.558	-26.215	-26.541
1968	-24.338	-24.885	-26.375	-26.183

	$\delta^{13}C$			
	TR EE 82		TR EE 88	
YEAR	RAW MEASURE	ERROR ADJUSTED	RAW MEASURE	ERROR ADJUSTED
1967	-24.235	-25.658	-26.285	-26.703
1966	-24.299	-25.522	-26.571	-26.853
1965	-24.764	-25.147	-26.156	-26.600
1964	-24.736	-24.875	-25.755	-26.513
1963	-24.303	-25.175	-26.042	-26.632
1962	-25.147	-25.108	-25.732	-26.364
1961	-25.337	-24.679	-26.109	-26.034
1960	-25.297	-24.774	-25.864	-26.140
1959	-25.048	-24.767	-26.306	-26.454
1958	-24.442	-24.683	-26.344	-26.224
1957	-24.412	-24.708	-26.097	-26.022
1956	-24.516	-24.865	-26.204	-26.219
1955	-24.855	-25.045	-26.142	-26.346
1954	-24.968	-25.147	-24.825	-26.317
1953	-25.002	-25.063	-25.621	-26.399
1952	-24.763	-24.981	-24.504	-26.475
1951	-25.573	-24.901	-26.420	-26.176
1950	-24.542	-24.513	-26.569	-25.871
1949	-24.464	-24.297	-25.647	-25.906
1948	-24.382	-24.254	-25.939	-25.943
1947	-24.657	-24.302	-26.461	-25.804
1946	-24.786	-24.555	-25.395	-26.032
1945	-25.156	-24.752	-25.011	-25.948
1944	-25.219	-24.708	-25.531	-26.057
1943	-25.616	-24.439	-24.975	-26.309
1942	-25.392	-24.642	-25.573	-26.312
1941	-24.924	-25.145	-25.127	-26.156
1940	-24.465	-25.302	-25.444	-26.159
1939	-24.433	-25.318	-25.372	-26.177
1938	-25.077	-25.232	-25.531	-25.870
1937	-24.723	-25.023	-26.181	-25.040
1936	-24.385	-24.620	-24.824	-25.399
1935	-24.146	-24.427	-25.130	-24.993
1934	-24.405	-24.431	-25.968	-25.189
1933	-24.788	-24.515	-25.596	-26.377
1932	-24.793	-24.719	-25.668	-26.479
1931	-25.088	-24.890	-25.534	-25.893
1930	-24.993	-24.966	-26.243	-25.812
1929	-24.490	-24.989	-25.637	-26.128
1928	-24.610	-24.876	-25.891	-26.227

	$\delta^{13}C$			
	TR EE 82		TR EE 88	
YEAR	RAW MEASURE	ERROR ADJUSTED	RAW MEASURE	ERROR ADJUSTED
1927	-25.098	-24.972	-26.004	-25.481
1926	-24.992	-25.403	-25.828	-25.113
1925	-24.408	-24.837	-25.347	-25.314
1924	-24.719	-24.504	-24.573	-25.309
1923	-25.079	-24.445	-25.391	-25.122
1922	-24.912	-24.407	-25.153	-25.466
1921	-24.310	-24.566	-25.196	-25.231
1920	-24.559	-24.712	-25.058	-25.328
1919	-24.493	-24.852	-23.827	-25.408
1918	-25.192	-25.104	-25.337	-25.416
1917	-25.068	-25.198	-24.974	-25.619
1916	-25.134	-25.370	-25.696	-25.997
1915	-25.170	-25.565	-25.225	-25.211
1914	-24.676	-25.411	-25.443	-24.990
1913	-24.052	-25.100	-25.524	-25.440
1912	-24.764	-24.752	-24.078	-25.864
1911	-24.598	-24.476	-25.261	-25.643
1910	-24.425	-24.461	-25.645	-25.651
1909	-24.278	-24.834	-24.235	-25.580
1908	-24.334	-24.945	-25.581	-25.880
1907	-24.601	-24.676	-25.362	-26.041
1906	-24.350	-24.423	-25.519	-25.713
1905	-24.235	-24.232	-25.112	-25.872
1904	-24.059	-24.255	-24.883	-25.971
1903	-24.834	-24.476	-25.728	-25.890
1902	-24.757	-24.739	-25.353	-25.600
1901	-25.646	-24.791	-25.319	-25.104
1900	-25.692	-24.926	-25.537	-24.762
1899	-24.868	-25.061	-24.784	-25.275
1898	-24.679	-24.956	-25.717	-25.202
1897	-23.650	-24.621	-24.647	-25.182
1896	-24.402	-24.553	-25.137	-25.130
1895	-24.791	-24.755	-26.126	-24.632
1894	-25.006	-25.052	-25.299	-24.202
1893	-24.497	-24.993	-25.552	-25.158
1892	-24.145	-24.637	-25.414	-25.074
1891	-24.110	-24.529	-25.470	-25.481
1890	-25.055	-24.779	-25.799	-25.434
1889	-25.023	-25.021	-25.766	-25.317
1888	-25.363	-24.956	-25.900	-25.459

	$\delta^{13}C$			
	TR EE 82		TR EE 88	
YEAR	RAW MEASURE	ERROR ADJUSTED	RAW MEASURE	ERROR ADJUSTED
1887	-25.223	-24.614	-25.736	-25.270
1886	-24.859	-24.386	-24.366	-24.366
1885	-25.003	-24.533	-25.311	-25.015
1884	-25.258	-24.528	-25.063	-25.511
1883	-24.401	-24.927	-25.726	-24.914
1882	-24.215	-25.141	-24.361	-24.749
1881	-24.104	-25.086	-25.235	-25.494
1880	-24.066	-25.127	-24.593	-25.400
1879	-24.665	-25.151	-25.035	-25.465
1878	-24.942	-24.894	-24.402	-25.195
1877	-25.194	-24.456	-25.542	-24.963
1876	-24.929	-24.207	-24.980	-25.328
1875	-24.263	-24.656	-24.306	-25.581
1874	-24.607	-24.642	-25.925	-25.349
1873	-24.544	-24.510	-25.330	-25.360
1872	-25.150	-24.381	-25.140	-25.439
1871	-24.762	-24.296	-25.259	-24.973
1870	-24.375	-24.341	-25.463	-25.425
1869	-24.591	-24.521	-26.028	-25.098
1868	-24.722	-24.467	-25.509	-24.870
1867	-24.901	-24.310	-24.035	-25.460
1866	-24.653	-24.204	-25.445	-25.909
1865	-24.835	-24.140	-25.293	-25.402
1864	-25.134	-24.625	-25.128	-25.503
1863	-24.821	-24.791	-25.255	-25.444
1862	-25.216	-25.087	-24.649	-25.453
1861	-24.958	-25.630	-25.418	-25.654
1860	-24.287	-25.607	-24.631	-25.787
1859	-24.965	-25.050	-25.926	-25.812
1858	-25.540	-24.753	-25.399	-25.859
1857	-24.844	-24.239	-24.961	-25.623
1856	-24.418	-23.862	-24.912	-25.019
1855	-24.337	-24.397	-24.974	-25.204
1854	-24.691	-24.734	-25.910	-25.144
1853	-24.903	-24.938	-25.416	-25.457
1852	-25.079	-24.745	-25.355	-25.075
1851	-23.980	-24.378	-24.837	-24.687
1850	-23.940	-24.148	-25.343	-25.046
1849	-24.754	-24.204	-24.622	-24.710
1848	-24.670	-24.843	-25.961	-24.917

	$\delta^{13}C$			
	TR EE 82		TR EE 88	
YEAR	RAW MEASURE	ERROR ADJUSTED	RAW MEASURE	ERROR ADJUSTED
1847	-24.232	-25.031	-26.010	-24.583
1846	-24.989	-25.178	-24.463	-25.254
1845	-24.193	-25.315	-25.768	-25.153
1844	-24.103	-25.165	-24.553	-24.593
1843	-24.706	-24.918	-25.241	-25.073
1842	-25.121	-24.973	-24.827	-25.703
1841	-24.910	-25.159	-25.634	-25.289
1840	-24.657	-24.873	-24.621	-25.173
1839	-24.833	-24.356	-24.957	-25.276
1838	-24.322	-24.209	-24.795	-25.480
1837	-24.518	-24.113	-25.211	-25.888
1836	-24.460	-24.093	-23.935	-25.629
1835	-25.071	-24.444	-25.794	-24.583
1834	-24.342	-24.793	-24.071	-24.787
1833	-24.082	-25.019	-25.241	-25.380
1832	-23.968	-25.128	-25.607	-25.237
1831	-24.418	-24.886	-24.709	-25.168
1830	-24.609	-24.407	-25.399	-25.136
1829	-24.346	-24.499	-26.200	-24.810
1828	-24.183	-24.572	-25.032	-25.242
1827	-24.590	-24.776	-25.159	-24.854
1826	-24.895	-25.037	-25.894	-25.568
1825	-24.937	-24.729	-24.243	-25.580
1824	-24.178	-24.450	-25.420	-25.150
1823	-24.261	-24.543	-25.193	-24.936
1822	-24.675	-24.673	-25.112	-24.933
1821	-24.452	-24.809	-25.332	-25.259
1820	-24.745	-24.812	-24.422	-25.760
1819	-24.397	-24.702	-25.086	-25.439
1818	-24.366	-24.865	-25.275	-25.292
1817	-24.891	-25.064	-24.364	-24.958
1816	-24.946	-24.907	-24.729	-25.202
1815	-24.845	-25.073	-25.201	-24.845
1814	-24.332	-25.091	-25.082	-25.518
1813	-24.742	-24.718	-25.208	-25.987
1812	-24.641	-24.473	-25.109	-25.217
1811	-24.853	-25.004	-25.376	-25.022
1810	-24.394	-25.403	-25.236	-25.331
1809	-23.859	-24.979	-25.746	-24.772
1808	-24.715	-24.556	-25.217	-25.119

	$\delta^{13}C$			
	TR EE 82		TR EE 88	
YEAR	RAW MEASURE	ERROR ADJUSTED	RAW MEASURE	ERROR ADJUSTED
1807	-24.927	-24.376	-24.690	-24.996
1806	-24.738	-24.487	-25.455	-25.419
1805	-24.505	-24.749	-25.554	-24.797
1804	-24.740	-24.928	-26.156	-24.885
1803	-25.013	-24.925	-25.990	-24.853
1802	-24.340	-24.156		-25.064
1801	-24.752	-23.971		-24.415
1800	-24.662	-24.464		-24.967
1799	-24.588	-24.708		-24.960
1798	-24.469	-24.492		-24.552
1797	-24.631	-24.461		-25.357
1796	-24.942	-24.793		-25.347
1795	-24.856	-24.252		-24.905
1794	-24.914	-24.159		-25.501
1793	-24.834	-24.581		-25.960
1792	-24.835	-24.984		-25.194
1791	-24.198	-25.002		-25.192
1790	-24.426	-24.798		-25.654
1789	-23.799	-24.719		-24.706
1788	-24.688	-24.699		-25.045
1787	-24.897	-24.387		-25.275
1786	-24.703	-24.491		-25.145
1785	-24.331	-24.507		-25.220
1784	-24.340	-24.894		-24.935
1783	-25.048	-24.592		-24.675
1782	-24.945	-24.197		-25.138
1781	-24.964	-24.032		-25.021
1780	-24.647	-24.124		-24.484
1779	-24.249	-24.456		-24.790
1778	-24.810	-24.552		-25.139
1777	-24.624	-24.357		-25.109
1776	-24.811	-24.237		-25.181
1775	-24.623	-24.507		-25.146
1774	-24.577	-24.805		-25.311
1773	-24.636	-24.923		-25.292
1772	-24.646	-24.558		-25.578
1771	-24.550	-24.213		-25.415
1770	-25.059	-24.391		-24.917
1769	-25.657	-24.611		-25.083
1768	-24.883	-24.517		-25.496

	$\delta^{13}C$			
	TR EE 82		TR EE 88	
YEAR	RAW MEASURE	ERROR ADJUSTED	RAW MEASURE	ERROR ADJUSTED
1767	-25.044	-24.676		-25.798
1766	-24.653	-24.454		-26.094
1765	-24.755	-24.398		-25.940
1764	-24.760	-24.738		
1763	-24.793	-24.927		
1762	-25.490	-24.896		
1761	-25.089	-24.619		
1760		-24.480		
1759		-24.703		
1758		-24.690		
1757		-24.761		
1756		-24.385		
1755		-24.010		
1754		-24.538		
1753		-24.866		
1752		-24.807		
1751		-24.610		
1750		-24.620		
1749		-24.847		
1748		-24.789		
1747		-24.465		
1746		-24.710		
1745		-24.657		
1744		-24.585		
1743		-24.502		
1742		-24.610		
1741		-24.854		
1740		-24.887		
1739		-24.890		
1738		-24.868		
1737		-24.835		
1736		-24.597		
1735		-24.282		
1734		-24.260		
1733		-24.017		
1732		-24.655		
1731		-24.852		
1730		-24.696		
1729		-24.400		
1728		-24.365		

	$\delta^{13}C$			
	TR EE 82		TR EE 88	
YEAR	RAW MEASURE	ERROR ADJUSTED	RAW MEASURE	ERROR ADJUSTED
1727		-24.844		
1726		-24.978		
1725		-24.951		
1724		-24.795		
1723		-24.463		
1722		-24.477		
1721		-24.739		
1720		-24.679		
1719		-24.757		
1718		-24.623		
1717		-24.593		
1716		-24.635		
1715		-24.639		
1714		-24.604		
1713		-24.981		
1712		-25.481		
1711		-25.118		
1710		-24.980		
1709		-24.807		
1708		-24.704		
1707		-24.755		
1706		-24.773		
1705		-25.054		
1704		-25.349		
1703		-24.986		

Table 11. Carbon Isotope Measurements for Tree 20.

	$\delta^{13}C$	
	TR EE 20	
YEAR	RAW MEASURE	ERROR ADJUSTED
2006	-27.138	-27.140
2005	-26.742	-26.799
2004	-26.144	-26.337
2003	-24.956	-25.548
2002	-25.638	-25.197
2001	-26.078	-25.709
2000	-26.211	-26.051
1999	-26.772	-26.210
1998	-26.242	-26.590
1997	-26.530	-26.487
1996	-26.680	-26.350
1995	-25.841	-26.560
1994	-25.840	-26.550
1993	-25.852	-25.970
1992	-25.446	-25.840
1991	-25.757	-25.846
1990	-25.906	-25.668
1989	-25.573	-25.551
1988	-26.224	-25.777
1987	-25.462	-25.857
1986	-25.459	-25.665
1985	-25.466	-26.018
1984	-25.978	-25.787
1983	-25.590	-25.460
1982	-25.431	-25.463
1981	-25.146	-25.566
1980	-25.143	-25.883
1979	-25.227	-25.656
1978	-25.219	-25.473
1977	-25.045	-25.267
1976	-25.005	-25.146
1975	-24.876	-25.169
1974	-25.158	-25.224
1973	-24.951	-25.197
1972	-24.737	-25.067
1971	-24.480	-25.014
1970	-25.291	-24.928
1969	-24.946	-25.025
1968	-24.849	-25.078

	$\delta^{13}C$	
	TR EE 20	
YEAR	RAW MEASURE	ERROR ADJUSTED
1967	-24.595	-24.896
1966	-24.681	-24.703
1965	-24.356	-24.598
1964	-24.356	-25.127
1963	-24.473	-25.038
1962	-24.868	-24.886
1961	-24.747	-24.723
1960	-24.543	-24.632
1959	-24.845	-24.588
1958	-24.529	-24.376
1957	-24.471	-24.374
1956	-24.590	-24.481
1955	-24.385	-24.771
1954	-24.233	-24.788
1953	-24.149	-24.632
1952	-24.393	-24.675
1951	-24.263	-24.732
1950	-24.727	-24.524
1949	-24.129	-24.495
1948	-24.521	-24.553
1947	-24.513	-24.407
1946	-24.900	-24.265
1945	-24.559	-24.179
1944	-24.752	-24.286
1943	-24.812	-24.330
1942	-24.522	-24.429
1941	-24.546	-24.557
1940	-24.879	-24.237
1939	-24.739	-24.483
1938	-24.790	-24.544
1937	-24.713	-24.803
1936	-24.890	-24.660
1935	-24.338	-24.680
1934	-24.527	-24.782
1933	-24.515	-24.683
1932	-24.144	-24.532
1931	-24.481	-24.638
1930	-24.767	-24.835
1929	-24.497	-24.759
1928	-24.553	-24.776

	$\delta^{13}C$	
	TR EE 20	
YEAR	RAW MEASURE	ERROR ADJUSTED
1927	-24.572	-24.735
1926	-24.045	-24.828
1925	-24.293	-24.523
1924	-24.536	-24.452
1923	-25.339	-24.525
1922	-24.932	-24.364
1921	-25.545	-24.256
1920	-25.778	-24.546
1919	-25.225	-24.701
1918	-25.021	-24.531
1917	-25.050	-24.546
1916	-25.103	-24.532
1915	-25.097	-24.174
1914	-25.249	-24.220
1913	-25.129	-24.451
1912	-25.423	-24.982
1911	-25.402	-25.147
1910	-25.076	-25.171
1909	-25.189	-25.610
1908	-24.956	-25.631
1907	-24.727	-25.216
1906	-24.208	-25.042
1905	-25.336	-25.052
1904	-25.692	-25.092
1903	-25.038	-25.108
1902	-25.589	-25.207
1901	-25.293	-25.172
1900	-25.461	-25.308
1899	-26.256	-25.409
1898	-26.289	-25.249
1897	-26.812	-25.125
1896	-25.426	-25.111
1895	-24.630	-24.901
1894	-24.583	-24.621
1893	-24.895	-24.449
1892	-24.997	-25.283
1891	-25.088	-25.577
1890	-24.930	-25.190
1889	-23.852	-25.460
1888	-23.673	-25.372

	$\delta^{13}C$	
	TR EE 20	
YEAR	RAW MEASURE	ERROR ADJUSTED
1887	-23.798	-25.421
1886	-23.734	-25.970
1885	-23.744	-26.278
1884	-24.011	-26.558
1883	-23.940	-26.187
1882	-24.600	-25.122
1881		-24.622
1880		-24.670
1879		-24.905
1878		-25.012
1877		-25.057
1876		-24.809
1875		-23.981
1874		-23.710
1873		-23.769
1872		-23.748
1871		-23.743
1870		-23.918
1869		-23.970
1868		-24.311
1867		-24.935

Biography

Hillary Sandford Jenkins was born on May 3, 1982 in New Brunswick, New Jersey, while her parents were in graduate school at Rutgers University. Before she was 4 years old, her family relocated to the desert of New Mexico and she spent her formative years in Albuquerque, amid the open expanse of sky and mesa. Growing up in the southwest birthed in her a love for the natural landscape and led her to choose Geology as her major at Wellesley College. In 2004, she graduated with a B.A. from Wellesley and a burgeoning desire to learn more about the history of the natural world. She continued her studies in the field of Paleoclimatology, coming to Duke University in the fall of 2004. Through several sampling trips and field excursions, she traversed the Amazon basin in search of the perfect climate record. It was during these adventures that she truly fell in love with this project, the Peruvian Amazon, and the fate of its people.